

**THE ANATOMY OF HYPERBOLIC TRAJECTORIES IN THE GULF OF
MEXICO**

by

Michael Weed

A thesis submitted to the faculty of the University of Delaware in partial
fulfillment of the requirements for the degree of Master of Science in Marine Studies

Winter 2006

Copyright 2006 Michael Weed
All Rights Reserved

UMI Number: 1432294



UMI Microform 1432294

Copyright 2006 by ProQuest Information and Learning Company.
All rights reserved. This microform edition is protected against
unauthorized copying under Title 17, United States Code.

ProQuest Information and Learning Company
300 North Zeeb Road
P.O. Box 1346
Ann Arbor, MI 48106-1346

**THE ANATOMY OF HYPERBOLIC TRAJECTORIES IN THE GULF OF
MEXICO**

by

Michael Weed

Approved: _____
A. D. Kirwan, Jr., Ph.D.
Professor in charge of thesis on behalf of the Advisory Committee

Approved: _____
Nancy M. Targett, Ph.D.
Dean of the Graduate College of Marine Studies

Approved: _____
Conrado M. Gempesaw II, Ph.D.
Vice Provost for Academic and International Programs

ACKNOWLEDGMENTS

This thesis would not have been possible without the financial support of the grant from the National Science Foundation (NSF) Transport- CMG Award #0222150. I would also like to thank the Office of Naval Research (ONR) for their support of many of my colleagues who assisted me in the completion of this thesis.

I am sincerely grateful to Dr. Kirwan for his patience, guidance and infinite knowledge. He led me through the challenging times with ease and led me on the right path. I'm indebted to Dr. Bruce Lipphardt for the countless hours he spent modifying code and for his help in revising this work, to Melissa Zweng for her assistance in Matlab programming, and to Dr. Fabrice Veron and his assistance in revising. I'm also grateful to all of the faculty and students in the College of Marine Studies at University of Delaware, Newark campus, for all of the knowledge and experience that they passed on.

Last but not least, I'd like to thank my family and friends for their continued support and confidence in me throughout my whole time at the University of Delaware. Their support helped me through the hard times and kept pushing me towards the end.

TABLE OF CONTENTS

| | |
|--|----|
| LIST OF TABLES | vi |
| LIST OF FIGURES | ix |
| ABSTRACT | xv |
| Chapter | |
| 1 Background..... | 1 |
| 1.1 Advection Studies..... | 1 |
| 1.1.1 Biological Studies | 1 |
| 1.1.2 Dynamical Systems Theory..... | 2 |
| 1.2 Toner et al. (2003)..... | 3 |
| 1.3 Research Questions | 6 |
| 2 Circulation in the Gulf of Mexico | 8 |
| 2.1 Introduction | 8 |
| 2.2 The Loop Current | 9 |
| 2.2.1 Loop Current Rings (LCR's)..... | 9 |
| 2.2.1.1 Shedding Rate..... | 9 |
| 2.2.2 Paths of Loop Current Rings | 11 |
| 2.2.3 Longevity..... | 11 |
| 2.3 Cyclones | 12 |
| 2.4 Eddy-Eddy Interaction..... | 12 |
| 2.6 Circulation Models | 14 |
| 3 Model..... | 15 |
| 3.1 Numerical Models of the Gulf of Mexico | 15 |
| 3.2 Model Validation..... | 16 |
| 4 Hyperbolic Trajectories..... | 19 |
| 4.1 Geopotential Height..... | 20 |
| 4.2 Simple Dynamical Model..... | 21 |
| 4.3 Kinematic Model | 25 |
| 4.4 Inflowing and Outflowing Manifolds..... | 26 |
| 4.5 Stagnation Point..... | 30 |
| 4.6 Hyperbolic Trajectory Characteristics..... | 31 |
| 5 Results | 34 |
| 5.1 Introduction | 34 |
| 5.2 Hyperbolic Structure A1..... | 36 |
| 5.2.1 Hyperbolic Trajectory Paths..... | 37 |
| 5.2.2 Distance Moved Per Day..... | 41 |

| | | |
|----------|---|-----|
| 5.2.3 | Chaotic Properties of the Hyperbolic Trajectories | 51 |
| 5.2.4 | Vertical Extent of Hyperbolic Structure A1 | 70 |
| 5.2.5 | Three-Dimensional Structure | 71 |
| 5.3 | Hyperbolic Structure A2..... | 83 |
| 5.3.1 | Hyperbolic Trajectory Paths..... | 83 |
| 5.3.2 | Distance Moved per Day | 85 |
| 5.3.3 | Chaotic Properties of the Hyperbolic Trajectories | 89 |
| 5.3.4 | Vertical Extent of Hyperbolic Structure A2..... | 94 |
| 5.3.5 | Three-Dimensional Structure | 96 |
| 5.4 | Advective Channel | 102 |
| 5.4.1 | Depth of the Channel..... | 103 |
| 5.4.2 | Three-Dimensional Channel..... | 106 |
| 5.4.3 | Volume Transport..... | 111 |
| 6 | Conclusions | 116 |
| 7 | Future Studies..... | 118 |
| Appendix | | |
| A | Material Curves | 121 |
| B | Hyperbolic Trajectory Tables | 123 |

LIST OF TABLES

| | | |
|-------------|---|----|
| Table 5-1: | Levels used..... | 35 |
| Table 5-2: | Table of distance traveled per day in kilometers for hyperbolic trajectory at 50 m for hyperbolic structure A1. The days with the minimum and maximum distance values are highlighted in yellow. | 44 |
| Table 5-3: | Table of distance traveled per day in kilometers for hyperbolic trajectory at 200 m for hyperbolic structure A1. The days with the minimum and maximum distance values are highlighted in yellow. | 45 |
| Table 5-4: | Table of distance traveled in per day kilometers for hyperbolic trajectory at 300 m for hyperbolic structure A1. The days with the minimum and maximum distance values are highlighted in yellow. | 46 |
| Table 5-5: | Table of distance traveled per day in kilometers for hyperbolic trajectory at 400 m for hyperbolic structure A1. The days with the minimum and maximum distance values are highlighted in yellow. | 47 |
| Table 5-6: | Table of distance traveled per day in kilometers for hyperbolic trajectory at 600 m for hyperbolic structure A1. The days with the minimum and maximum distance values are highlighted in yellow. | 48 |
| Table 5-7: | Table of distance traveled per day in kilometers for hyperbolic trajectory at 1100 m for hyperbolic structure A1. The days with the minimum and maximum distance values are highlighted in yellow. | 49 |
| Table 5-8: | Variability of distance traveled in km with depth for A1 from April 11-12, April 24-25 and April 25-26 for hyperbolic trajectories associated with A1..... | 50 |
| Table 5-9: | Mean distance traveled for hyperbolic structure A1. The distances are in km/day. | 51 |
| Table 5-10: | Table of distance traveled in kilometers for hyperbolic trajectory at 10 m for hyperbolic structure A2. The minimum and maximum values are highlighted in yellow..... | 86 |

| | |
|--|-----|
| Table 5-11: Table of distance traveled in kilometers for hyperbolic trajectory at 50 m for hyperbolic structure A2. The minimum and maximum values are highlighted in yellow..... | 87 |
| Table 5-12: Table of distance traveled in kilometers for hyperbolic trajectory at 125 m for hyperbolic structure A2. The minimum and maximum values are highlighted in yellow..... | 88 |
| Table 5-13: Depth-to-depth variability in km on April 10-11 and April 15-16..... | 88 |
| Table 5-14: Mean distance traveled for hyperbolic structure A2. The distances are in km/day. | 89 |
| Table 5-15: Details of the volume flux estimate calculation along two transects spanning the advect channel on April 16, 1998. | 113 |
| Table B-1: Table of Distances traveled at 0 m for hyperbolic structure A1. | 124 |
| Table B-2: Table of Distances traveled at 10 m for hyperbolic structure A1. | 125 |
| Table B-3: Table of Distances traveled at 20 m for hyperbolic structure A1. | 126 |
| Table B-4: Table of Distances traveled at 30 m for hyperbolic structure A1. | 127 |
| Table B-5: Table of Distances traveled at 75 m for hyperbolic structure A1. | 128 |
| Table B-6: Table of Distances traveled at 100 m for hyperbolic structure A1. | 129 |
| Table B-7: Table of Distances traveled at 125 m for hyperbolic structure A1. | 130 |
| Table B-8: Table of Distances traveled at 150 m for hyperbolic structure A1. | 131 |
| Table B-9: Table of Distances traveled at 250 m for hyperbolic structure A1. | 132 |
| Table B-10: Table of Distances traveled at 500 m for hyperbolic structure A1. | 133 |
| Table B-11: Table of Distances traveled at 700 m for hyperbolic structure A1. | 134 |
| Table B-12: Table of Distances traveled at 800 m for hyperbolic structure A1. | 135 |
| Table B-13: Table of Distances traveled at 900 m for hyperbolic structure A1. | 136 |
| Table B-14: Table of Distances traveled at 1000 m for hyperbolic structure A1. | 137 |
| Table B-15: Table of Distances traveled at 1200 m for hyperbolic structure A1. | 138 |

Table B-16: Table of Distances traveled at 1300 m for hyperbolic structure A1. 139

Table B-17: Table of Distances traveled at 1400 m for hyperbolic structure A1. 140

Table B-18: Table of Distances traveled at 1500 m for hyperbolic structure A1. 141

Table B-19: Table of Distances traveled at 1750 m for hyperbolic structure A1. 142

Table B-20: Table of Distances traveled at 2000 m for hyperbolic structure A1. 143

Table B-21: Table of Distances traveled at 2500 m for hyperbolic structure A1. 144

Table B-22: Table of Distances traveled at 3000 m for hyperbolic structure A1. 145

Table B-23: Table of Distances traveled at 0 m for hyperbolic structure A2. 146

Table B-24: Table of Distances traveled at 20 m for hyperbolic structure A2. 146

Table B-25: Table of Distances traveled at 30 m for hyperbolic structure A2. 147

Table B-26: Table of Distances traveled at 75 m for hyperbolic structure A2. 147

Table B-27: Table of Distances traveled at 100 m for hyperbolic structure A2. 148

LIST OF FIGURES

| | | |
|-------------|--|----|
| Figure 1-1: | Study area, denoted by the red box. Photo courtesy of The National Weather Service http://www.srh.noaa.gov/mob/MOB_chart.png | 3 |
| Figure 1-2: | SeaWiFS images showing chlorophyll distribution on (a) April 1 and (b) April 17. The white boxes are the area of interest. The black and white contours are sea surface height. | 4 |
| Figure 1-3: | Advective channel in the Gulf of Mexico. The red curves are the unstable manifolds and the blue curves are the stable manifolds. The green is ocean color, representing high concentrations of chlorophyll. A1 and A2 are the two hyperbolic trajectories found by Toner et al. (2003). The contours are sea-surface height anomaly and the dashed line is the 110 m isobar. (Figure from Toner et al. 2003) | 6 |
| Figure 2-1: | Bottom bathymetry of the Gulf of Mexico. Deep blue represents water deeper than 3000 meters, light blue represents the shelf with depths less than 200 meters and mid-blue represents a depth of around 1200 meters. | 8 |
| Figure 2-2: | The northern movement of the Loop Current, the pinching event and the subsequent westward motion of the anticyclone. http://oceanexplorer.noaa.gov/explorations/02mexico/background/currents/media/gulf_loop.html | 10 |
| Figure 2-3: | Advective channel in the Gulf of Mexico on April 17, 1998. The red (blue) curves are the unstable (stable) manifolds. The green is ocean color representing high concentrations of chlorophyll. A1 and A2 are the two hyperbolic trajectories found by Toner et al. (2003). The contours are sea-surface height anomaly and the dashed line is the 110-m isobar. (From Toner et al. 2003) | 14 |
| Figure 4-1: | Geopotential height anomaly of our study area in the Gulf of Mexico at 10 m on April 6, 1998. | 21 |

| | | |
|-------------|---|----|
| Figure 4-2: | Examples of inflowing and outflowing manifolds. The lines depict the inflowing (blue) and outflowing (red) manifolds at 50 m on April 17, 1998. The inflowing manifold was initialized on April 26, 1998 and the outflowing manifold was initialized on April 6, 1998. The filled contours are geopotential height in m^2/s^2 | 29 |
| Figure 4-3: | The stretching and compression of a blob of particles around the hyperbolic trajectory. The green circles are initialized particles. The blue square is the location of the stagnation point and the pink diamond in the location of the hyperbolic trajectory. | 32 |
| Figure 4-4: | Paths of the hyperbolic trajectory (red) and stagnation point (blue) in a velocity field with background flow. | 33 |
| Figure 5-1: | Paths of hyperbolic trajectories at six depths ranging from 10 to 300 m. The colors correspond to the depths as shown in the legend. The large diamonds denote the initial position of the hyperbolic trajectory on April 6. The 3000 m isobar is also shown. | 38 |
| Figure 5-2: | Paths of hyperbolic trajectories at six depths ranging from 300 to 800 m. The colors correspond to the depths as shown in the legend. The large diamonds denote the initial position of the hyperbolic trajectory on April 6. The 3000 m isobar is also shown. | 39 |
| Figure 5-3: | Paths of hyperbolic trajectories at six depths ranging from 900 to 3000 m. The colors correspond to the depths as shown in the legend. The large diamonds denote the initial position of the hyperbolic trajectory on April 6. The 3000 m isobar is also shown. | 40 |
| Figure 5-4: | Vertical profiles of temperature and salinity at the location of the hyperbolic trajectory at 50 m on April 6. Top panels show full vertical structure while the bottom panels focus on the upper 1000 m. The transition layer is between 300 and 400 m, denoted by red lines. | 41 |

| | | |
|--------------|---|----|
| Figure 5-5: | Paths of the hyperbolic trajectory and four particles initialized 1 km north, south, east, and west of the hyperbolic trajectory at 100 m. The colors correspond to the particle positions as shown in the legend. The image to the right is zoomed in on the initial positions. The particles and the hyperbolic trajectories are shown from April 6 to April 26. The contours are bottom bathymetry in meters. | 54 |
| Figure 5-6: | Same as Figure 5-5 for 200 m. | 55 |
| Figure 5-7: | Same as Figure 5-5 for 300 m. | 56 |
| Figure 5-8: | Same as Figure 5-5 for 400 m. | 57 |
| Figure 5-9: | Same as Figure 5-5 for 1100 m. | 58 |
| Figure 5-10: | Natural log of separation/initial separation versus time for the hyperbolic trajectory and four particles initialized 1km to the north, south, east, and west of the hyperbolic trajectory at 100 m. The colors correspond to the positions as noted in the legend above. The green line is a line with slope of f (Coriolis parameter)..... | 60 |
| Figure 5-11: | Same as Figure 5-10 for 200 m. | 61 |
| Figure 5-12: | Same as Figure 5-10 for 300 m. | 62 |
| Figure 5-13: | Same as Figure 5-10 for 400 m. | 63 |
| Figure 5-14: | Same as Figure 5-10 for 1100 m. | 64 |
| Figure 5-15: | Time series (April 6 - April 26) of geopotential (m^2/s^2 , top), temperature ($^{\circ}C$, middle), and salinity (PSU, bottom) for the hyperbolic trajectory at 100 m (green) and nearby particles. The line colors for the nearby particles correspond to their positions as shown in the legend..... | 66 |
| Figure 5-16: | Same as Figure 5-15 for 200 m. | 67 |
| Figure 5-17: | Same as Figure 5-15 for 300 m. | 68 |
| Figure 5-18: | Same as Figure 5-15 for 400 m. | 69 |
| Figure 5-19: | Same as Figure 5-15 for 1100 m. | 70 |

| | |
|--|----|
| Figure 5-20: Position of hyperbolic structures A1 and A2. The colored dots correspond to times and position as shown in the legend. The contours are the bottom topography (in m)..... | 71 |
| Figure 5-21: Plan view of the hyperbolic structure A1. This figure shows the position of the hyperbolic trajectory in each of the 27 depths on April 7. The blue dot denotes the position at 10 meters..... | 72 |
| Figure 5-22: Three-dimensional view of the hyperbolic structure A1. This figure shows the position of the hyperbolic trajectory in each of the 27 depths on April 7. The blue dot denotes the position at 10 meters. | 73 |
| Figure 5-23: Plan view of the hyperbolic structure A1. This figure shows the position of the hyperbolic trajectory in each of the 27 depths on April 11. The blue dot denotes the position at 10 meters..... | 74 |
| Figure 5-24: Three-dimensional view of the hyperbolic structure A1. This figure shows the position of the hyperbolic trajectory in each of the 27 depths on April 11. The blue dot denotes the position at 10 meters. | 75 |
| Figure 5-25: Three-dimensional view of the hyperbolic structure A1. This figure shows the position of the hyperbolic trajectory in each of the 27 depths from April 6 (red) to April 26 (blue). The changing colors from red to blue represent passing time. The green diamond denotes the position at 10 m..... | 76 |
| Figure 5-26: Same as Figure 5-25 but shown at a perspective from the right. | 77 |
| Figure 5-27: Velocities near hyperbolic structure A1 at 50 m on April 16. The red diamond denotes position of the hyperbolic trajectory..... | 79 |
| Figure 5-28: Velocities near hyperbolic structure A1 at 300 m on April 16. The red diamond denotes the position of hyperbolic trajectory..... | 80 |
| Figure 5-29: Velocities near hyperbolic structure A1 at 400 m on April 16. The red diamond denotes the position of hyperbolic trajectory..... | 81 |
| Figure 5-30: Velocities near hyperbolic structure A1 at 1100 m on April 16. The red diamond denotes the position of the hyperbolic trajectory..... | 82 |

| | |
|---|-----|
| Figure 5-31: Path of the hyperbolic structure A2 from 10 to 125 m. The colors correspond to the depths as noted in the legend. The large diamonds denote the initial position of the hyperbolic trajectory on April 10. The contours are bottom bathymetry (in m). | 84 |
| Figure 5-32: Paths of the hyperbolic trajectory and four particles initialized 1 km north, south, east and west of it at 10 m from April 10 to April 20. Colors correspond to positions as noted by the legend. The image to the right is zoomed in on the initial positions. The contours are bottom bathymetry (in m)..... | 90 |
| Figure 5-33: Same as Figure 5-32 for 50 m. | 91 |
| Figure 5-34: Natural log of separation/initial separation versus time for the hyperbolic trajectory and four particles initialized 1km to the north, south, east, and west of hyperbolic trajectory A2 at 10 m. The colors correspond to the positions as noted in the legend. The green line is a line with slope of f (Coriolis parameter)..... | 92 |
| Figure 5-35: Same as Figure 5-34 for 50 m. | 93 |
| Figure 5-36: Difference in geopotential, temperature and salinity from the hyperbolic trajectory's initial value for the hyperbolic trajectory and four particles initialized 1 km north, south, east and west of the hyperbolic trajectory at 10 m. The colors correspond to positions as denoted in the legend above. Shown from April 10 to April 20. | 94 |
| Figure 5-37: Positions of the hyperbolic trajectories associated with A2 for five depths ranging from 30 to 125 m on April 10. The colors correspond to the depths as noted in the legend..... | 95 |
| Figure 5-38: Plan view of the hyperbolic structure A2 on April 11. The blue dot denotes the position at 10 m..... | 97 |
| Figure 5-39: Three-dimensional view of the hyperbolic structure A2 on April 11. The blue dot denotes the position at 10 m..... | 98 |
| Figure 5-40: Plan view of the hyperbolic structure A2 on April 15. The blue dot denotes the position at 10 m..... | 99 |
| Figure 5-41: Three-dimensional view of the hyperbolic structure A2 on April 15. The blue dot denotes the position at 10 m..... | 100 |

| | |
|--|-----|
| Figure 5-42: Three-dimensional view of the evolution of hyperbolic structure A2 from April 10 (red) to April 20 (blue). The green diamond denotes the position at 10 m..... | 101 |
| Figure 5-43: Same as Figure 5-42 but at a perspective from the right..... | 102 |
| Figure 5-44: Inflowing and outflowing manifolds for depths 10-50 m for both A1 and A2 on April 16, 1998..... | 104 |
| Figure 5-45: Inflowing and outflowing manifolds at depths 75-125 m for both A1 and A2 and 150 m for A1 on April 16, 1998..... | 105 |
| Figure 5-46: Advective channel formed by the inflowing A2 manifolds (blue) and the outflowing manifolds (red) on April 14, 1998 for depths 10-100 m. The shade of the manifold gets darker with depth..... | 107 |
| Figure 5-47: Same as Figure 5-46 for April 15, 1998..... | 108 |
| Figure 5-48: Same as Figure 5-46 for April 16, 1998..... | 109 |
| Figure 5-49: Same as Figure 5-46 for April 17, 1998..... | 110 |
| Figure 5-50: Same as Figure 5-46 for April 18, 1998..... | 111 |
| Figure 5-51: Position of transects A (green) and B (light blue) used for the volume flux estimates on April 16, 1998 at 50 m. The inflowing (outflowing) manifolds of A1 are shown in blue (red) and the inflowing (outflowing) manifolds of A2 are shown in black (magenta). The vectors are the model velocity vectors at grid points..... | 114 |

ABSTRACT

The eastern Gulf of Mexico is an area of strong interaction between eddies (cyclones and anticyclones). The presence of the Loop current and shed Loop Current Eddies intensifies this interaction. Toner et al., (2003, Chlorophyll dispersal by eddy-eddy interactions in the Gulf of Mexico. *J. Geophys. Res.* Vol. 108(C4), 3105. doi:10.1029/2002JC001499) found that the material curves of the two hyperbolic trajectories (A1 and A2) in the area of this interaction created an advective channel. The channel was verified by using ocean color data, signifying a chlorophyll plume. This study uses all available layers of the Colorado University Princeton Ocean Model (CUPOM), to study 1) the depth to which the hyperbolic structures are present, 2) the vertical structure of these hyperbolic structure and 3) the depth of the advective channel. In the process, we examine both the path of the hyperbolic trajectories in each level and the chaotic nature of these hyperbolic trajectories.

Material curves are initialized in all available layers in order to study the vertical characteristics of the hyperbolic structures. Both hyperbolic structures extend from the surface to the bottom at their respective locations, which for A1 is from the surface to 3000 m while for A2 is from the surface to 125 m. Hyperbolic trajectory A2 follows the bottom topography of the shelf from 50 m to 125 m. The hyperbolic trajectories of A1 follow similar pathways from the surface to 300 m and another similar pattern from 400-3000 m. The hyperbolic structures have chaotic characteristics with particles initialized 1 km to the north, south, east, and west of the structure separating from the structure at a rate $.125 f$ for the upper levels and

decreasing to $.075 f$ in the lower levels for A1 where f is the Coriolis parameter. The particles separate at a rate of $.05 f$ for A2. The advective channel of Toner et al. (2003), which was delineated by a chlorophyll plume, is also studied through the water column. It is present only up to 75 meters and is most clearly delineated by the material curves from 30-75 m. The advective channel has an associated volume transport of 1.4 Sverdrups and 2.6 Sverdrups at two different transects.

Chapter 1

BACKGROUND

1.1 Advection Studies

1.1.1 Biological Studies

There have been a number of biological studies showing that advection plays a role in determining ocean color patterns in the Gulf of Mexico. Gower et al (1980) and Denman and Abbot (1994) studied the importance of advection on the distribution of plankton and Muller-Karger et al. (1991), Biggs and Muller-Karger (1994) and Perez et al. (1999) examined the effect that eddies have on biological transport in the Gulf of Mexico.

Other studies have used ocean color data to analyze the role of advection in determining ocean color patterns. Muller-Karger et al. (1991) studied near-surface phytoplankton from a multi-year series of the Coastal Zone Color Scanner (CZCS). They found that high-pigment water from the Mississippi River was advected offshore, wrapped around the cyclonic edge of an anticyclonic eddy pinched off from the loop current and then was advected through the Florida Straits. Biggs and Muller-Karger (1994) found that cyclone-anticyclone pairs influence the surface circulation over the continental slope and rise. Using the CZCS images, they found that cyclone-anticyclone geometries transport high-chlorophyll shelf water 100-200 km off of the shelf. Again using CZCS, Gilbes et al. (1996) found episodic formation of an

extensive plume on the West Florida Shelf that extended southward from Cape San Blas toward the Florida Keys. They concluded that this plume was possibly due to the circulation of water associated with the Loop Current and its intrusions. Finally, Toner et al. (2003) studied several examples of advective transport in the Gulf of Mexico. That work is the motivation for this study and is discussed further in Section 1.2.

1.1.2 Dynamical Systems Theory

Many recent studies have used dynamical systems theory to study Lagrangian transport quantities and other geometric structures that quantify transport. Using a three-layer model, Couillette and Wiggins (2000) used special material curves initialized in the vicinity of structures known as hyperbolic trajectories to analyze flux. (Hyperbolic trajectories are explained in detail in Chapter 4). They showed that dynamical systems techniques aid in studying Lagrangian transport and ring formation. Using the Colorado University Princeton Ocean Model (CUPOM), Kuznetsov et al. (2002) showed that these dynamical systems methods are capable of defining channels for advective transport in the realistic setting of the Gulf of Mexico. Again using CUPOM, Kirwan et al. (2003) studied Lagrangian predictability of ocean flow in the Gulf of Mexico using the concepts from dynamical systems theory. They found that this approach is capable of separating the flow fields into regions with distinct advective fates or destinations. Toner et al. (2003) then used the dynamical systems idea in order to study an advective channel in the Gulf of Mexico extending from the Yucatan Shelf to the West Florida Shelf. For more details on dynamical systems theory and use in geophysical fluid dynamics, see Kirwan et al. (2003) and Kirwan (2005).

1.2 Toner et al. (2003)

Toner et al. (2003) were the first study that combined dynamical systems theory with ocean color data from satellite imagery. They studied a 500 by 509 km region that extends from the Yucatan Shelf to the southern West Florida Shelf during the month of April 1998 after a pinching event of the Loop Current. This area is denoted by the red box in Figure 1-2.

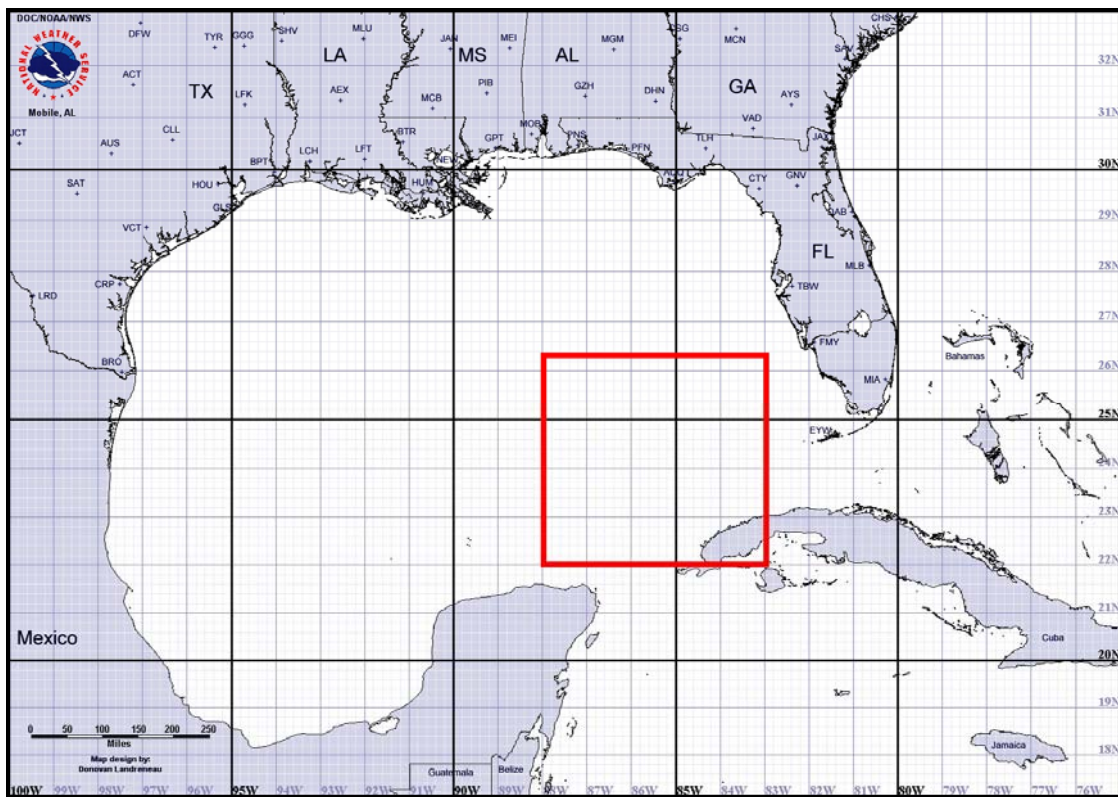


Figure 1-1: Study area, denoted by the red box. Photo courtesy of The National Weather Service (http://www.srh.noaa.gov/mob/MOB_chart.png)

First, using satellite images from SeaWiFS (Sea-viewing Wide-Field-of-View Sensor), they showed that chlorophyll was advected off of the Campeche Shelf across the deep Gulf to the West Florida Shelf. This advection is shown in Figure 1-2. In the white box of Figure 1-2a, only a small amount of light green color is in the deep Gulf. This changes in Figure 1-2b where a much more noticeable light green plume is detected.

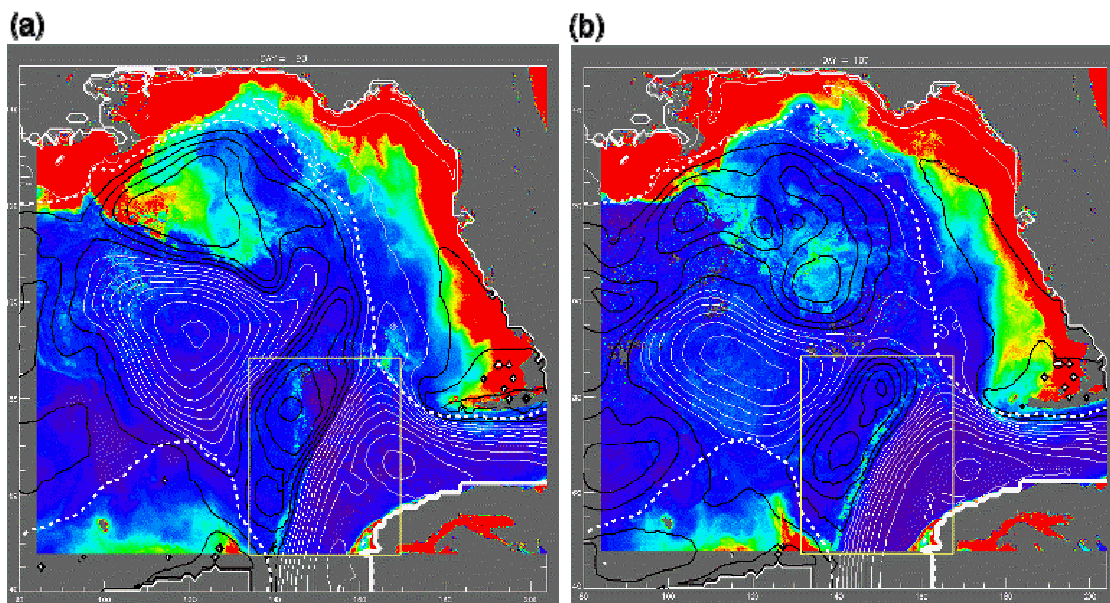


Figure 1-2: SeaWiFS images showing chlorophyll distribution on (a) April 1 and (b) April 17. The white boxes are the area of interest. The black and white contours are sea surface height.

They then used the dynamical systems technique to study this advection. They located two dynamical structures known as hyperbolic trajectories. A hyperbolic trajectory acts as a simultaneous attractor and repeller for nearby fluid particles. Particles lying on or near the negative eigendirections of the velocity

gradient are attracted towards the hyperbolic trajectory while those lying along or near the positive eigendirection are repelled. These structures are referred to as A1 and A2 (Figure 1-3). The continuous stream of particles directly repelled from the hyperbolic trajectory create the material curve known as the outflowing manifold and the particles attracted directly to the hyperbolic trajectory create the inflowing manifold. They are the red and blue curves shown in Figure 1-3. (Material curves are discussed more extensively in Appendix A). The intersection of these impermeable curves defines the position of the hyperbolic trajectory. Using the outflowing manifold of hyperbolic trajectory A1 and the inflowing manifold of hyperbolic trajectory A2, they identified a narrow advective channel at 50 meters depth between the Loop Current and an adjacent cyclone. Comparing this channel to SeaWiFS images, the chlorophyll plume aligned remarkably well with the channel, as shown in Figure 1-3.

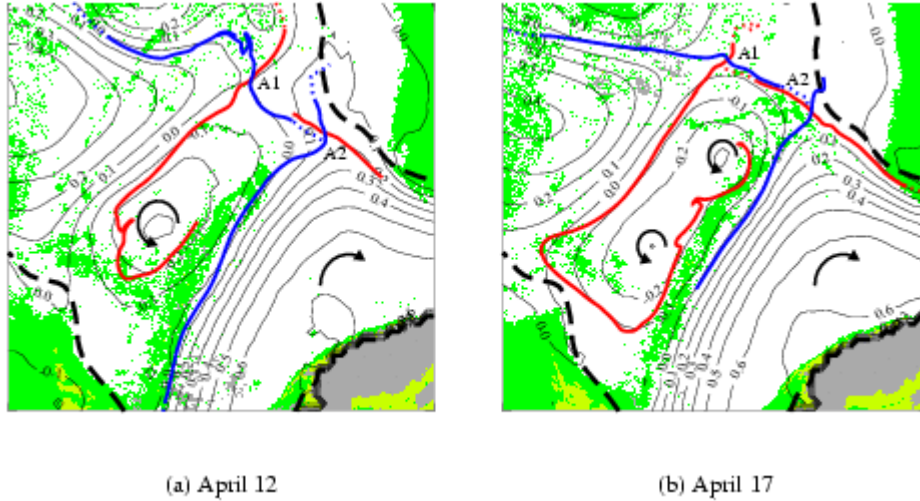


Figure 1-3: Advective channel in the Gulf of Mexico. The red curves are the unstable manifolds and the blue curves are the stable manifolds. The green is ocean color, representing high concentrations of chlorophyll. A1 and A2 are the two hyperbolic trajectories found by Toner et al. (2003). The contours are sea-surface height anomaly and the dashed line is the 110 m isobar. (Figure from Toner et al. 2003)

1.3 Research Questions

The pioneering work of Toner et al. (2003) provides the first observational evidence of the existence of hyperbolic trajectories in the ocean. By combining the use of satellite imagery with dynamical systems techniques, they clearly illustrated how powerful and accurate the dynamical systems theory can be in analyzing these Lagrangian properties. This work opened the door to a new level of questions:

- Are these structures confined to the near surface or do they live throughout the water column? If they are found throughout the water column, is there any

relation between the deeper structures and the near surface features reported by Toner et al. (2003)?

- How are they affected by the thermocline and halocline?
- How do the structures move?
- What other properties do they possess?

The work also opens questions about the advective channel:

- How deep is the advective channel?
- How long is the advective channel present?
- What is the volume transport associated with it?

Using Toner et al. (2003) as a foundation, this research attempts to bring clarification of the issues above. By looking at all available levels of CUPOM, a new picture of hyperbolic regions in the ocean emerges. For the first time, the entire anatomy of the hyperbolic structure will be studied.

Chapter 2

CIRCULATION IN THE GULF OF MEXICO

2.1 Introduction

Kantha (2004, private communication) describes the Gulf of Mexico as a three-layer ocean. The upper layer characteristic depth goes from the surface to about 50m, which roughly corresponds to the sill depth of the Straits of Florida. The intermediate layer characteristic depth is from 50m to about 1200m, which is characteristic of the sill depth across the Yucatan Channel. The abyssal layer is from 1200m to about 2500m, roughly the abyssal plain of the Gulf. These two sill depths are shown in Figure 2-1.



Figure 2-1: Bottom bathymetry of the Gulf of Mexico. Deep blue represents water deeper than 3000 meters, light blue represents the shelf with depths less than 200 meters and mid-blue represents a depth of around 1200 meters.

2.2 The Loop Current

The Loop Current is the dominant circulation feature in the eastern Gulf of Mexico. It is known as the Yucatan Current as it enters the Gulf of Mexico via the Yucatan channel. Between 23 and 28 Sverdrups of warm subtropical water enter the Gulf from the Yucatan Channel (Candela et al. 2003). Once in the Gulf of Mexico, the Loop Current flows clockwise and penetrates northward and westward. Once it exits through the Straits of Florida, it is known as the Gulf Stream.

2.2.1 Loop Current Rings (LCR's)

The majority of the observational studies have dealt with the Loop Current variability and its anticyclonic eddy shedding. Ichiye (1962) was the first to show that the large anticyclonic rings shed by the Loop Current are a dominant factor in the circulation of the Gulf of Mexico. Later, Elliot (1979; 1982) showed that these anticyclonic features are important with respect to the salt and heat budgets, as well as a dominant factor in momentum balance. They are among some of the most energetic mesoscale ocean structures (Indest et al., 1989). The radii of these rings can reach 100 km, the swirl velocities can exceed 1 m/s, and the thermal signatures can be found as deep as 1000 m (Kirwan et al., 1984a; Lewis and Kirwan, 1985; 1987; Lewis et al., 1989, Indest et al. 1989).

2.2.1.1 Shedding Rate

The Loop Current sheds eddies approximately once every 11 months but there is great variability (Vukovich, 1995; Sturges and Leben, 2000). Oey et al. (2003) showed that both winds and the Caribbean eddies play a role in determining when the Loop Current will shed an eddy. This process and the subsequent westward motion are shown in Figure 2-2.

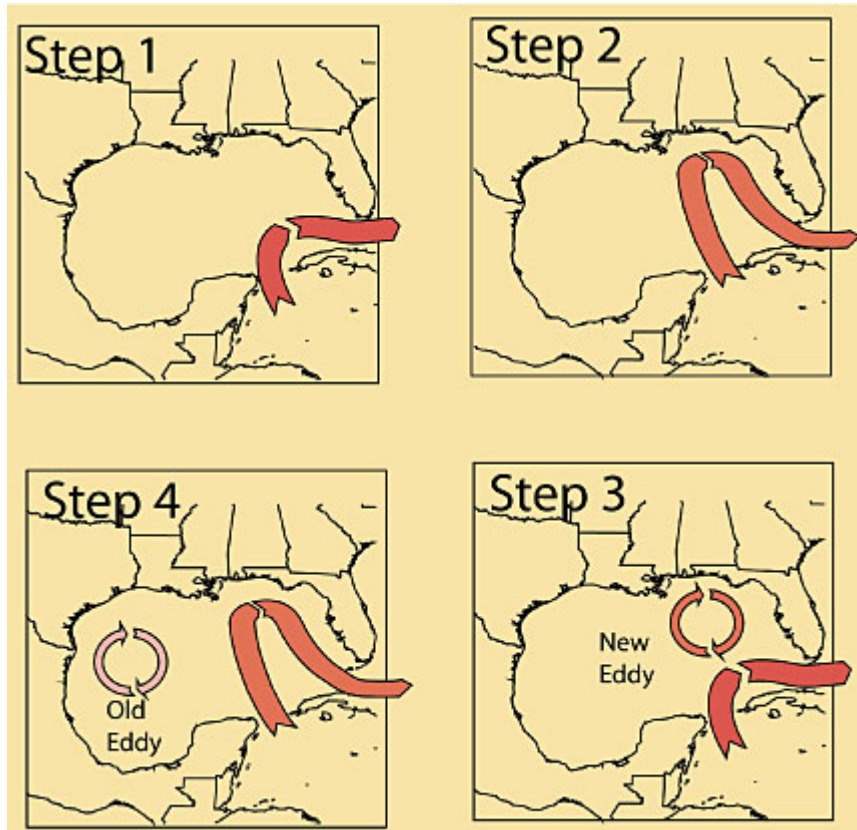


Figure 2-2: The northern movement of the Loop Current, the pinching event and the subsequent westward motion of the anticyclone.
http://oceanexplorer.noaa.gov/explorations/02mexico/background/currents/media/gulf_loop.html

Sturges et al. (1993) showed that there is no clear way of determining the moment when the eddies separate; the ring may appear to be separated, yet later information shows that parts are still attached. Sturges et al. (1993) also showed that recirculation can occur in the interior of the ring while the ring is still attached. Oey et al. (2003) studied causes of the irregular eddy shedding by the Loop Current and Oey (2004) found that the potential vorticity flux might serve as an indicator of eddy

shedding. Despite many theoretical and observational studies, the dynamics causing the shedding are still unknown.

2.2.2 Paths of Loop Current Rings

Cochrane (1969), Elliot (1982) and Kirwan et al., (1984a,b 1988) found that the primary path of the rings is westward through the deepest portion of Gulf, but the route may have a northern variation (Vukovich and Crissman, 1986). Biggs et al (1996) studied one Loop Current eddy *Triton* for a period of one year as it drifted southwest across the Gulf and documented its behavior as it reached the Western Shelf region.

The pinched-off eddies have a warm-water core and thus rotate anticyclonically as they propagate to the west. These warm core rings transport a significant amount of heat, momentum and salt across the Gulf (Kirwan et al., 1984b; Lewis and Kirwan, 1985). They have typical translation velocities of approximately 2 cm/s, estimated from data and models in the eastern Gulf (Lewis and Kirwan, 1985; Lewis et al. 1989). The anticyclones retain much of their structure during the very slow westward propagation and therefore have a major impact on processes in the Gulf of Mexico (Elliot, 1982).

2.2.3 Longevity

A number of these anticyclones can exist in the Gulf of Mexico at a given time (Lewis and Kirwan, 1985, 1987), and they may persist for months or even years before they dissipate (Lewis, 1990). These anticyclones eventually dissipate as they reach the shelf in the western Gulf of Mexico.

2.3 Cyclones

Associated with the Loop Current Rings are smaller but intense cyclones. Although ubiquitous, their role in the overall circulation dynamics of the Gulf of Mexico is not well understood, due to the very little attention they have received. Lewis and Kirwan (1987) found and documented persistent cyclones to the northwest of the Loop Current. Hamilton et al. (2002) showed that the Loop Current eddies play a role in the position of the cyclones on the northern slope of the Gulf of Mexico. And it is known that the Campeche Bank Cyclone and the Dry Tortugas Cyclonic Eddy often form on the southwest and southeast sides of the Loop Current during the process of a warm-core eddy pinch off from the Loop Current (Kantha et al. 2005). Kuznetsov et al. (2002), in an analysis during a 20-day period starting June 1, 1998, affirmed this fact during one shedding event. They found that a cyclone moved south and positioned itself between the Loop Current and the newly formed ring.

These cyclones are much smaller than anticyclones and have swirl velocities between 0.3 and 0.7 m/s, which is considerably less than that of the large anticyclonic eddies with swirl velocities of 1-2 m/s. Their thermal signatures have been found as deep as 1000 m, their sea-surface-height (SSH) signature is smaller (0.1-0.5 m) and their typical lifespan is only a few months (Lewis and Kirwan, 1985; 1987; Kuznetsov et al., 2002).

2.4 Eddy-Eddy Interaction

Interactions between cyclones and anticyclones locally affect water movement in the Gulf. Merrell and Morrison (1981) and Merrell and Vasquez (1983) found offshore transport between a cyclone and an anticyclone in the western Gulf to

be 30 Sverdrups, approximately the same volume that enters the Gulf through the Straits of Yucatan.

Toner et al. (2003) documented the formation of an advective channel due to the interaction between a cyclone, anticyclone, and the Loop Current. They studied the eastern Gulf region during the month of April 1998 after a pinching event of the Loop Current. At the 50-meter depth between counter rotating eddies, they located two dynamical structures known as hyperbolic trajectories. These structures, which simultaneously attract and repel particles, are referred to as A1 and A2 in Figure 2-3 below. Hyperbolic trajectories are discussed further in Chapter 6. They also calculated the material curves, which are the particles that leave (arrive at) the hyperbolic trajectory over time. These curves intersect at the hyperbolic trajectory and are aligned with the directions of maximum compression and stretch. They are referred to as inflowing and outflowing manifolds and are shown in red and blue in Figure 2-3. See Chapter 5 for more discussion of material curves.

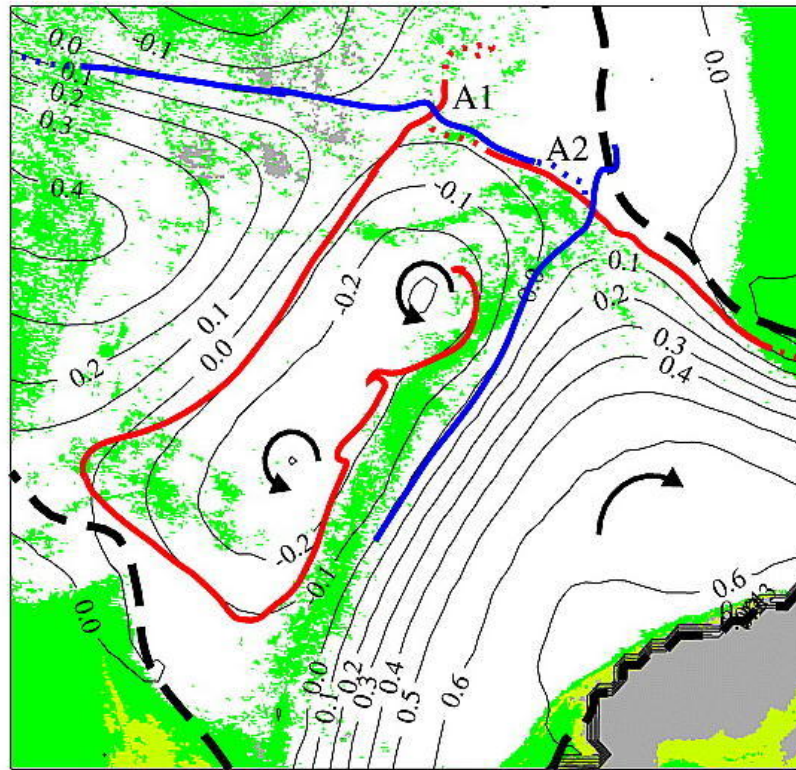


Figure 2-3: Advective channel in the Gulf of Mexico on April 17, 1998. The red (blue) curves are the unstable (stable) manifolds. The green is ocean color representing high concentrations of chlorophyll. A1 and A2 are the two hyperbolic trajectories found by Toner et al. (2003). The contours are sea-surface height anomaly and the dashed line is the 110-m isobar. (From Toner et al. 2003)

2.6 Circulation Models

Romanou and Chassignet (2004) and Kantha et al. (2005) have examined the circulation in the Gulf of Mexico using high-resolution models that accurately run both hindcasts and forecasts of Loop Current Eddy shedding and associated warm and cold eddy movement. Circulation models are discussed more in Chapter 3.

Chapter 3

MODEL

3.1 Numerical Models of the Gulf of Mexico

Numerical models are now a standard tool for process studies. With their ability to accurately reproduce velocity fields, they provide us with a wealth of data about the state of the ocean. Specifically, they are able to reproduce the Loop Current and eddies, which provides us with accurate phenomenology in the Gulf of Mexico.

Hurlburt and Thomson (1980) developed the first primitive equation numerical model of the Gulf of Mexico. They used a two-layer barotropic reduced gravity model. Sturges et al. (1993) later used a 12-level primitive equation model, followed by Deitrich and Lin (1994) who used a 16-level version of the Sandi Ocean Modeling System. Dietrich et al. (1997) increased the resolution to 1/12-degree, increased the vertical layers to 20, and extended the boundaries into the Caribbean. See Romanou (2004) for a detailed history of numerical models.

For the analysis here, the Colorado University Princeton Ocean Model (CUPOM) is used. This is a modified version of the original Princeton Ocean Model (POM) (Kantha et al., 1999; Lopez and Kantha, 2000). It is a data assimilating state-of-the-art primitive equation model. It has a horizontal resolution of 1/12° and a vertical resolution of 24 sigma layers. It uses realistic bottom topography for the Gulf of Mexico prescribed from ETOPO5 with no effort to correct the well-known inaccuracies in the shelf regions. TOPEX/Poseidon and ERS-2 provide the altimeter

data and near-real-time sea surface temperature is assimilated. Atmospheric forcing comes from the Navy Operational Global Atmospheric Prediction System (NOGAPS) wind data. Inflow through the Yucatan Channel is prescribed from climatological data (mean of 28 Sv) and outflow through the Florida Straits evolves with model physics. The model uses a Mellor and Yamada (1982) turbulence closure submodel. Modification (Kantha and Clayson, 1994) of the original mixed layer parameterization (Galperin et al., 1988) has improved depiction of near-surface currents, sea-surface-temperature (SST), and upper layer heat content.

Since it is a data-assimilating model, it is especially useful when comparing the chlorophyll plume shown by SeaWiFS in Figure 1-2 to the advective channel shown in Figure 1-3. Therefore, this data-assimilating model will continue to be used for this research and will allow us similar comparisons.

3.2 Model Validation

In order to use the CUPOM for this study, it is important to have some level of validation. Specifically, the model must be able to accurately reproduce velocity fields, particle paths, and eddies in order for it to be considered useful for research. Toner et al. (2001) compared the model velocities to drifter velocities. They found, using a filtered time-series for both of the velocity components, that the correlation between the model velocities and the drifter data is very high; between 0.77 and 0.94. This means that the model accurately reproduced both the shape and the magnitudes of the velocities at these frequencies. Toner et al. (2001) also used an Eulerian error metric to compare the velocity field of the model and velocities of the drifters, reproduced using both an unconstrained geometrical orthogonal function (UGOF) and a constrained geometrical orthogonal function (CGOF). The CGOF

exactly reproduced the drifter velocity at the drifter location. The Eulerian error metric for CGOF maintained a low error with a mean of 4.53 percent for the CGOF with percent error defined as $\left| \frac{\text{observed velocity} - \text{model velocity}}{\text{observed velocity}} \right| * 100$.

Toner et al. (2001) also used a Lagrangian error metric to compare the particle trajectories of the model and drifters. He analyzed both the position of the particles and the shape of the trajectory. He found that both the position and the shape of the model trajectories agreed fairly well with the drifters, though as expected, there is some divergence.

Toner et al (2003) used a Lagrangian analysis of the transport of chlorophyll plumes from satellite-derived ocean color compared to model particle trajectories and found that the two were in agreement, further validating the similarities between model and actual trajectory data at 50 meters.

Kantha et al. (2005) showed that the model shedding of Loop Current Rings was consistent with observations. They compared model results with the Eddy Joint Industry Project (EJIP) database of Loop Current Rings from 1966 to 1991. They found consistency between the model and observations for both the timing of the shedding and the tracks of the shed eddies. The frequency of shedding was also consistent with the observations of Sturges and Leben (2000), as was the size of the shed rings. They also noted that, even though translational speeds of the rings are variable, modeled rings speeds were consistent with observations.

Finally, Toner et al. (2003) used CUPOM to calculate hyperbolic trajectories and their corresponding material curves. They examined ocean color data and found that chlorophyll plumes aligned well with the outflowing material associated with the hyperbolic trajectories at 50 meters.

These studies have shown that CUPOM is capable of accurately reproducing the velocity fields, particle trajectories, eddies, and the shedding of the Loop Current in the upper levels of the model. Validation of the deep Gulf is impossible due to the lack of observational data.

Chapter 4

HYPERBOLIC TRAJECTORIES

There are two equivalent descriptions of oceanic conditions. The Eulerian approach reports oceanographic conditions at fixed geographic positions as a function of time. In contrast, the Lagrangian approach reports oceanographic conditions at particles as a function of time. Although the Eulerian and Lagrangian descriptions are mathematically equivalent, each is best suited for different types of studies. Most models and observations follow the Eulerian approach. However, as the focus of this study is advective transport, the Lagrangian description is more appropriate and will be used for most of this analysis.

As noted by Haller (2000) and others, hyperbolic trajectories are very important for characterizing mixing and transport. A hyperbolic trajectory acts as a simultaneous attractor and repeller for nearby fluid particles. Particles lying on or near the negative eigendirections of the velocity gradient are attracted towards the hyperbolic trajectory while those lying along or near the positive eigendirection are repelled. The continuous stream of particles directly repelled from the hyperbolic trajectory creates the material curve known as the outflowing manifold and the particles attracted directly to the hyperbolic trajectory create the inflowing manifold. Both the inflowing manifolds and outflowing manifolds create impermeable boundaries for advection. The theory of material curves is reviewed in Appendix A.

Haller (2000) provided some results that can be used to identify hyperbolic trajectories and their manifolds in any finite-time numerically or

experimentally generated velocity field. He was able to isolate the hyperbolic trajectory for velocity fields where the time scale for the deformation rates was slow compared to the time scale for the individual particles.

4.1 Geopotential Height

In the study of material curves and hyperbolic trajectories in the Gulf of Mexico, we use the geopotential height. Of special importance in oceanography, a geopotential surface is the level surface on which the potential energy of a mass remains constant (Neumann and Pierson, 1966). The geopotential, then, is the work done in raising a mass a mass of water through a vertical distance against the force of gravity (Pond and Pickard, 1983). Its unit is energy per unit mass (J/kg or m^2/s^2). In many oceanic applications, particles tend to flow along the lines of constant geopotential. Therefore it is widely used to show current patterns. Figure 4-1 shows an example of the geopotential height field anomaly for our study area in the Gulf of Mexico. The red denotes the large anticyclonic Loop Current Eddy and the Loop Current itself. The dark blue area to the north-east of the Loop Current is the cyclone. The white dot is missing geopotential data in that grid.

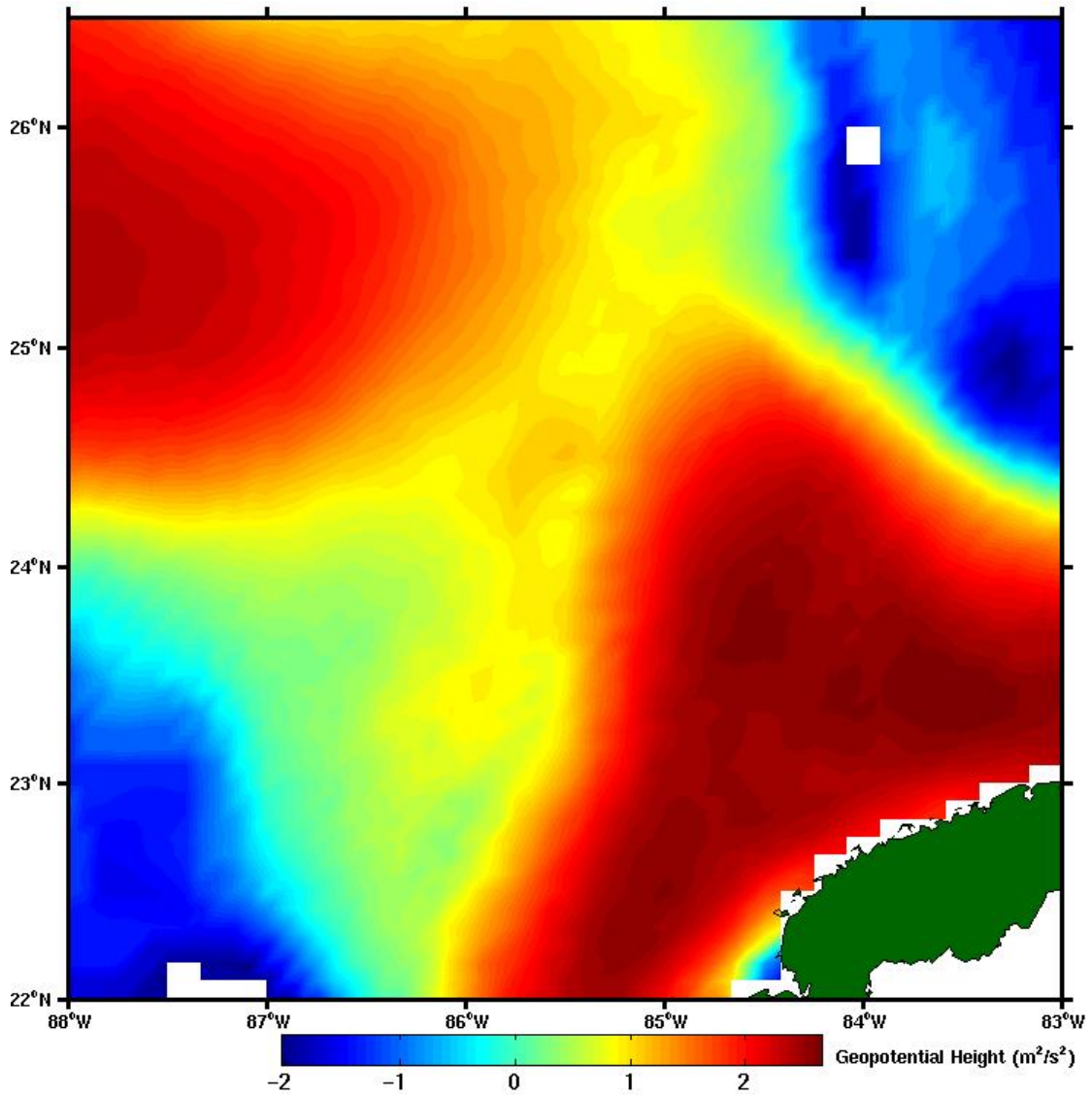


Figure 4-1: Geopotential height anomaly of our study area in the Gulf of Mexico at 10 m on April 6, 1998.

4.2 Simple Dynamical Model

The hyperbolic trajectory and associated manifolds can be illustrated with the use of a simple dynamical model. For a geostrophic flow, the equations of motion

reduce to a balance of the Coriolis acceleration and the gradients of the geopotential Ψ specified as a function of time and space.

The relevant equations are

$$fv = \frac{\partial \Psi}{\partial x} \quad (1)$$

$$fu = -\frac{\partial \Psi}{\partial y}. \quad (2)$$

As this is a local analysis, a Taylor expansion around (x_0, y_0) for the geopotential is used. Therefore, when all terms up to second order are used, we have

$$\begin{aligned} \Psi(x, y, t) = & \Psi_0(x_0, y_0, t) + \frac{\partial \Psi}{\partial x} \Big|_{x_0, y_0} (x - x_0) + \frac{\partial \Psi}{\partial y} \Big|_{x_0, y_0} (y - y_0) \\ & + \frac{1}{2} \frac{\partial^2 \Psi}{\partial x^2} \Big|_{x_0, y_0} (x - x_0)^2 + \frac{1}{2} \frac{\partial^2 \Psi}{\partial y^2} \Big|_{x_0, y_0} (y - y_0)^2 + \frac{\partial^2 \Psi}{\partial x \partial y} \Big|_{x_0, y_0} (x - x_0)(y - y_0). \end{aligned} \quad (3)$$

For later convenience, (3) is rewritten as

$$\Psi = \left(\frac{B}{2} + B_N \right) x^2 + \left(\frac{B}{2} - B_N \right) y^2 + 2B_S xy + g(t)x + h(t)y + \Psi_0(x_0, y_0) \quad (4)$$

where

$$\begin{aligned} (g, h) = & \left(\frac{\partial \Psi}{\partial x} \Big|_{x_0, y_0}, \frac{\partial \Psi}{\partial y} \Big|_{x_0, y_0} \right) \\ B = & \left(\frac{\partial^2 \Psi}{\partial x^2} + \frac{\partial^2 \Psi}{\partial y^2} \right) \Big|_{x_0, y_0} \\ B_N = & \left(\frac{1}{2} \right) \left(\frac{\partial^2 \Psi}{\partial x^2} - \frac{\partial^2 \Psi}{\partial y^2} \right) \Big|_{x_0, y_0} \\ B_S = & \left(\frac{1}{2} \right) \left(\frac{\partial^2 \Psi}{\partial x \partial y} \right) \Big|_{x_0, y_0} \end{aligned} \quad (5)$$

Observations in oceanic hyperbolic regions suggest that the Hessian of the geopotential must vary on a slow time scale relative to a fast time scale of typical particle velocities. The Hessian is composed of the four components (three independent) of the second order partial derivative. For present purposes, it is sufficient to take the Hessian as time independent while prescribing the first order terms as functions of time. The geopotential gradients are then given by

$$\frac{\partial \Psi}{\partial x} = (B + 2B_N)x + 2B_S y + g(t) \quad (6)$$

$$\frac{\partial \Psi}{\partial y} = 2B_S x + (B - 2B_N)y + h(t). \quad (7)$$

The equations of motions, (1) and (2) then become

$$fv = (B + 2B_N)x + 2B_S y + g(t) \quad (8)$$

$$fu = -2B_S x - (B - 2B_N)y - h(t). \quad (9)$$

To study the hyperbolic trajectory, we take the Laplace transform of (8) and (9) which gives the frequency relation

$$p^2 - H^2 = 0 \quad (10)$$

where p is the transform variable and

$$H^2 = (B + 2B_N)(B - 2B_N) - 4B_S^2. \quad (11)$$

Using $g(t) = E \cos(\omega t)$ and $h(t) = F \cos(\omega t)$, the trajectories of individual particles can be expressed as

$$\begin{aligned}
x = & \left(\frac{(X - X_s)}{2} + \frac{(U - U_s)}{2\frac{H}{f}} \right) e^{\frac{H}{f}t} + \left(\frac{(X - X_s)}{2} - \frac{(U - U_s)}{2\frac{H}{f}} \right) e^{-\frac{H}{f}t} \\
& + X_s \cos(\omega t) + \left(\frac{U_s}{\omega} \right) \sin(\omega t)
\end{aligned} \tag{12}$$

$$\begin{aligned}
y = & \left(\frac{(Y - Y_s)}{2} + \frac{(V - V_s)}{2\frac{H}{f}} \right) e^{\frac{H}{f}t} + \left(\frac{(Y - Y_s)}{2} - \frac{(V - V_s)}{2\frac{H}{f}} \right) e^{-\frac{H}{f}t} \\
& + Y_s \cos(\omega t) + \left(\frac{V_s}{\omega} \right) \sin(\omega t)
\end{aligned} \tag{13}$$

with the following equations for the trajectory (x_s, y_s) , initial position (X_s, Y_s) and velocity (U_s, V_s) of the hyperbolic trajectory as well as the initial velocity (U, V) of other particles within the flow field.

$$\begin{aligned}
x_s = & X_s \cos(\omega t) + \left(\frac{U_s}{\omega} \right) \sin(\omega t) \\
y_s = & Y_s \cos(\omega t) + \left(\frac{V_s}{\omega} \right) \sin(\omega t)
\end{aligned} \tag{14}$$

$$\begin{aligned}
X_s = & \frac{(B - B_N)E + \omega f F}{f^2 \left(\omega^2 + \frac{H^2}{f^2} \right)} \\
Y_s = & \frac{-2B_s E}{f^2 \left(\omega^2 + \frac{H^2}{f^2} \right)}
\end{aligned} \tag{15}$$

$$\begin{aligned}
U_s &= \frac{-2\omega B_s F}{f^2 \left(\omega^2 + \frac{H^2}{f^2} \right)} \\
V_s &= \frac{\omega (\omega f E + (B + 2B_N) F)}{f^2 \left(\omega^2 + \frac{H^2}{f^2} \right)}
\end{aligned} \tag{16}$$

$$\begin{aligned}
U &= -2 \frac{B_s}{f} X + \left(\frac{2B_N - B}{f} \right) Y + E \\
V &= \left(2 \frac{B_N + B}{f} \right) X + 2 \frac{B_s}{f} Y
\end{aligned} \tag{17}$$

From equations (10), (11) and (14), we note that a particle initialized on the hyperbolic trajectory will remain on the hyperbolic trajectory for all time.

4.3 Kinematic Model

The geostrophic model can be related to the gradient of the velocity field of Okubo's (1970) kinematic model. The kinematic model is useful since values for N , the normal deformation, S , the shear deformation, and C the vorticity, can be estimated near the hyperbolic trajectories. Typical values are given in section 4.6.

Recall this model as

$$u = \frac{\partial x}{\partial t} = \frac{\partial u}{\partial x} x + \frac{\partial u}{\partial y} y + g(t) = Nx + \left(S - \frac{C}{2} \right) y + g(t) \tag{18}$$

$$v = \frac{\partial y}{\partial t} = \frac{\partial v}{\partial x} x + \frac{\partial v}{\partial y} y + h(t) = \left(S + \frac{C}{2} \right) x - Ny + h(t) \tag{19}$$

where C , N , and S are the vorticity, normal deformation and shear deformation and the velocity gradients are constant, defined by

$$\begin{aligned}
\frac{\partial u}{\partial x} &= N \\
\frac{\partial u}{\partial y} &= S - \frac{C}{2} \\
\frac{\partial v}{\partial x} &= S + \frac{C}{2} \\
\frac{\partial v}{\partial y} &= -N
\end{aligned}
\tag{20}$$

with

$$\frac{\partial u}{\partial x} + \frac{\partial v}{\partial y} = 0.
\tag{21}$$

Inspection of the equations of motion for both models shows that (18) and (19) are equivalent to (6) and (7) with

$$\begin{aligned}
S &= 2 \frac{B_N}{f} \\
N &= -2 \frac{B_S}{f} \\
\frac{C}{2} &= \frac{B}{f} \\
\gamma^2 &= N^2 + S^2 - \frac{C^2}{4} = \frac{H^2}{f^2}.
\end{aligned}
\tag{22}$$

This equivalence will be used to connect the kinematic model to the geostrophic dynamics.

4.4 Inflowing and Outflowing Manifolds

Inflowing and outflowing manifolds are important since their intersection defines the location of the hyperbolic trajectory. Using (10) and (11), the manifolds can be seen as the values of (X, Y) that make the appropriate exponential terms zero. So the inflowing manifolds are the (X, Y) values that make

$$\begin{aligned} \left(\frac{(X - X_s)}{2} + \frac{(U - U_s)}{2\gamma} \right) &= 0 \\ \left(\frac{(Y - Y_s)}{2} + \frac{(V - V_s)}{2\gamma} \right) &= 0 \end{aligned} \quad (23)$$

and the outflowing flowing manifolds are the values of (X, Y) that make

$$\begin{aligned} \left(\frac{(X - X_s)}{2} - \frac{(U - U_s)}{2\gamma} \right) &= 0 \\ \left((Y - Y_s) - \frac{(V - V_s)}{2\gamma} \right) &= 0 \end{aligned} \quad (24)$$

Solving (23) simultaneously and substituting

$$\begin{aligned} U &= NX + \left(S - \frac{C}{2} \right) Y + E \\ V &= \left(S + \frac{C}{2} \right) X - NY \end{aligned} \quad (25)$$

we get two equations, X inflowing and Y inflowing (X_I and Y_I). These two equations imply that X_I and Y_I are linearly related. Therefore, we can write the manifold equations as

$$Y_I = \gamma_I X_I + \beta_I \quad (26)$$

where γ_I is the slope and β_I is the intercept of the inflowing manifold. We then have a family of lines all with the same slope

$$\gamma_I = - \frac{\left(\frac{1 + \frac{N}{\gamma}}{S - \frac{C}{2}} \right)}{\left(\frac{\gamma}{1 - \frac{N}{\gamma}} \right)} = - \frac{\left(\frac{S + \frac{C}{2}}{\gamma} \right)}{\left(\frac{\gamma}{1 - \frac{N}{\gamma}} \right)}. \quad (27)$$

It can be shown, then, if we chose

$$\beta_I = \frac{R_1}{\left(\frac{S - \frac{C}{2}}{\gamma} \right)} = \frac{R_2}{1 - \frac{N}{\gamma}} \quad (28)$$

where

$$\begin{aligned} R_1 &= X_S + \frac{U_S - A}{\gamma} \\ R_2 &= Y_S + \frac{V_S}{\gamma} \end{aligned} \quad (29)$$

that the family of lines collapses to a single straight line. A similar process is followed for the outflowing manifold using the condition (24). Therefore, we have the initial manifolds as

$$\begin{aligned} Y_I &= \gamma_I X_I + \beta_I \\ Y_O &= \gamma_O X_O + \beta_O \end{aligned} \quad (31)$$

The manifolds are in terms of X_S , Y_S , U_S , and V_S . If we plot these two lines Y_I and Y_O simultaneously, then the intersection is at the hyperbolic trajectory.

Toner et al. (2003) used inflowing and outflowing manifolds to locate hyperbolic trajectories in the ocean. Examples of inflowing and outflowing manifolds are shown in Figure 4-2.

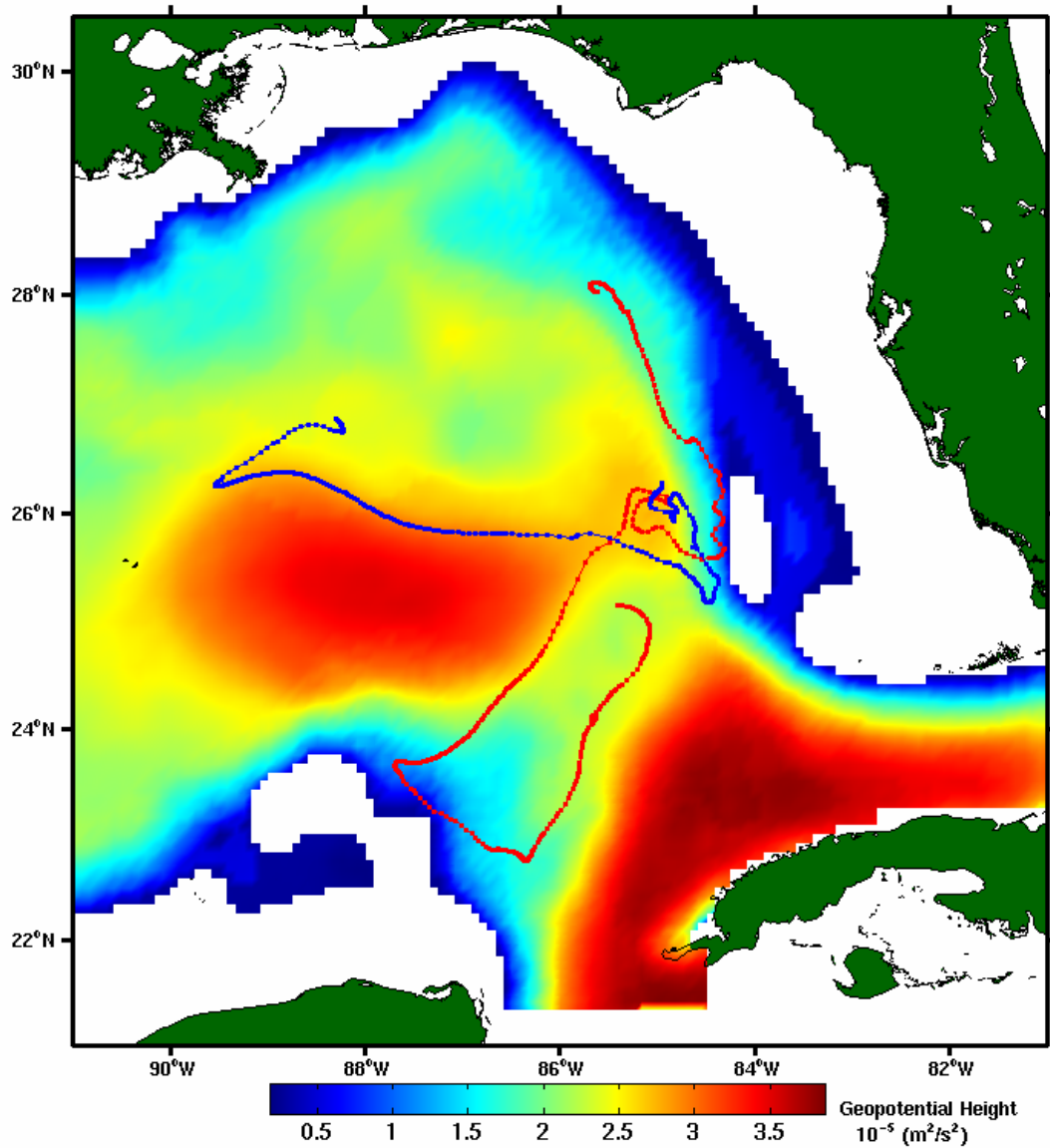


Figure 4-2: Examples of inflowing and outflowing manifolds. The lines depict the inflowing (blue) and outflowing (red) manifolds at 50 m on April 17, 1998. The inflowing manifold was initialized on April 26, 1998 and the outflowing manifold was initialized on April 6, 1998. The filled contours are geopotential height in m^2/s^2 .

For my research, I will use the inflowing and outflowing manifolds at depths where they are present to determine the shape of both the inflowing and outflowing material surfaces and locate the hyperbolic trajectory in each level.

Determining manifolds from data is tedious and calculation intensive. The two manifolds in Figure 4-2 were created using daily velocities from CUPOM. The outflowing (inflowing) manifolds were found by initializing particles in the vicinity of the hyperbolic region and running time forwards (backwards). In order to retain the detailed shape of the material curve, particles were reseeded whenever separation between two neighboring particles reached 5 km.

4.5 Stagnation Point

Another structure found within flow fields is the stagnation point. This is the point where the velocity is always zero. From (16) and (17), the equation of the stagnation point is given by

$$\begin{aligned}
 x_{SP} &= -E\left(\frac{N}{\gamma^2}\right)\cos \omega t - F\left(\frac{S - \frac{C}{2}}{\gamma^2}\right)\sin \omega t \\
 y_{SP} &= F\left(\frac{N}{\gamma^2}\right)\sin \omega t - E\left(\frac{S + \frac{C}{2}}{\gamma^2}\right)\cos \omega t
 \end{aligned} \tag{32}$$

The equations of the hyperbolic trajectory (14) and the stagnation point (32) are clearly different. This means that a particle initialized at the stagnation point will diverge from the path of the stagnation point while a particle initialized at the hyperbolic trajectory will remain on the hyperbolic trajectory at all times.

4.6 Hyperbolic Trajectory Characteristics

The following figures illustrate some of the characteristics of hyperbolic trajectories. They are created in the context of the kinematic model due to the fact that we can find or estimate typical values for N , the normal deformation, S , the shear deformation, and C the vorticity. Here, I take

$$\begin{aligned}C &= 0.4 \bullet 10^{-4} \text{ s}^{-1} \\N &= 0.6 \bullet 10^{-4} \text{ s}^{-1} \\S &= 0.6 \bullet 10^{-4} \text{ s}^{-1}.\end{aligned}\tag{33}$$

Clearly these values satisfy the hyperbolic condition that $N^2 + S^2 - \frac{C^2}{4} > 0$. We also choose $E = 0.1$ and $F = 0.15$ so that we have an approximate velocity of .1 m/s, which is a typical velocity in an oceanic flow field. Finally, we chose $\omega = .5f = .5 \bullet 10^{-4}$.

Plugging in all of these values leads to length scales in x and y on the order of kilometers, which are typical length scales of the trajectories.

Figure 4-3 is an illustration of the stretching and compression of initialized particles. It shows the attracting and repelling behavior of four circles of particles initialized on the inflowing and outflowing manifolds and around the hyperbolic trajectory. The circles are stretched along the outflowing manifold and compressed along the inflowing manifold.

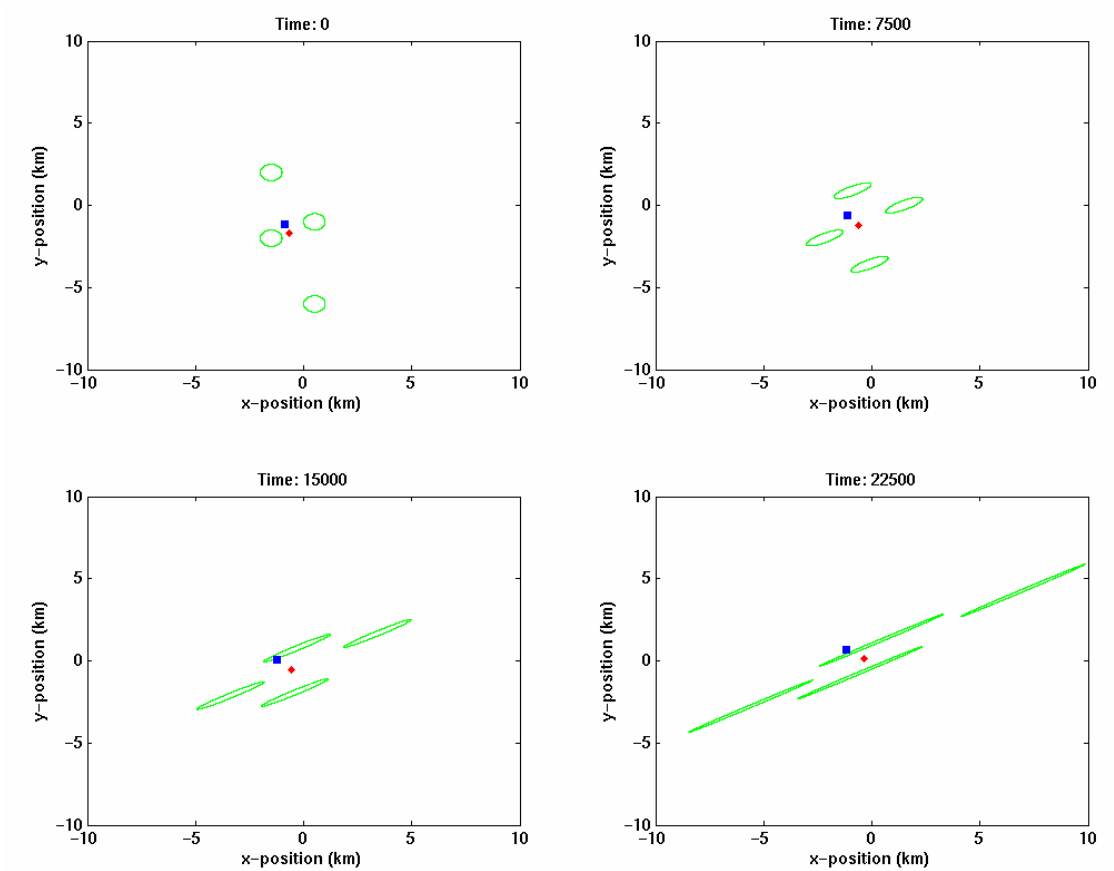


Figure 4-3: The stretching and compression of a blob of particles around the hyperbolic trajectory. The green circles are initialized particles. The blue square is the location of the stagnation point and the pink diamond in the location of the hyperbolic trajectory.

Figure 4-4 illustrates the trajectories of both the hyperbolic trajectory and the stagnation point. The same parameter values as above for N , S , and C are used. The major axis of the hyperbolic trajectory is on the order of 2 kilometers while the major axis of the stagnation point is on the order of 5 kilometers.

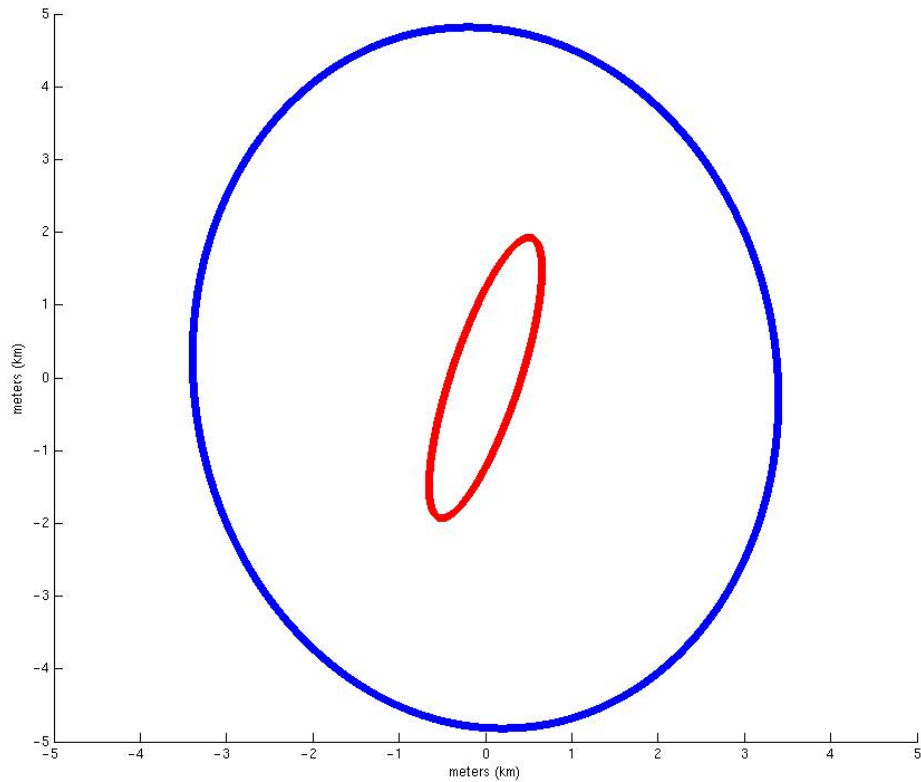


Figure 4-4: Paths of the hyperbolic trajectory (red) and stagnation point (blue) in a velocity field with background flow.

This is a case where the Eulerian stagnation point implies a Lagrangian hyperbolic trajectory, as found by Haller and Poje (1998). However, Coulliette and Wiggins (2000) found examples in a numerical model where the stagnation point and the hyperbolic trajectory are unrelated.

Chapter 5

RESULTS

5.1 Introduction

As with many numerical models, CUPOM is formulated as a sigma layer model. Sigma coordinates are attractive since they follow the bottom topography and thus are a natural way to characterize vertical motion. However, for technical reasons, it is necessary to use z-levels in this study. The 24 sigma levels of CUPOM were interpolated to 28 z-levels using a cubic spline. The 28 z-levels for this analysis are shown in Table 5-1.

Table 5-1: Levels used.

| Level | Depth (m) | Level | Depth (m) |
|-------|-----------|-------|-----------|
| 1 | 0 | 15 | 600 |
| 2 | 10 | 16 | 700 |
| 3 | 20 | 17 | 800 |
| 4 | 30 | 18 | 900 |
| 5 | 50 | 19 | 1000 |
| 6 | 75 | 20 | 1100 |
| 7 | 100 | 21 | 1200 |
| 8 | 125 | 22 | 1300 |
| 9 | 150 | 23 | 1400 |
| 10 | 200 | 24 | 1500 |
| 11 | 250 | 25 | 1750 |
| 12 | 300 | 26 | 2000 |
| 13 | 400 | 27 | 2500 |
| 14 | 500 | 28 | 3000 |

As discussed in Chapter 4, manifolds are critical in the study of hyperbolic trajectories. The intersection of inflowing and outflowing manifolds defines the position of the hyperbolic trajectory. Using CUPOM, inflowing and outflowing manifolds were constructed in every level available, giving a three-dimensional structure.

Other than Mezic and Wiggins (1994) there is little theoretical work on the three-dimensional structure of hyperbolic regions that is applicable to geophysical fluid dynamics.

For this research, the two hyperbolic structures shown in Figure 1-3 will be studied in more detail. These will be referred to as hyperbolic structures A1 and A2. The rest of the chapter is organized as follows. In 5.2, hyperbolic structure A1 is examined. Paths of hyperbolic trajectories for each level are determined and the differences and similarities of the paths are examined. The distance moved per day

for the hyperbolic trajectory in each level is also completed. Along with the variability of the speed and direction, the chaotic nature of hyperbolic trajectories is examined. This is demonstrated by initializing particles close to the hyperbolic trajectory at any level. They quickly diverge from the path of the hyperbolic trajectory. After that, the baroclinicity of the hyperbolic structure is examined. Finally, the three-dimensional structure of A1 throughout its life cycle is studied. In 5.3, a similar analysis for hyperbolic structure A2 is presented. In 5.4, the advective channel, which is created by the outflowing manifold of A1 and the inflowing manifold of A2, is examined. The depth to which the channel is present is found and the time dependent three-dimensional structure of this channel is examined. An estimate of the volume transport from the advective channel is also given.

Results from the surface are inconsistent with the other levels. Since the model is strongly affected by air-sea exchange, this is not unexpected as effects of these processes are confined to the first few meters. Therefore the data from the first level is not considered in the analysis.

5.2 Hyperbolic Structure A1

Hyperbolic structure A1 was studied from April 6 to April 26, 1998. These dates are consistent with the work of Toner et al. (2003). Further analysis of this hyperbolic structure has shown that it is present for two days before and two days after this time period (April 4 to April 28). To maintain consistency, the analysis is restricted to the time periods reported by Toner et al. (2003).

5.2.1 Hyperbolic Trajectory Paths

Hyperbolic trajectories at each depth for hyperbolic structure A1 were found by initializing inflowing and outflowing manifolds and calculating their intersection. Figures 5-1 through 5-3 show the position of the hyperbolic trajectory in different depths over those 21 days. The figures are broken down such that Figure 5-1 shows the upper depths, Figure 5-2 shows the transitional middle depths, and Figure 5-3 shows the lower depths.

In the upper depths (Figure 5-1) all of the hyperbolic trajectories begin to the southeast and work their way in an arc to the northeast then down to the southwest. All the paths are similar in shape and the hyperbolic trajectory paths are very similar moving down through this portion of the water column.

In the transitional middle depths, the hyperbolic trajectory paths are less organized. The shallower mid-depths follow a pattern similar to the upper-depth hyperbolic trajectories. The 300-meter depth is overlapped to illustrate that the shapes of the trajectories are similar to the upper-depths. There is an abrupt change in the shape between 300 m and 400 m. The deeper mid-depths then follow a new pattern where the hyperbolic trajectories start in the northeast and work their way to the southwest.

In the lower depths (Figure 5-3), the hyperbolic trajectories move similar to the deep mid-depths. These deep hyperbolic trajectories follow similar patterns to each other and once again seem to be translated from north to south with depth.

The abrupt change in hyperbolic trajectory shape occurs between 300 and 400 m. Figure 5-4 shows the vertical profile of the temperature and salinity. It shows that the bottom of the thermocline and the halocline are located around 400 m, the exact location where the hyperbolic trajectories change shape. This poses the

question, is this one hyperbolic structure, uniform through the water column, or is it two structures, one upper and one lower?

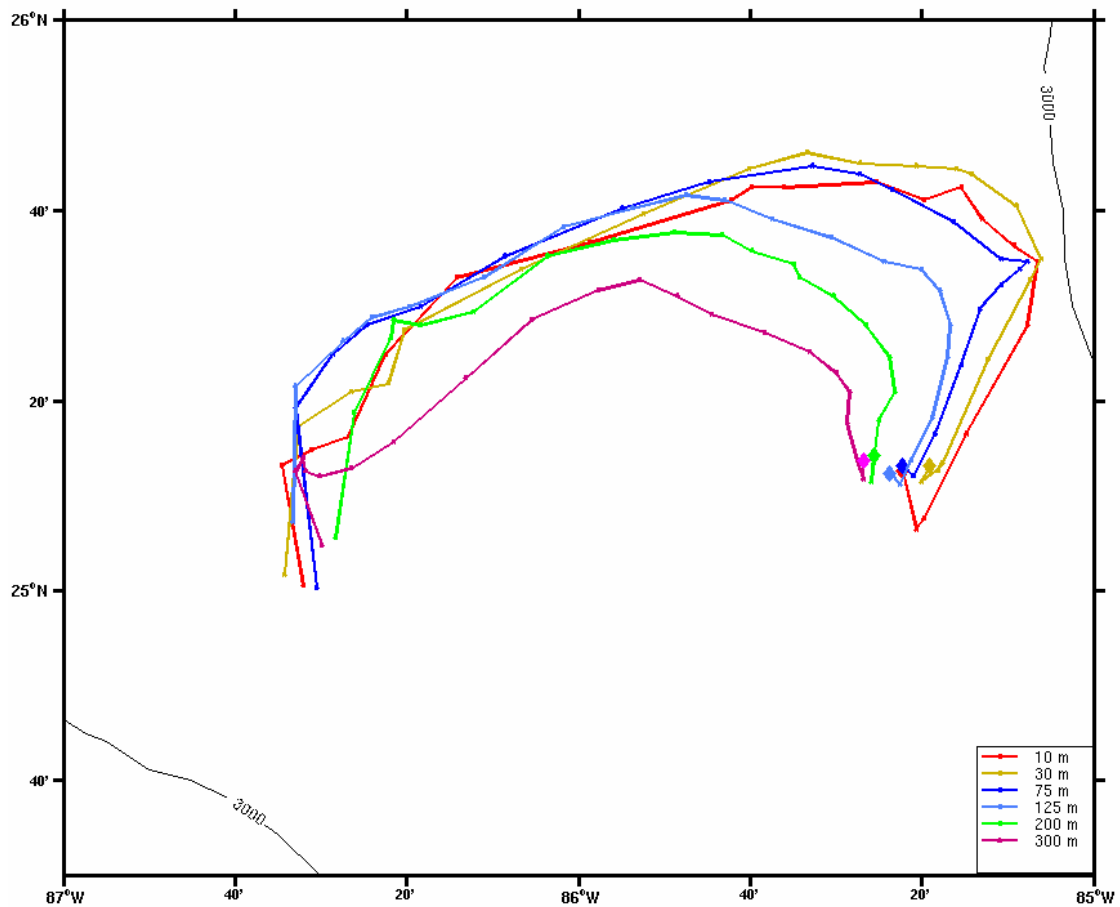


Figure 5-1: Paths of hyperbolic trajectories at six depths ranging from 10 to 300 m. The colors correspond to the depths as shown in the legend. The large diamonds denote the initial position of the hyperbolic trajectory on April 6. The 3000 m isobar is also shown.

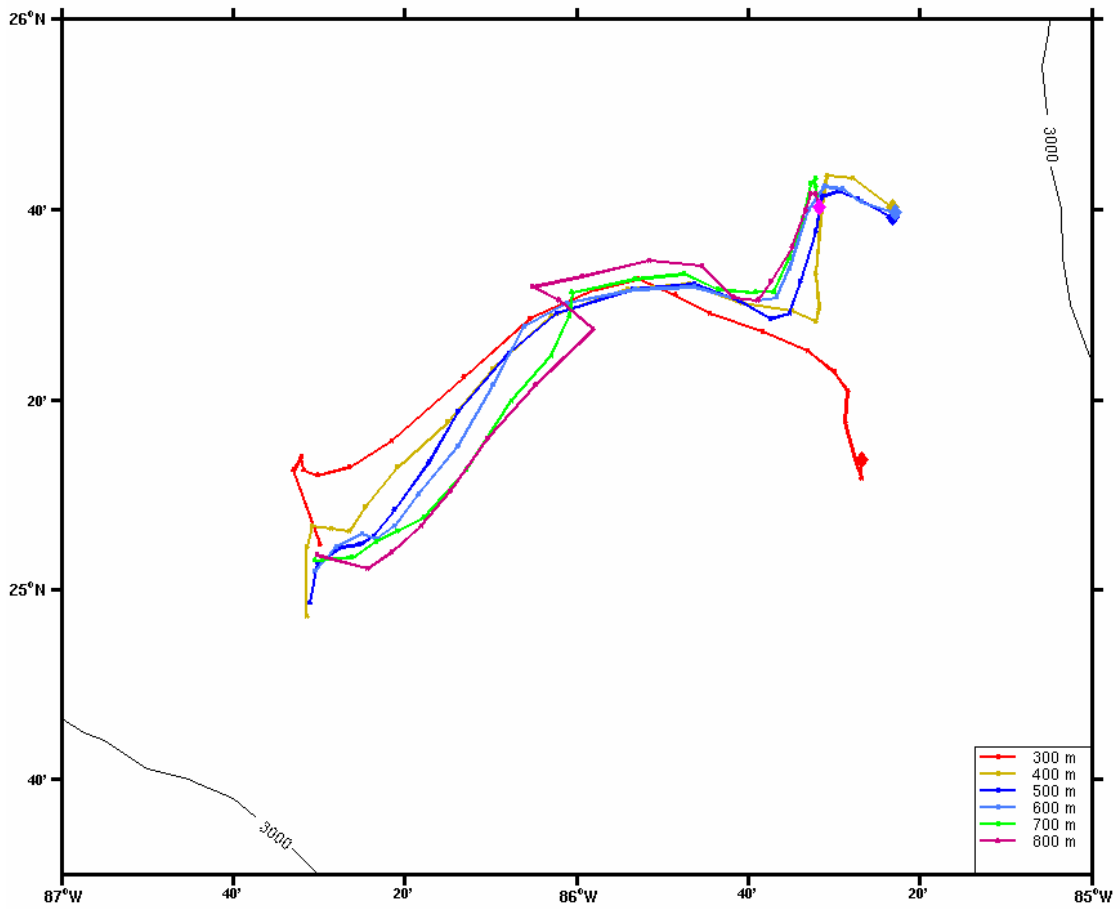


Figure 5-2: Paths of hyperbolic trajectories at six depths ranging from 300 to 800 m. The colors correspond to the depths as shown in the legend. The large diamonds denote the initial position of the hyperbolic trajectory on April 6. The 3000 m isobar is also shown.

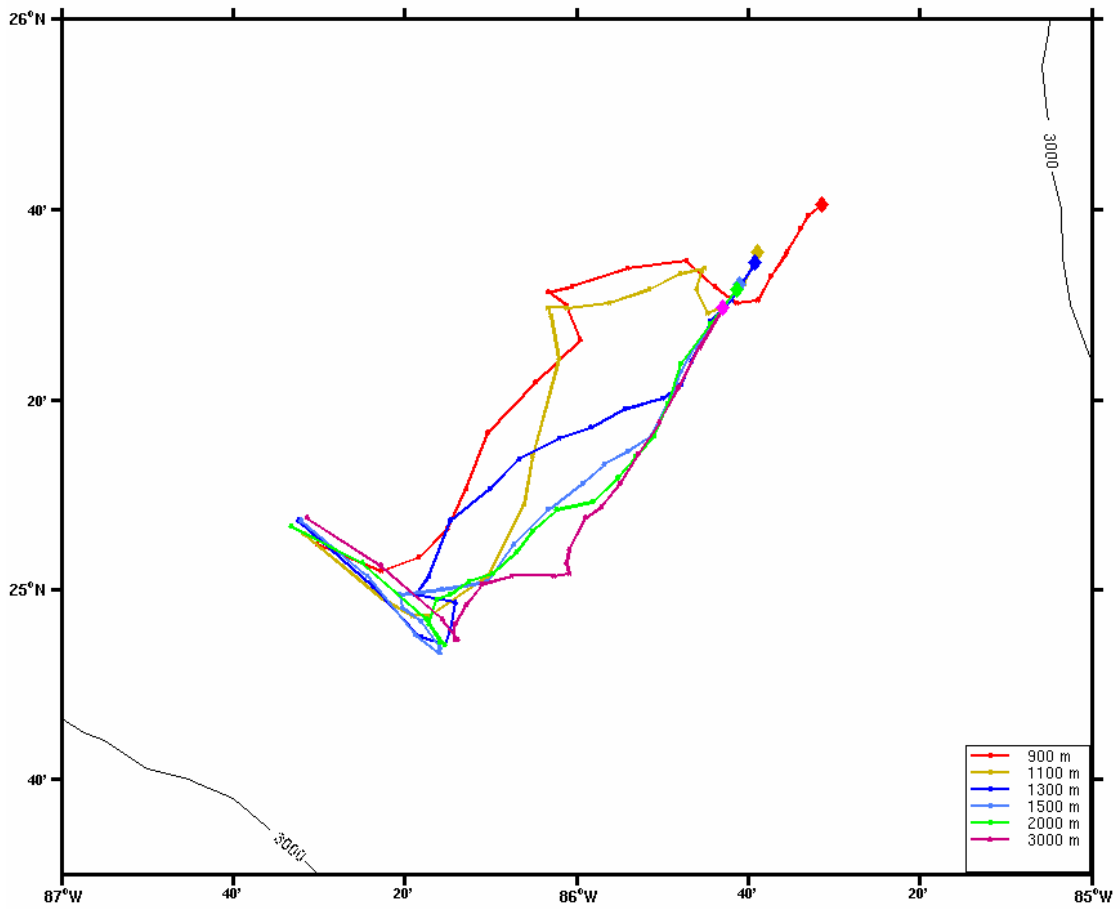


Figure 5-3: Paths of hyperbolic trajectories at six depths ranging from 900 to 3000 m. The colors correspond to the depths as shown in the legend. The large diamonds denote the initial position of the hyperbolic trajectory on April 6. The 3000 m isobar is also shown.

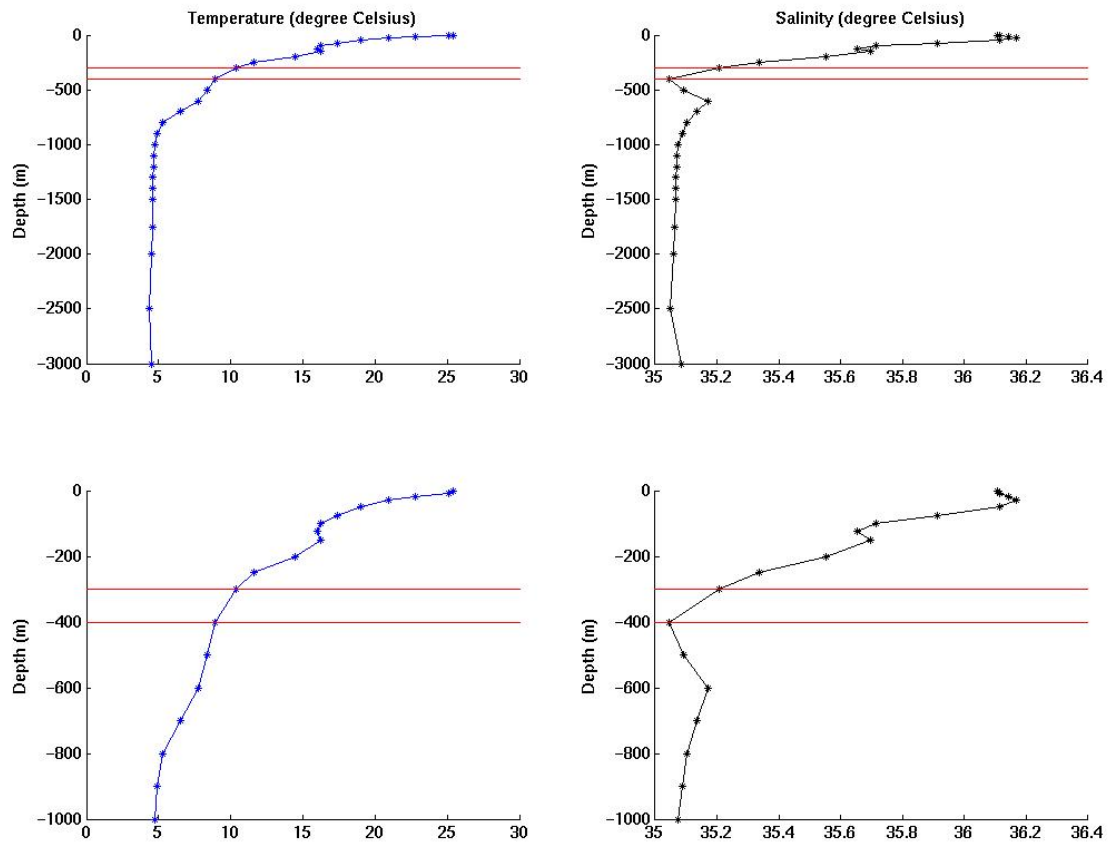


Figure 5-4: Vertical profiles of temperature and salinity at the location of the hyperbolic trajectory at 50 m on April 6. Top panels show full vertical structure while the bottom panels focus on the upper 1000 m. The transition layer is between 300 and 400 m, denoted by red lines.

5.2.2 Distance Moved Per Day

Figure 5-1, 5-2 and 5-3 show the path of the hyperbolic trajectories at each depth for A1. The hyperbolic trajectories move different distances every day. These distances illustrate two points about the variability associated with hyperbolic structure A1. First, it illustrates the day-to-day variability. There is a large spread in

the distance values within one depth. This demonstrates that hyperbolic trajectories do not move at a uniform speed. Second, it shows the depth-to-depth variability on a same day. There is a large variation between different depths in the distance values on a given day. The main points of this analysis were made using 6 depths. Appendix B has tables for the remaining 22 depths.

The day-to-day variability is examined first. Table 5-2 through Table 5-5 show the distances moved each day from April 6 to April 26. The rows with the minimum and maximum values are colored yellow. At 50 m (Table 5-2), there is a minimum of 4.17 km from April 6 to April 7 and a maximum of 27.47 km from April 25 to April 26. At 200 m (Table 5-3), we find a minimum distance of 2.77 km from April 15 to April 16 and a maximum of 24.53 from April 25 to April 26. At 300 m, (Table 5-4), there is a minimum of 2.63 km from April 23 to April 24 and a maximum of 18.68 km from April 19 to April 20. At 400 m (Table 5-5), there is a minimum of 2.63 km from April 11 to April 12 and a maximum of 15.87 km from April 16 to April 17. At 600 m (Table 5-6), there is a minimum of 2.80 from April 23 to April 24 and a maximum of 19.77 from April 19 to April 20. At 1100 m (Table 5-7), we have smaller minimums, as expected, since the water velocities decrease with depth but, surprisingly, we find no decrease in the maximum. The minimum at 1100 m is 0.73 from April 11 to April 12 and the maximum is 19.77 from April 19 to April 20. Overall, the minimum and maximum distance values differ by an average of 18.4 km, a surprisingly large spread.

Table 5-8 shows the distances traveled per day for several depths for the hyperbolic trajectories associated with A1. Three one-day intervals are shown. These days illustrate the large range of values associated with different depths on these given

days. April 12 had a minimum of 0.73 km traveled at 1100 m up to a maximum of 10.79 km at 50 m. April 25 had a minimum of 3.01 km traveled at 300 m up to a maximum of 16.15 km at 200 m. April 26 had a minimum of 6.24 km at 600 m up to a maximum of 27.47 km at 50 m. This illustrates that there is comparable variability between the day-to-day and the depth-to-depth variability.

Table 5-2: Table of distance traveled per day in kilometers for hyperbolic trajectory at 50 m for hyperbolic structure A1. The days with the minimum and maximum distance values are highlighted in yellow.

| Date | Longitude (°W) | Latitude (°N) | East (km) | North (km) | Dist (km) |
|-------------|-----------------------|----------------------|----------------------------------|-------------------|------------------|
| 4/6/98 | -85.35 | 25.22 | | | |
| 4/7/98 | -85.33 | 25.19 | 2.08 | -3.61 | 4.17 |
| 4/8/98 | -85.30 | 25.27 | 3.11 | 8.77 | 9.31 |
| 4/9/98 | -85.26 | 25.33 | 4.15 | 6.70 | 7.88 |
| 4/10/98 | -85.21 | 25.47 | 5.18 | 15.97 | 16.79 |
| 4/11/98 | -85.12 | 25.55 | 8.80 | 8.75 | 12.41 |
| 4/12/98 | -85.05 | 25.62 | 7.76 | 7.20 | 10.59 |
| 4/13/98 | -85.09 | 25.66 | -4.65 | 5.14 | 6.94 |
| 4/14/98 | -85.21 | 25.70 | -11.37 | 4.11 | 12.09 |
| 4/15/98 | -85.28 | 25.72 | -7.24 | 2.57 | 7.68 |
| 4/16/98 | -85.35 | 25.74 | -7.23 | 1.54 | 7.40 |
| 4/17/98 | -85.45 | 25.76 | -9.82 | 2.57 | 10.15 |
| 4/18/98 | -85.54 | 25.80 | -8.78 | 4.11 | 9.70 |
| 4/19/98 | -85.68 | 25.74 | -14.46 | -6.68 | 15.93 |
| 4/20/98 | -85.87 | 25.69 | -19.63 | -5.14 | 20.30 |
| 4/21/98 | -86.09 | 25.60 | -21.19 | -10.29 | 23.56 |
| 4/22/98 | -86.30 | 25.50 | -21.21 | -10.29 | 23.57 |
| 4/23/98 | -86.42 | 25.44 | -11.91 | -6.69 | 13.66 |
| 4/24/98 | -86.47 | 25.41 | -5.70 | -3.61 | 6.74 |
| 4/25/98 | -86.55 | 25.34 | -7.77 | -8.25 | 11.33 |
| 4/26/98 | -86.58 | 25.09 | -2.59 | -27.35 | 27.47 |
| | | | | | |
| | | | Average Velocity (km/day) | | 12.88 |

Table 5-3: Table of distance traveled per day in kilometers for hyperbolic trajectory at 200 m for hyperbolic structure A1. The days with the minimum and maximum distance values are highlighted in yellow.

| Date | Longitude (°W) | Latitude (°N) | East (km) | North (km) | Dist (km) |
|-------------|-----------------------|----------------------|----------------------------------|-------------------|------------------|
| 4/6/98 | -85.43 | 25.24 | | | |
| 4/7/98 | -85.43 | 25.19 | -0.52 | -5.16 | 5.19 |
| 4/8/98 | -85.43 | 25.23 | 0.52 | 3.61 | 3.65 |
| 4/9/98 | -85.42 | 25.30 | 1.04 | 8.25 | 8.32 |
| 4/10/98 | -85.39 | 25.35 | 3.11 | 5.67 | 6.47 |
| 4/11/98 | -85.40 | 25.41 | -1.04 | 6.70 | 6.78 |
| 4/12/98 | -85.44 | 25.47 | -4.66 | 6.18 | 7.74 |
| 4/13/98 | -85.50 | 25.52 | -6.21 | 5.66 | 8.41 |
| 4/14/98 | -85.57 | 25.55 | -6.73 | 3.60 | 7.63 |
| 4/15/98 | -85.58 | 25.57 | -1.03 | 2.57 | 2.77 |
| 4/16/98 | -85.66 | 25.60 | -8.28 | 2.57 | 8.67 |
| 4/17/98 | -85.72 | 25.63 | -5.69 | 3.09 | 6.47 |
| 4/18/98 | -85.81 | 25.63 | -9.31 | 0.51 | 9.32 |
| 4/19/98 | -85.93 | 25.62 | -11.89 | -1.54 | 11.99 |
| 4/20/98 | -86.06 | 25.59 | -12.93 | -3.09 | 13.29 |
| 4/21/98 | -86.20 | 25.49 | -14.49 | -10.81 | 18.07 |
| 4/22/98 | -86.31 | 25.47 | -10.35 | -2.57 | 10.67 |
| 4/23/98 | -86.36 | 25.48 | -5.18 | 1.03 | 5.28 |
| 4/24/98 | -86.36 | 25.44 | -0.52 | -3.61 | 3.64 |
| 4/25/98 | -86.44 | 25.31 | -7.25 | -14.43 | 16.15 |
| 4/26/98 | -86.47 | 25.10 | -3.63 | -24.26 | 24.53 |
| | | | | | |
| | | | Average Velocity (km/day) | | 9.25 |

Table 5-4: Table of distance traveled in per day kilometers for hyperbolic trajectory at 300 m for hyperbolic structure A1. The days with the minimum and maximum distance values are highlighted in yellow.

| Date | Longitude (°W) | Latitude (°N) | East (km) | North (km) | Dist (km) |
|-------------|-----------------------|----------------------|----------------------------------|-------------------|------------------|
| 4/6/98 | -85.45 | 25.23 | | | |
| 4/7/98 | -85.45 | 25.20 | 0.00 | -3.61 | 3.61 |
| 4/8/98 | -85.46 | 25.23 | -1.04 | 3.61 | 3.76 |
| 4/9/98 | -85.48 | 25.30 | -2.08 | 7.22 | 7.51 |
| 4/10/98 | -85.47 | 25.35 | 0.52 | 6.19 | 6.21 |
| 4/11/98 | -85.50 | 25.38 | -2.59 | 3.61 | 4.44 |
| 4/12/98 | -85.55 | 25.42 | -5.18 | 4.12 | 6.62 |
| 4/13/98 | -85.64 | 25.45 | -8.81 | 3.61 | 9.52 |
| 4/14/98 | -85.74 | 25.49 | -10.36 | 3.60 | 10.97 |
| 4/15/98 | -85.81 | 25.52 | -6.73 | 3.60 | 7.64 |
| 4/16/98 | -85.88 | 25.55 | -7.25 | 3.09 | 7.88 |
| 4/17/98 | -85.96 | 25.53 | -8.28 | -2.06 | 8.53 |
| 4/18/98 | -86.09 | 25.48 | -12.94 | -5.66 | 14.12 |
| 4/19/98 | -86.22 | 25.37 | -12.95 | -11.33 | 17.21 |
| 4/20/98 | -86.36 | 25.26 | -13.99 | -12.38 | 18.68 |
| 4/21/98 | -86.44 | 25.22 | -8.30 | -5.16 | 9.77 |
| 4/22/98 | -86.50 | 25.20 | -6.23 | -1.55 | 6.42 |
| 4/23/98 | -86.53 | 25.21 | -2.59 | 1.03 | 2.79 |
| 4/24/98 | -86.53 | 25.23 | -0.52 | 2.58 | 2.63 |
| 4/25/98 | -86.55 | 25.21 | -1.56 | -2.58 | 3.01 |
| 4/26/98 | -86.50 | 25.08 | 5.19 | -14.46 | 15.36 |
| | | | | | |
| | | | Average Velocity (km/day) | | 8.33 |

Table 5-5: Table of distance traveled per day in kilometers for hyperbolic trajectory at 400 m for hyperbolic structure A1. The days with the minimum and maximum distance values are highlighted in yellow.

| Date | Longitude (°W) | Latitude (°N) | East (km) | North (km) | Dist (km) |
|-------------|-----------------------|----------------------|----------------------------------|-------------------|------------------|
| 4/6/98 | -85.39 | 25.67 | | | |
| 4/7/98 | -85.46 | 25.72 | -7.75 | 5.65 | 9.60 |
| 4/8/98 | -85.51 | 25.73 | -5.17 | 0.51 | 5.19 |
| 4/9/98 | -85.52 | 25.67 | -1.03 | -6.17 | 6.25 |
| 4/10/98 | -85.54 | 25.56 | -1.03 | -12.86 | 12.90 |
| 4/11/98 | -85.53 | 25.50 | 0.52 | -6.69 | 6.71 |
| 4/12/98 | -85.54 | 25.47 | -0.52 | -2.57 | 2.63 |
| 4/13/98 | -85.58 | 25.49 | -4.66 | 2.06 | 5.10 |
| 4/14/98 | -85.68 | 25.50 | -9.84 | 1.54 | 9.96 |
| 4/15/98 | -85.78 | 25.54 | -10.35 | 3.60 | 10.96 |
| 4/16/98 | -85.90 | 25.53 | -11.90 | -1.03 | 11.95 |
| 4/17/98 | -86.05 | 25.48 | -15.01 | -5.15 | 15.87 |
| 4/18/98 | -86.16 | 25.39 | -11.39 | -10.30 | 15.36 |
| 4/19/98 | -86.25 | 25.30 | -8.81 | -10.31 | 13.56 |
| 4/20/98 | -86.35 | 25.22 | -9.85 | -8.77 | 13.19 |
| 4/21/98 | -86.41 | 25.15 | -6.23 | -7.74 | 9.94 |
| 4/22/98 | -86.44 | 25.10 | -3.12 | -4.65 | 5.60 |
| 4/23/98 | -86.48 | 25.11 | -3.64 | 0.52 | 3.67 |
| 4/24/98 | -86.51 | 25.11 | -3.64 | 0.52 | 3.67 |
| 4/25/98 | -86.52 | 25.08 | -1.04 | -4.13 | 4.26 |
| 4/26/98 | -86.52 | 24.96 | 0.00 | -13.44 | 13.44 |
| | | | | | |
| | | | Average Velocity (km/day) | | 8.99 |

Table 5-6: Table of distance traveled per day in kilometers for hyperbolic trajectory at 600 m for hyperbolic structure A1. The days with the minimum and maximum distance values are highlighted in yellow.

| Date | Longitude (°W) | Latitude (°N) | East (km) | North (km) | Dist (km) |
|-------------|-----------------------|----------------------|----------------------------------|-------------------|------------------|
| 4/6/98 | -85.38 | 25.66 | | | |
| 4/7/98 | -85.45 | 25.68 | -6.72 | 2.06 | 7.03 |
| 4/8/98 | -85.48 | 25.70 | -3.62 | 2.57 | 4.44 |
| 4/9/98 | -85.52 | 25.71 | -3.62 | 0.51 | 3.65 |
| 4/10/98 | -85.55 | 25.67 | -3.10 | -4.63 | 5.57 |
| 4/11/98 | -85.59 | 25.57 | -3.62 | -11.32 | 11.88 |
| 4/12/98 | -85.61 | 25.51 | -2.59 | -5.66 | 6.22 |
| 4/13/98 | -85.65 | 25.51 | -3.62 | -0.51 | 3.66 |
| 4/14/98 | -85.70 | 25.51 | -5.18 | 0.51 | 5.20 |
| 4/15/98 | -85.77 | 25.53 | -7.25 | 2.06 | 7.53 |
| 4/16/98 | -85.89 | 25.53 | -11.39 | -0.51 | 11.40 |
| 4/17/98 | -86.02 | 25.50 | -13.46 | -2.57 | 13.70 |
| 4/18/98 | -86.10 | 25.46 | -8.28 | -4.63 | 9.49 |
| 4/19/98 | -86.16 | 25.36 | -6.21 | -11.34 | 12.93 |
| 4/20/98 | -86.23 | 25.25 | -6.74 | -11.86 | 13.64 |
| 4/21/98 | -86.31 | 25.17 | -7.78 | -9.29 | 12.12 |
| 4/22/98 | -86.35 | 25.11 | -4.67 | -6.20 | 7.76 |
| 4/23/98 | -86.39 | 25.09 | -3.64 | -2.58 | 4.46 |
| 4/24/98 | -86.42 | 25.10 | -2.60 | 1.03 | 2.80 |
| 4/25/98 | -86.47 | 25.08 | -5.19 | -2.58 | 5.80 |
| 4/26/98 | -86.51 | 25.03 | -4.16 | -4.65 | 6.24 |
| | | | | | |
| | | | Average Velocity (km/day) | | 7.78 |

Table 5-7: Table of distance traveled per day in kilometers for hyperbolic trajectory at 1100 m for hyperbolic structure A1. The days with the minimum and maximum distance values are highlighted in yellow.

| Date | Longitude (°W) | Latitude (°N) | East (km) | North (km) | Dist (km) |
|-------------|-----------------------|----------------------|----------------------------------|-------------------|------------------|
| 4/6/98 | -85.65 | 25.59 | | | |
| 4/7/98 | -85.67 | 25.54 | -2.59 | -6.18 | 6.70 |
| 4/8/98 | -85.71 | 25.50 | -3.62 | -4.12 | 5.49 |
| 4/9/98 | -85.75 | 25.49 | -3.62 | -1.54 | 3.94 |
| 4/10/98 | -85.77 | 25.53 | -2.07 | 4.63 | 5.08 |
| 4/11/98 | -85.76 | 25.56 | 1.04 | 3.60 | 3.75 |
| 4/12/98 | -85.75 | 25.57 | 0.52 | 0.51 | 0.73 |
| 4/13/98 | -85.80 | 25.56 | -4.66 | -1.03 | 4.77 |
| 4/14/98 | -85.86 | 25.53 | -6.21 | -3.09 | 6.94 |
| 4/15/98 | -85.94 | 25.50 | -7.76 | -2.57 | 8.18 |
| 4/16/98 | -86.02 | 25.50 | -8.28 | -1.03 | 8.35 |
| 4/17/98 | -86.06 | 25.50 | -3.62 | 0.00 | 3.62 |
| 4/18/98 | -86.05 | 25.48 | 0.52 | -1.54 | 1.63 |
| 4/19/98 | -86.03 | 25.41 | 1.55 | -8.24 | 8.39 |
| 4/20/98 | -86.09 | 25.23 | -5.18 | -19.08 | 19.77 |
| 4/21/98 | -86.10 | 25.15 | -1.56 | -9.29 | 9.42 |
| 4/22/98 | -86.17 | 25.03 | -7.27 | -13.95 | 15.73 |
| 4/23/98 | -86.29 | 24.96 | -11.43 | -7.76 | 13.82 |
| 4/24/98 | -86.32 | 24.96 | -3.12 | 0.00 | 3.12 |
| 4/25/98 | -86.38 | 24.99 | -6.24 | 3.62 | 7.21 |
| 4/26/98 | -86.53 | 25.10 | -15.08 | 12.40 | 19.52 |
| | | | | | |
| | | | Average Velocity (km/day) | | 7.81 |

Table 5-8: Variability of distance traveled in km with depth for A1 from April 11-12, April 24-25 and April 25-26 for hyperbolic trajectories associated with A1.

| Depths (m) | <i>12-Apr</i> | <i>25-Apr</i> | <i>26-Apr</i> |
|-------------------|---------------|---------------|---------------|
| <i>50</i> | 10.59 | 11.33 | 27.47 |
| <i>200</i> | 7.47 | 16.15 | 24.53 |
| <i>300</i> | 6.62 | 3.01 | 15.36 |
| <i>400</i> | 2.63 | 4.26 | 13.44 |
| <i>600</i> | 6.22 | 5.8 | 6.24 |
| <i>1100</i> | 0.73 | 7.21 | 19.52 |

Table 5-9 summarizes the average distance moved per day at each depth. Moving down the water column, the average distances moved decrease in a fairly even increment. This decrease is expected since the velocities decrease with depth. The uniform decrease is unexpected, though, since daily values vary widely at each depth. Another interesting finding is the mean distance moved of the hyperbolic trajectory at 3000 m. This value of 6.48 is surprisingly high since it is widely believed that flow at the bottom is on the order of 1 km/day. There is little difference in the average speeds of the hyperbolic trajectories between 300 and 400 m, where the thermocline is located.

Table 5-9: Mean distance traveled for hyperbolic structure A1. The distances are in km/day.

| | Mean Distance | | | Mean Distance |
|-----------|---------------|--|-----------|---------------|
| Depth (m) | km/day | | Depth (m) | km/day |
| 0 | N/A | | 600 | 7.78 |
| 10 | 13.43 | | 700 | 7.33 |
| 20 | 13.11 | | 800 | 8.16 |
| 30 | 12.66 | | 900 | 7.69 |
| 50 | 12.88 | | 1000 | 7.62 |
| 75 | 12.38 | | 1100 | 7.81 |
| 100 | 11.35 | | 1200 | 7.37 |
| 125 | 10.46 | | 1300 | 7.58 |
| 150 | 10.09 | | 1400 | 7.60 |
| 200 | 9.25 | | 1500 | 7.34 |
| 250 | 8.61 | | 1750 | 7.16 |
| 300 | 8.33 | | 2000 | 6.83 |
| 400 | 8.99 | | 2500 | 6.71 |
| 500 | 8.18 | | 3000 | 6.48 |

The results shown in Table 5-9 suggest that A1 is a single hyperbolic structure organized throughout the water column.

5.2.3 Chaotic Properties of the Hyperbolic Trajectories

Particles initialized close to the hyperbolic trajectory in the toy model diverge at an exponential rate from it. This is shown for the hyperbolic trajectories in the Gulf of Mexico. Particles initialized very close to the hyperbolic trajectory will diverge greatly from the path of the hyperbolic trajectory.

For hyperbolic structure A1, we find that the paths the hyperbolic trajectory and four particles initialized 1 km to the north, south, east and west of it are completely different:

- At 100 m (Figure 5-5), the hyperbolic trajectory follows the circular motion first to the northeast and then back to the southwest, similar to those shown before in Figure 5.1. The particles initialized to the north (magenta), south (green) and east (blue) of the hyperbolic trajectory travel to the north of the hyperbolic trajectory while the particle initialized to the west (red) travels south away from the path of the hyperbolic trajectory and then makes a turn north back towards its initial position.
- At 200 m (Figure 5-6), the hyperbolic trajectory follows a similar arcing pattern as in Figure 5-1 and the particles initialized near the hyperbolic trajectory again diverge. The particles initialized to the north (magenta), south (green) and east (blue) of the hyperbolic trajectory travel north while the particle initialized to the west (red) travels to the southwest and then back up to the north-east.
- At 300 m (Figure 5-7), the hyperbolic trajectory follows the arcing pattern as before and the particles to the north (magenta), south (green) and west (red) travel to the south-west and then back up to the north east, similar to those at 100 m (Figure 5-5) and 200 m (Figure 5-6). The particle to the east (blue) travels to the north and then circles back to the west.
- At 400 m (Figure 5-8), the hyperbolic trajectory follows the northeast to southwest pattern as described in 5.2.1. The particles to the north (magenta), south (green) and east (blue) travel to the north and then

circle to the west while the particle to the west (red) follows a pattern to the south-west and then back up to the north-east.

- At 1100 m (Figure 5-9), the hyperbolic trajectory follows the same pattern as at 400 m. The particles to the north (magenta), east (blue) and west (red) all move to the north while the particle to the south follows the same southern route with a northern turn at the end.

All trajectories were similar in shape. Particles that were drawn to the north stayed to the north and then circled to the west while the particles drawn to the south moved to the southwest and then circled back to the northeast. There was no clear pattern as to which particles were drawn in each direction. There was also no distinct change in the shape or direction of the particle trajectories between 300 and 400 m at the thermocline, unlike the change in shape of the hyperbolic trajectories that we found at the thermocline.

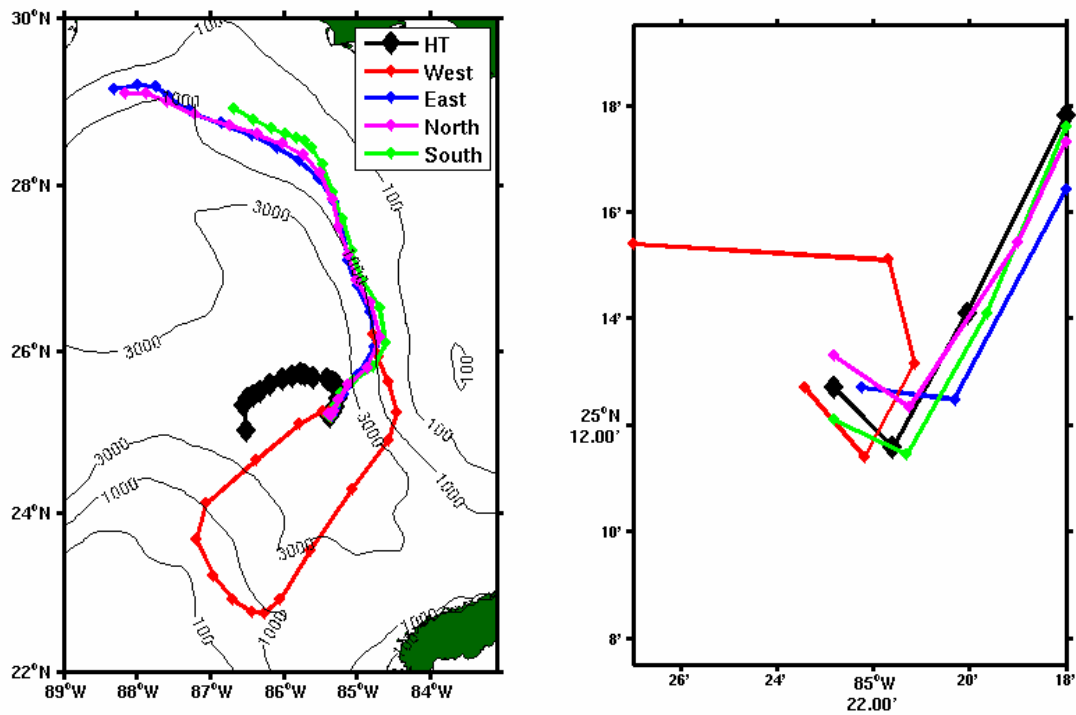


Figure 5-5: Paths of the hyperbolic trajectory and four particles initialized 1 km north, south, east, and west of the hyperbolic trajectory at 100 m. The colors correspond to the particle positions as shown in the legend. The image to the right is zoomed in on the initial positions. The particles and the hyperbolic trajectories are shown from April 6 to April 26. The contours are bottom bathymetry in meters.

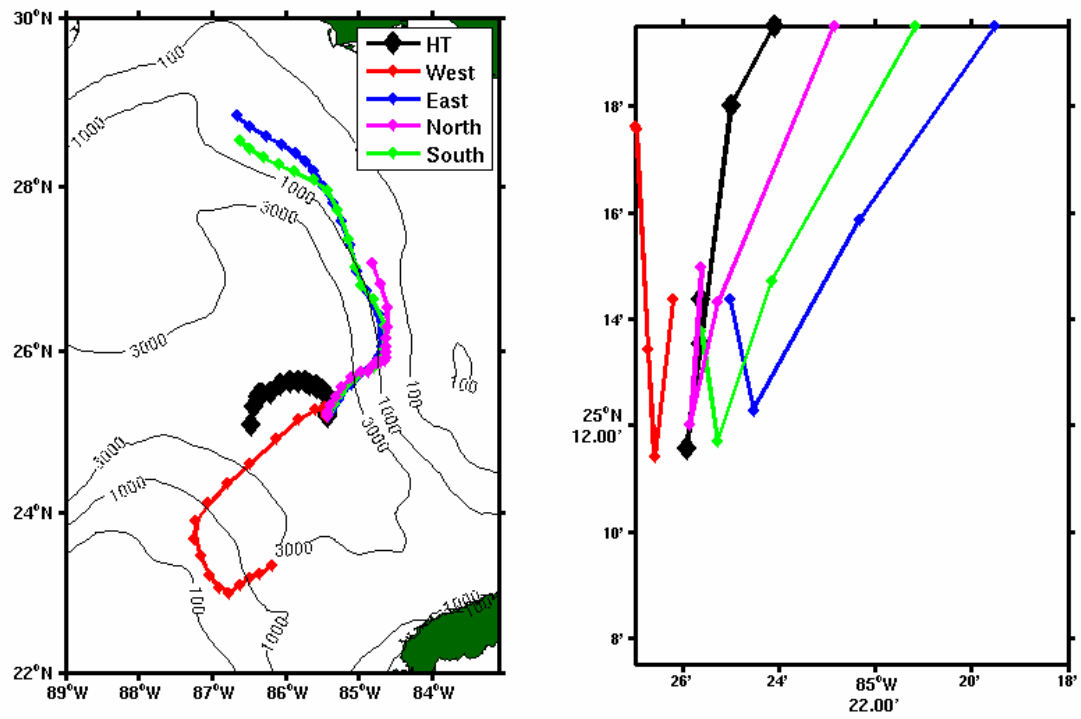


Figure 5-6: Same as Figure 5-5 for 200 m.

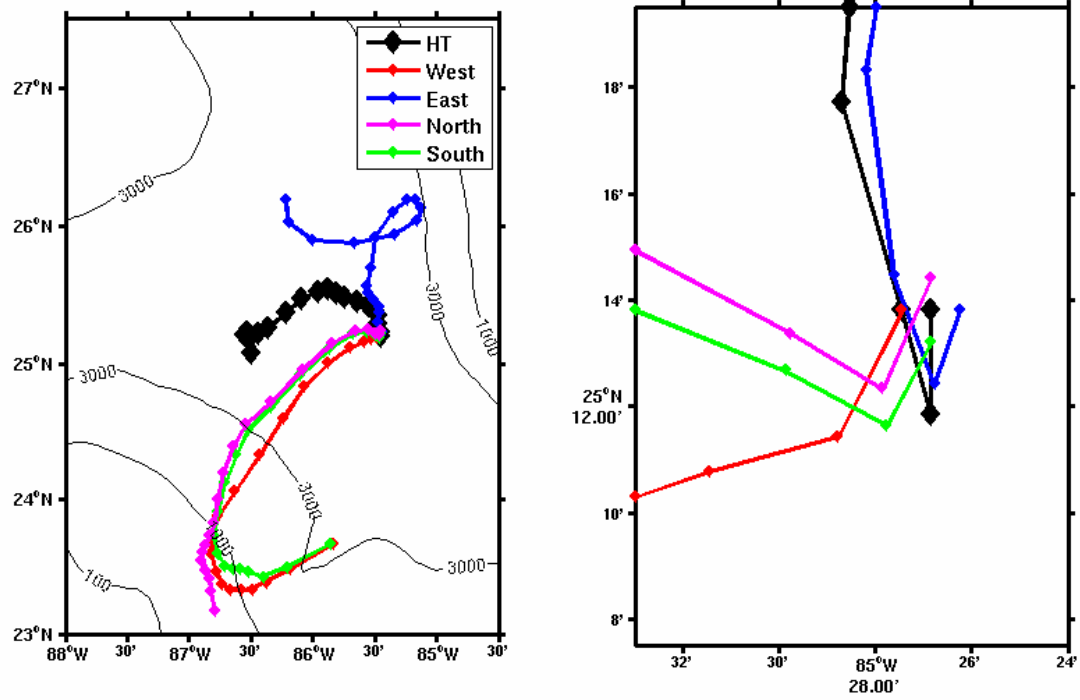


Figure 5-7: Same as Figure 5-5 for 300 m.

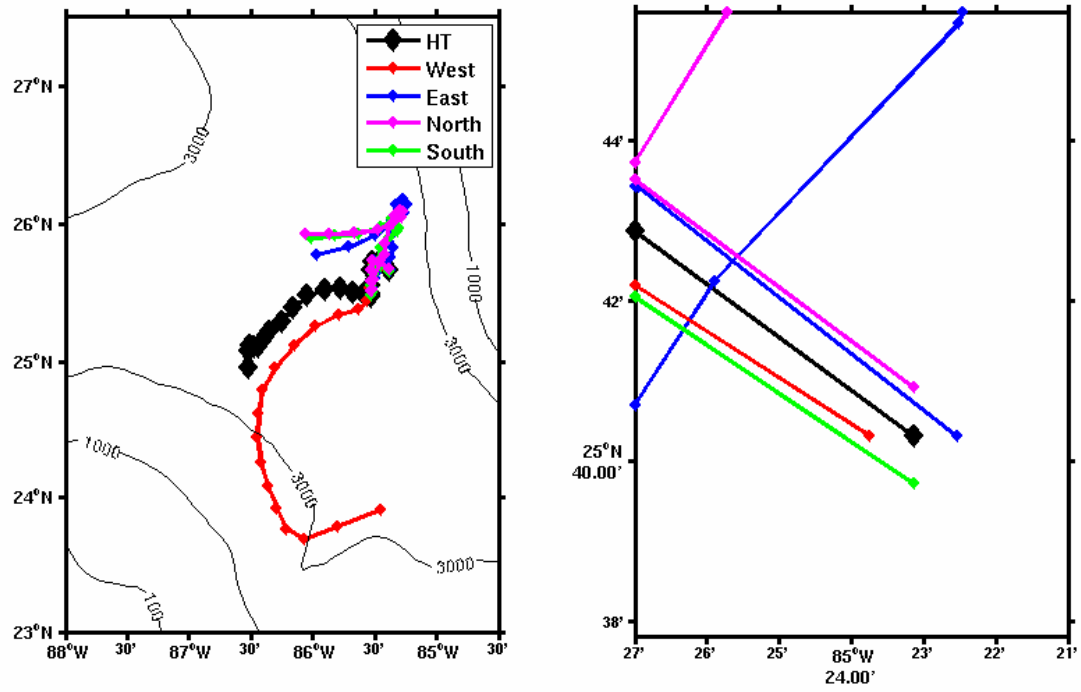


Figure 5-8: Same as Figure 5-5 for 400 m.

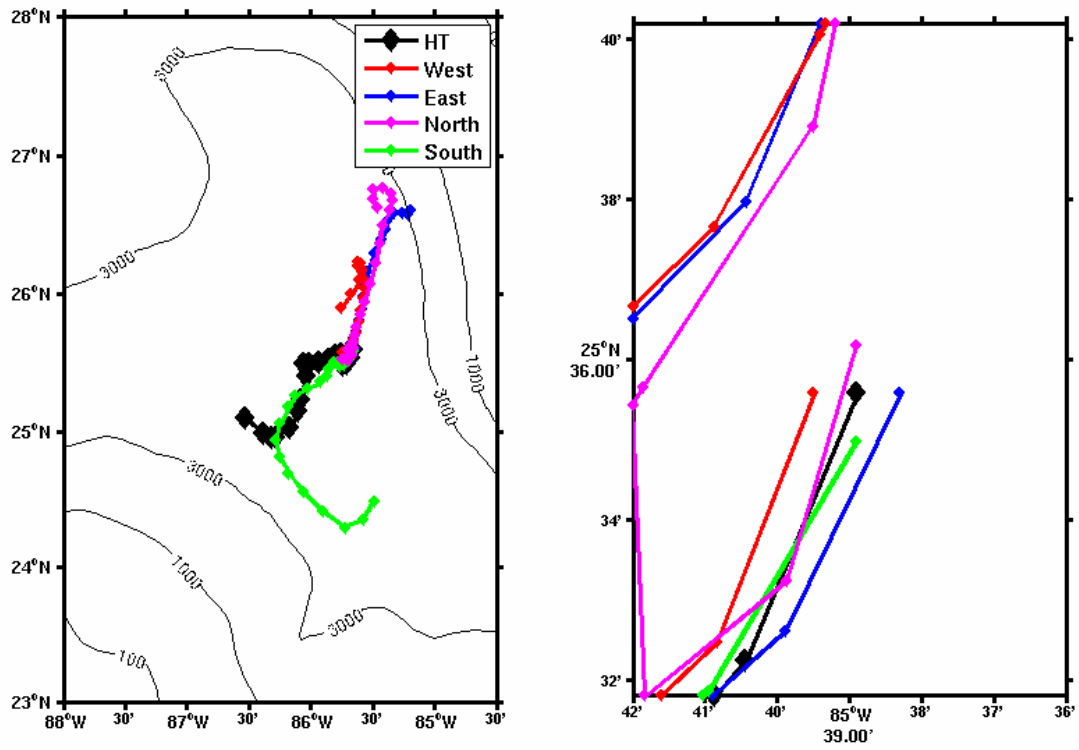


Figure 5-9: Same as Figure 5-5 for 1100 m.

The dispersion illustrated in the previous figures, 5-5 through 5-9, can be attributed to the chaotic nature of hyperbolic trajectories. Nearby particles diverge rapidly from the hyperbolic trajectory. The separation between the particle and the hyperbolic trajectory can be defined by $S = S_o e^{\lambda t}$. Therefore, the $\ln\left(\frac{S}{S_o}\right) = \lambda t$ and

$$\frac{d\left(\ln\left(\frac{S}{S_o}\right)\right)}{dt} = \lambda$$

so that λ is the exponential rate of separation, referred to as a Finite

Time Lyapunov Exponent.

The distances between the nearby particles and the hyperbolic trajectory (Figures 5-5 through 5-9) grow rapidly with time, as is expected with chaotic hyperbolic structures. Figures 5-10 through 5-14 show the natural log of the separation as a function of time. The $\ln\left(\frac{\text{separation}(t)}{\text{separation}(t_o)}\right)$ is shown where *separation* (t_o) is specified as 1 km. A line is also plotted with a slope equal to f , the Coriolis parameter (1×10^{-4}).

The maximum separation occurred in the first six days, April 6 to April 11. Figure 5-10 shows that all the particles at 100 meters depth separate from the hyperbolic trajectory at roughly the same rate, roughly $\frac{f}{8}$.

Figures 5-11 through 5-14 show that the separation rate decreases with depth. For depths between 200 and 1100 m, the separation rates are similar, roughly equal to $0.075 f$. There is no significant change in the separation rate across the thermocline from 300 to 400 m.

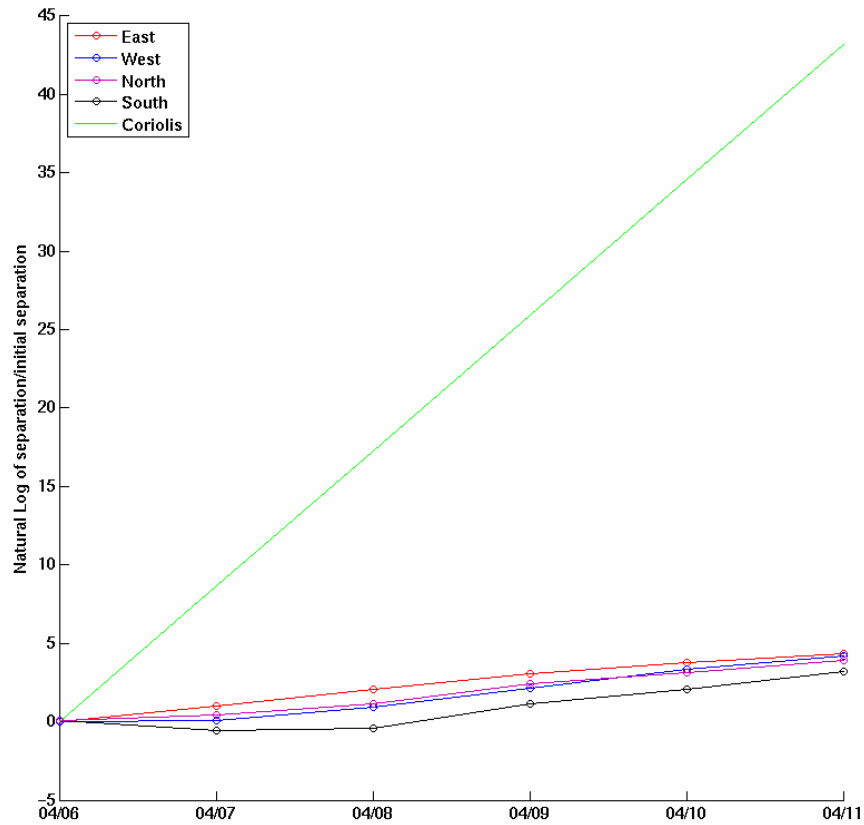


Figure 5-10: Natural log of separation/initial separation versus time for the hyperbolic trajectory and four particles initialized 1km to the north, south, east, and west of the hyperbolic trajectory at 100 m. The colors correspond to the positions as noted in the legend above. The green line is a line with slope of f (Coriolis parameter).

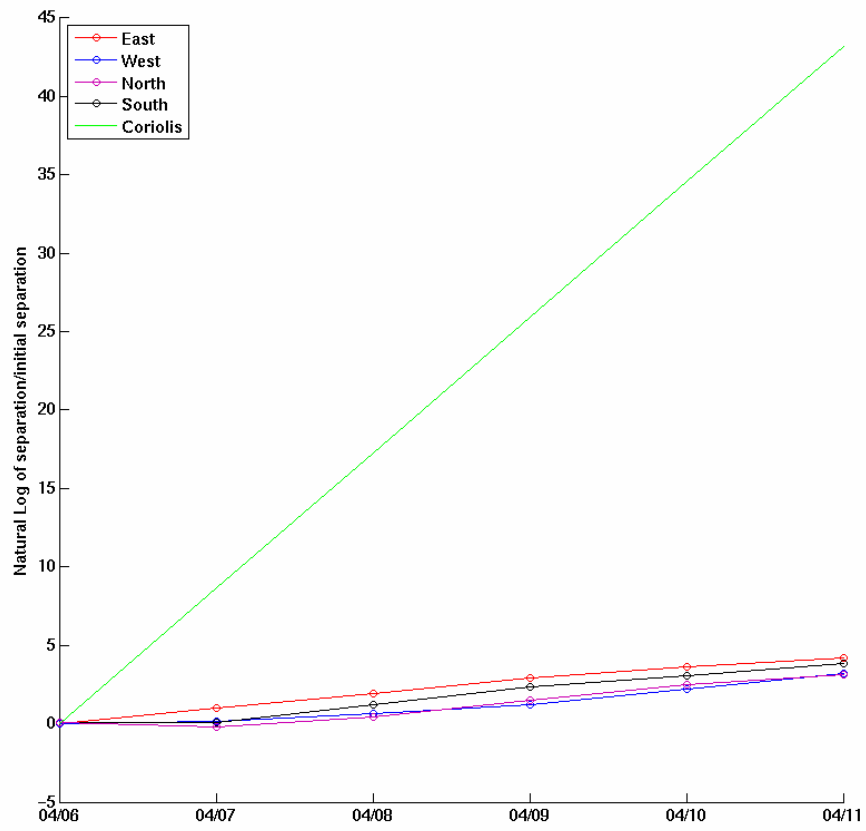


Figure 5-11: Same as Figure 5-10 for 200 m.

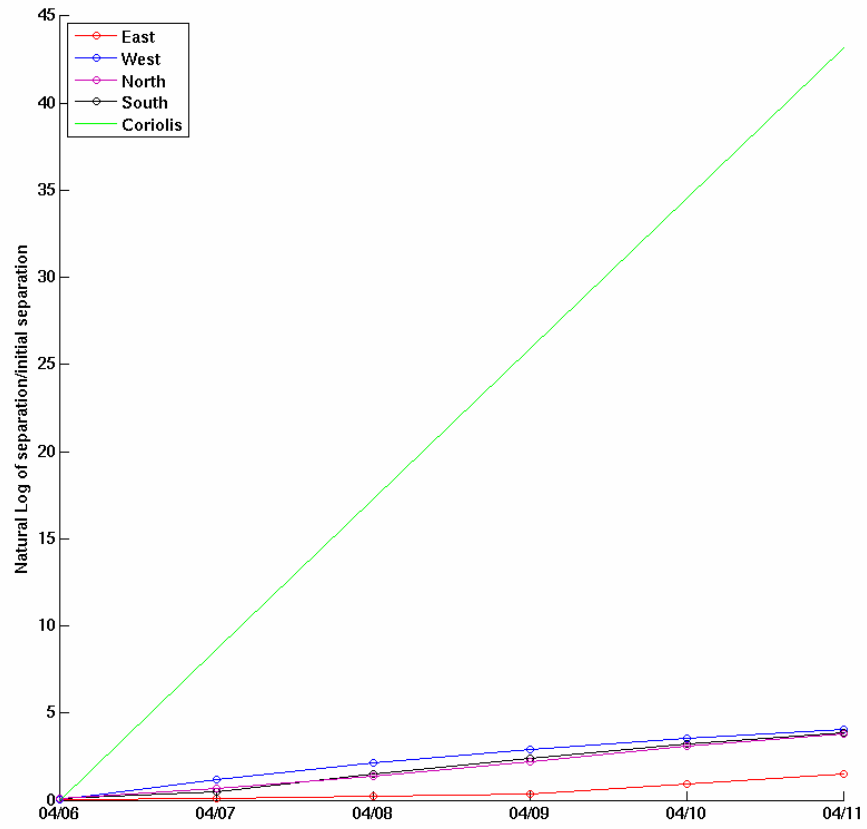


Figure 5-12: Same as Figure 5-10 for 300 m.

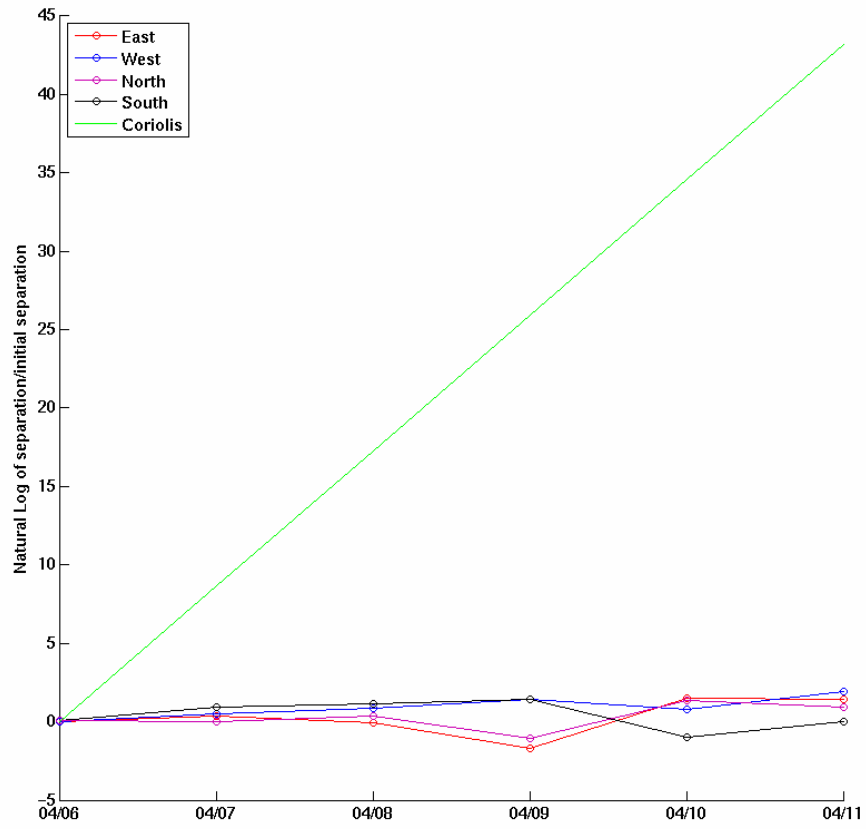


Figure 5-13: Same as Figure 5-10 for 400 m.

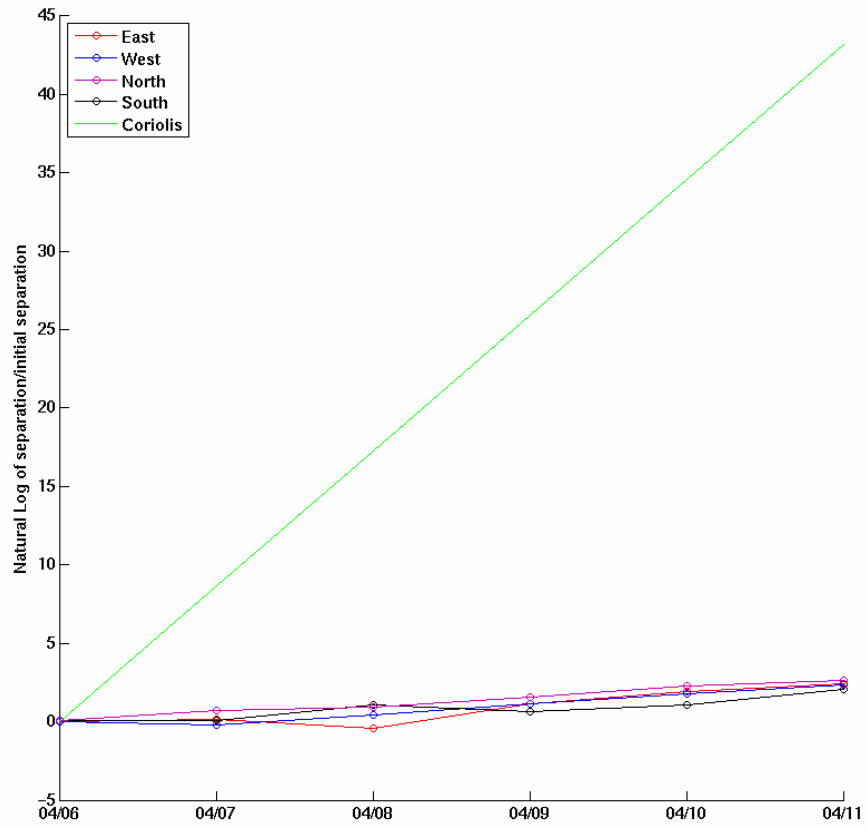


Figure 5-14: Same as Figure 5-10 for 1100 m.

Particles nearby the hyperbolic trajectory encounter different values of geopotential, salinity, and temperature as they diverge from it. At 100 m (Figure 5-15), differences between the hyperbolic trajectory geopotential and that of the other particles are evident after 4 days. Differences in temperature and salinity are evident after 2 days. At 200 m (Figure 5-16), the geopotential differences are again evident after 4 days and the temperature and salinity differences are evident after 2 days. At 300 m (Figure 5-17), the geopotential differences occur after 6 days, although the value for the particle to the north (magenta) remains similar to the hyperbolic trajectory value. Temperature and salinity values diverge after 3 days. At 400 m (Figure 5-18), the particles to the north, south and west follow similar geopotential throughout while the particle to the east diverges after 14 days. The particles separate from temperature and salinity after 6 days. At 1100 m (Figure 5-19), all the particles separate from the geopotential after 5 days and they separate from the temperature and salinity after 4 days.

There is no clear pattern as to when the particles separate from the geopotential or salinity. It is evident, though, that even if a particle follows similar geopotential, it does not maintain similar temperature and salinity for the entire time period. Again, there is no clear change in geopotential, salinity, or temperature patterns when we move through the thermocline from 300 to 400 m.

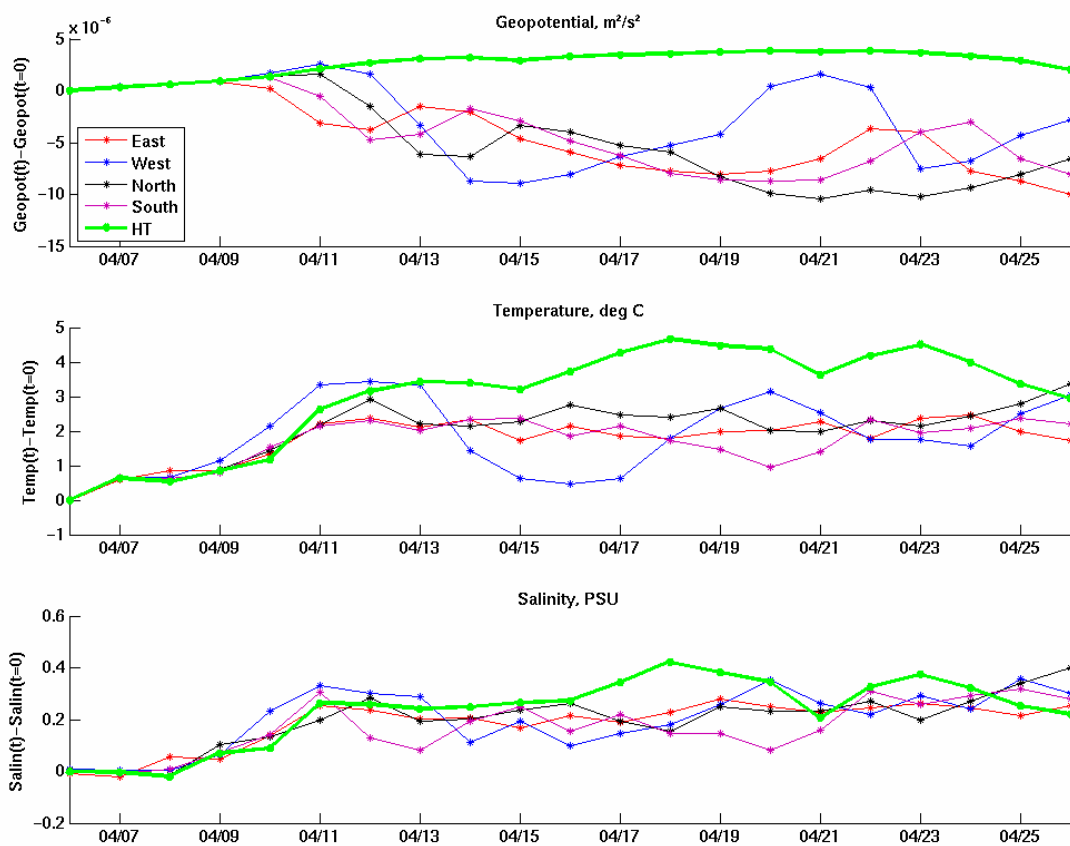


Figure 5-15: Time series (April 6 - April 26) of geopotential (m^2/s^2 , top), temperature ($^{\circ}C$, middle), and salinity (PSU, bottom) for the hyperbolic trajectory at 100 m (green) and nearby particles. The line colors for the nearby particles correspond to their positions as shown in the legend.

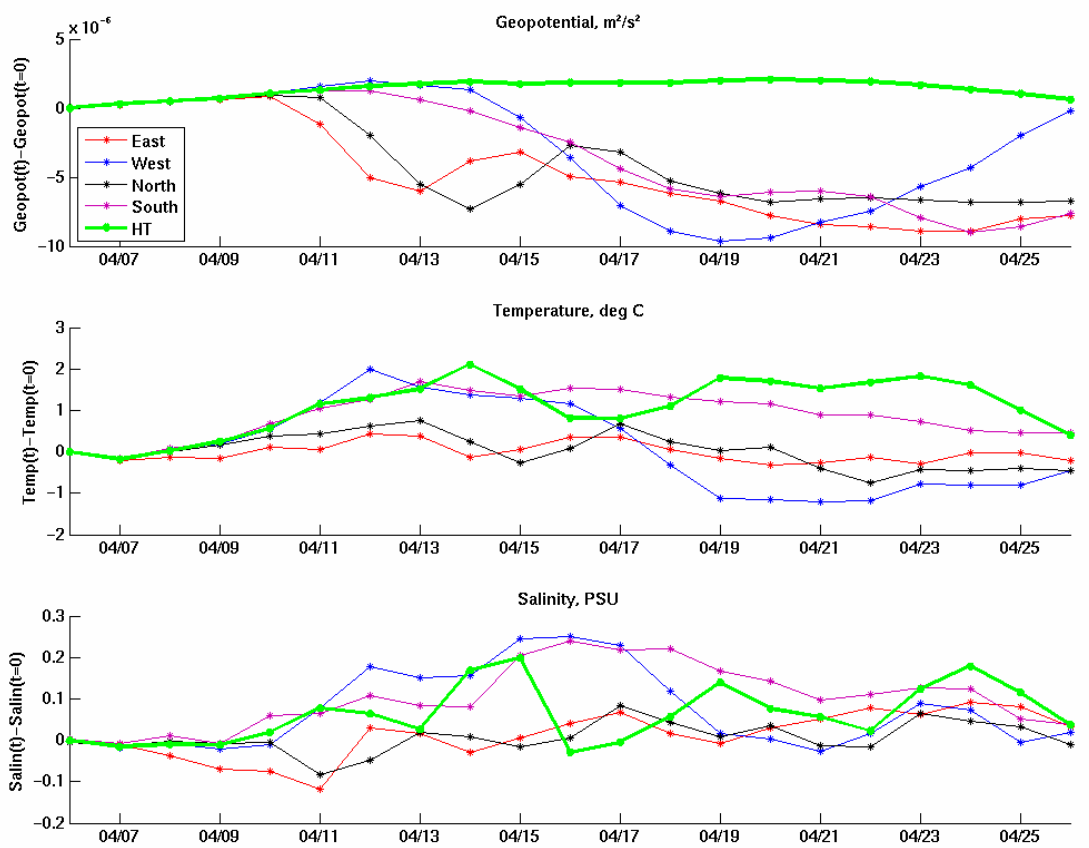


Figure 5-16: Same as Figure 5-15 for 200 m.

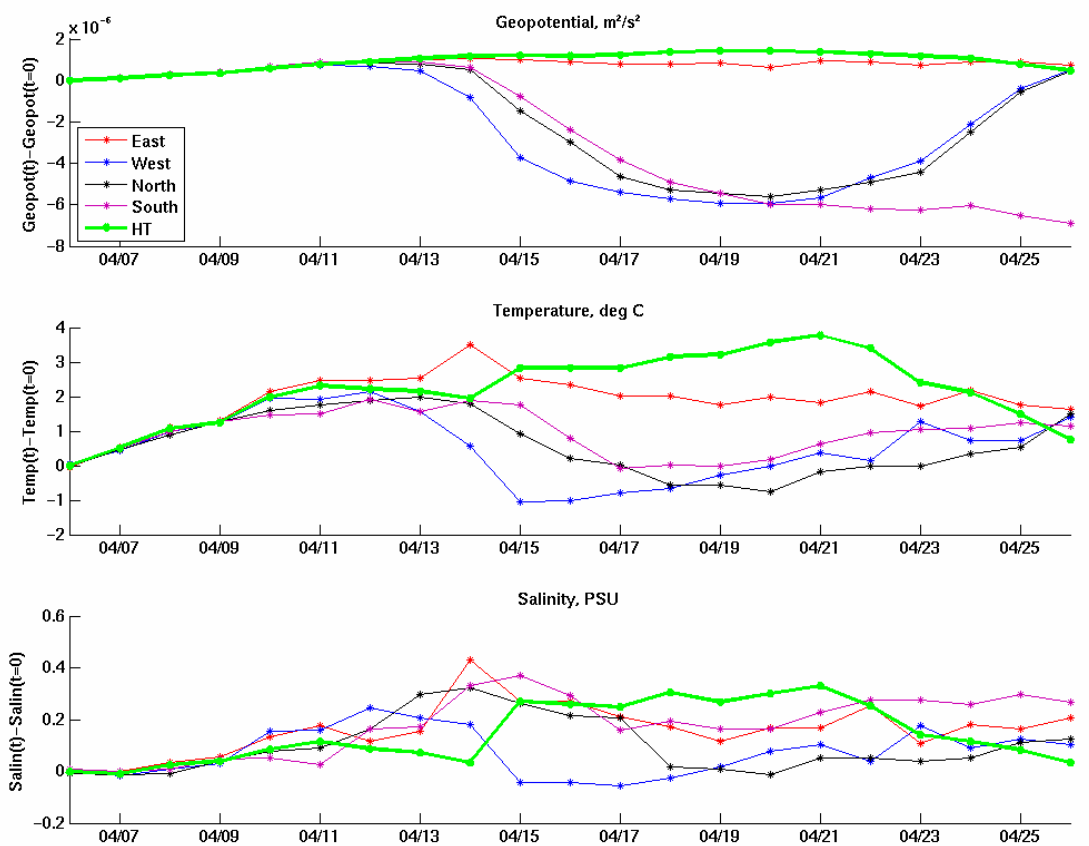


Figure 5-17: Same as Figure 5-15 for 300 m.

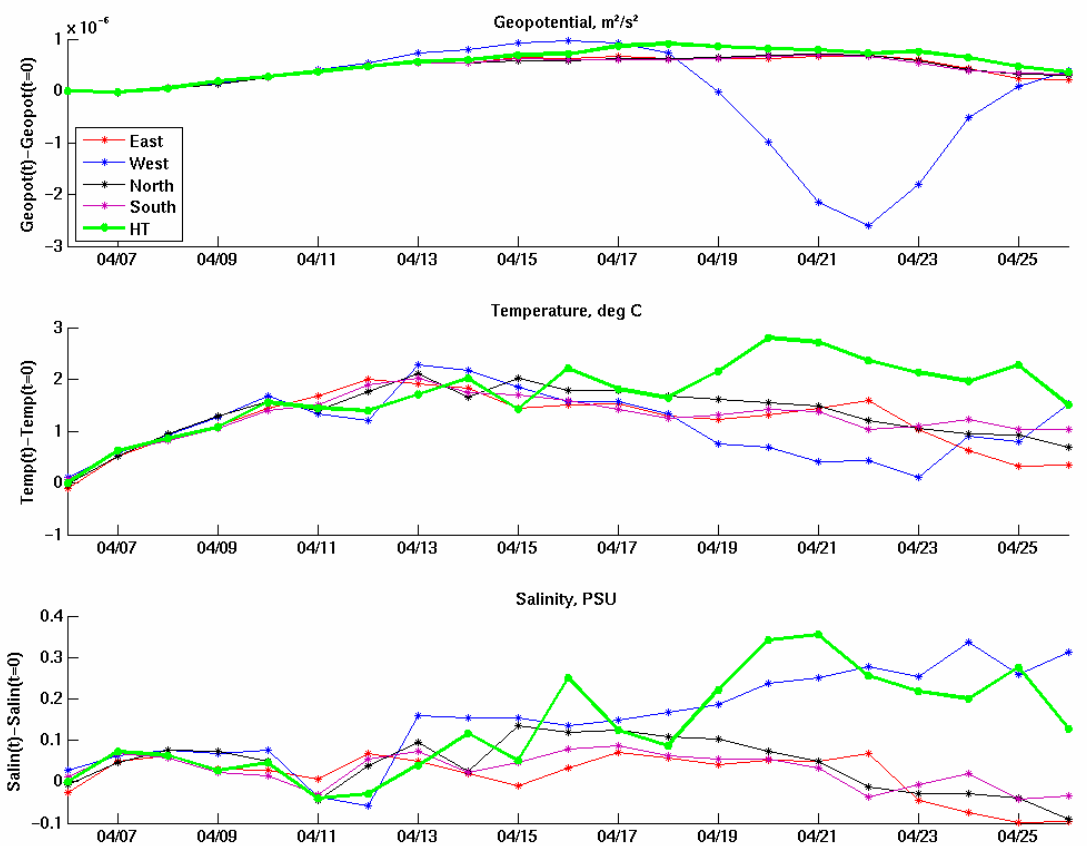


Figure 5-18: Same as Figure 5-15 for 400 m.

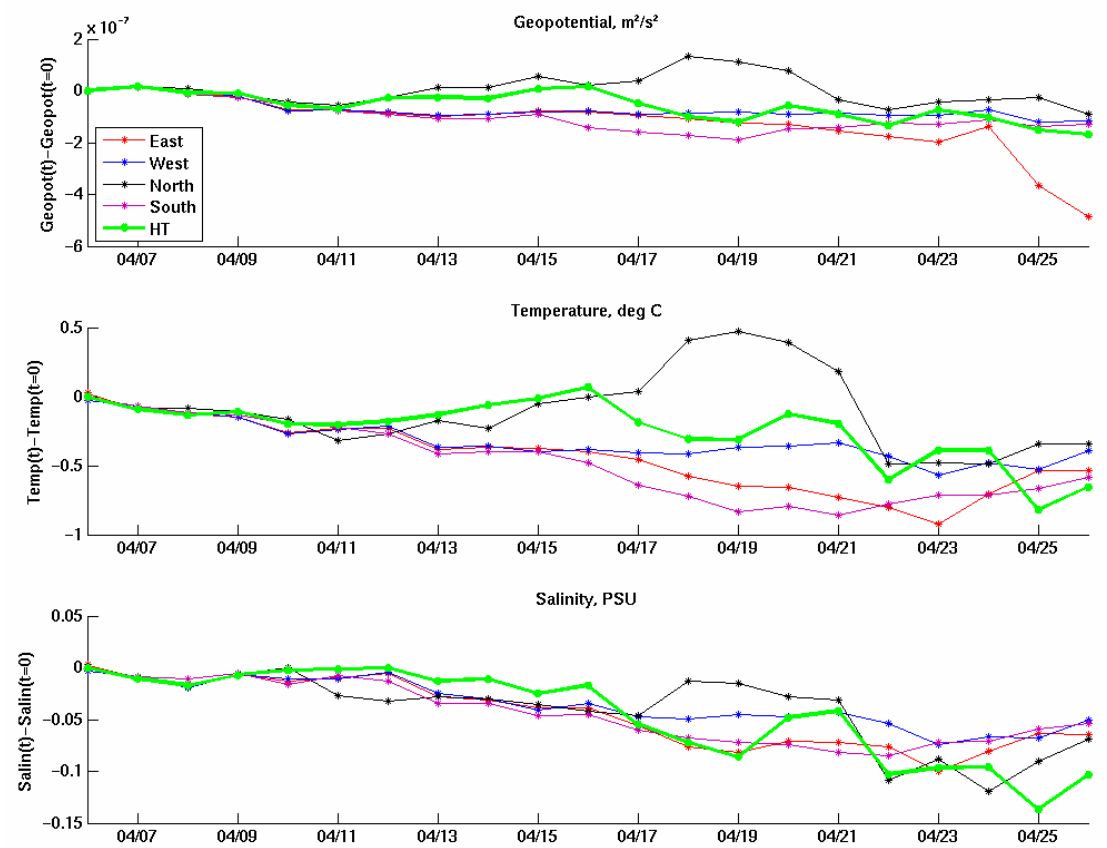


Figure 5-19: Same as Figure 5-15 for 1100 m.

5.2.4 Vertical Extent of Hyperbolic Structure A1

Hyperbolic structure A1 was tracked at all depths (surface to 3000 m) during the period of April 6 to 26, 1998. Figure 5-20 shows A1's position for April 6 and April 26 at 10 and 3000 m.

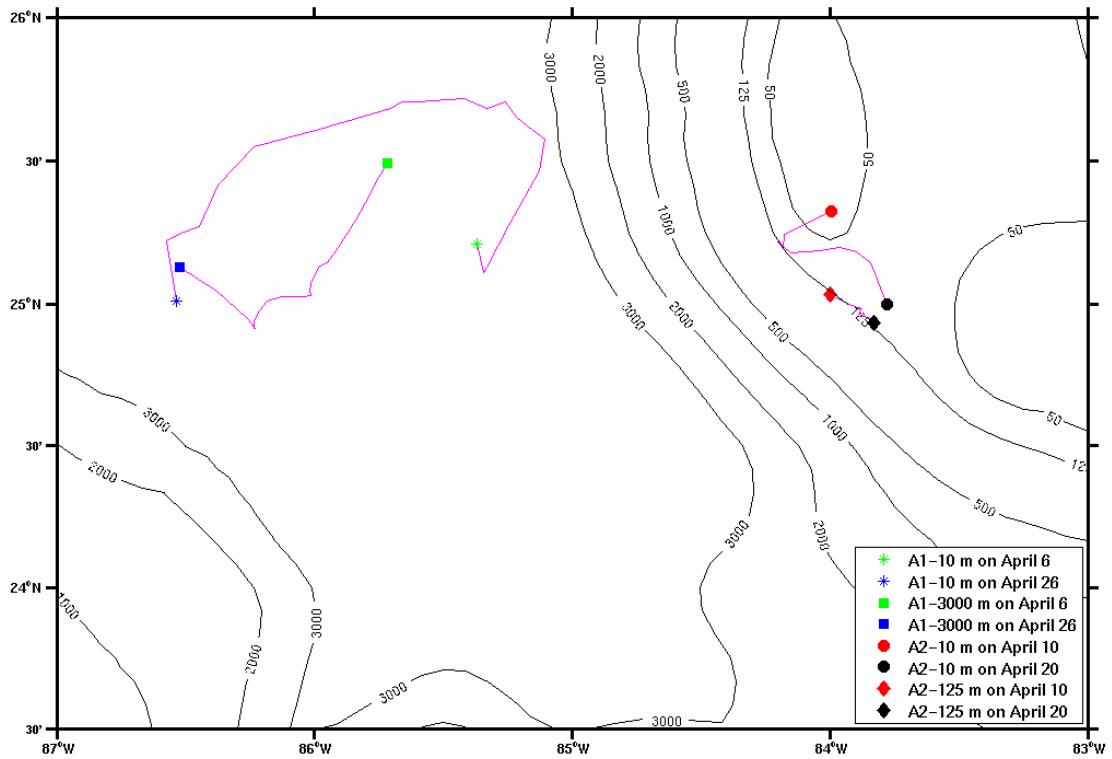


Figure 5-20: Position of hyperbolic structures A1 and A2. The colored dots correspond to times and position as shown in the legend. The contours are the bottom topography (in m).

5.2.5 Three-Dimensional Structure

The three-dimensional character of hyperbolic structure A1 is evident when A1's position at all depths is viewed simultaneously. Figures 5-21 through Figure 5-24 show the both plan and the three-dimensional views of the vertical structure on April 7 and April 11 in a 110 km x 110 km area around the structure. In the shallower depths, A1 is located more to the southeast and while at deeper depths, it is located farther to the northwest. The plan views (Figures 5-21 and 5-23) show this offset with depth, which occurs between 300 and 400 m. This is the location of the

thermocline and halocline, as shown in Figure 5-4. Figures 5-25 and 5-26 show the evolution of the three dimensional structure of A1 from April 6 to April 26.

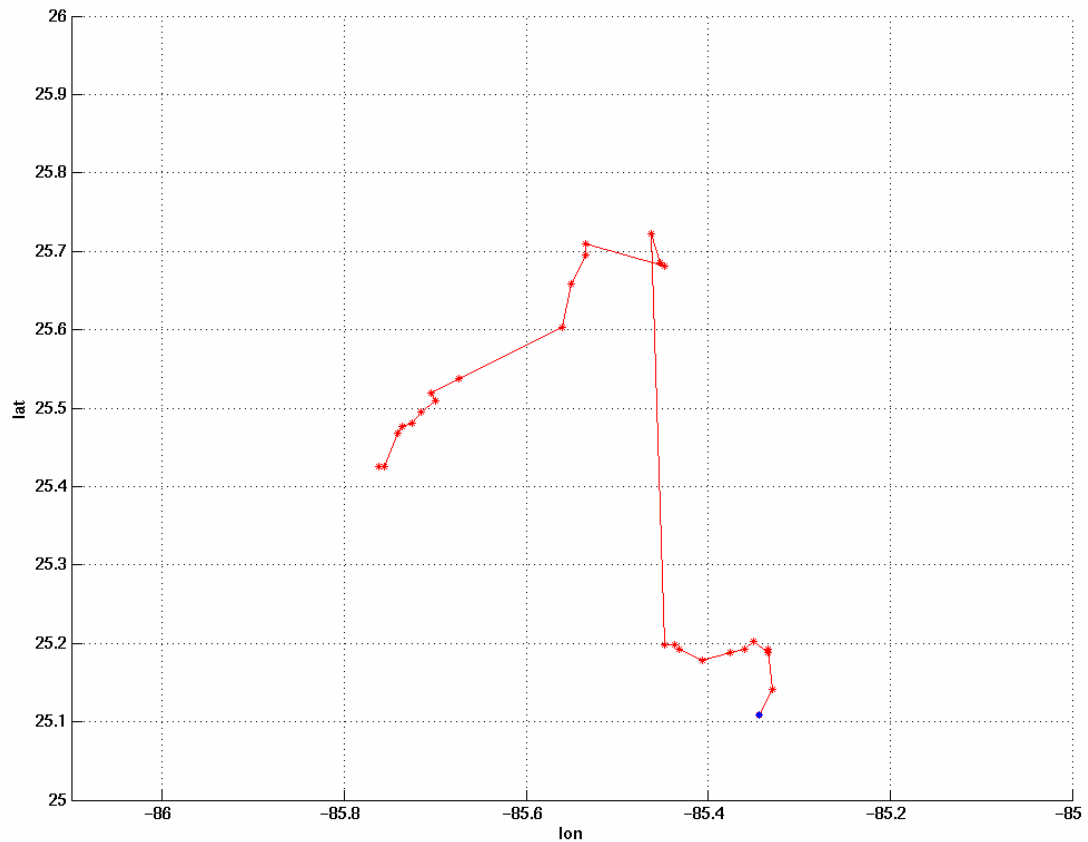


Figure 5-21: Plan view of the hyperbolic structure A1. This figure shows the position of the hyperbolic trajectory in each of the 27 depths on April 7. The blue dot denotes the position at 10 meters.

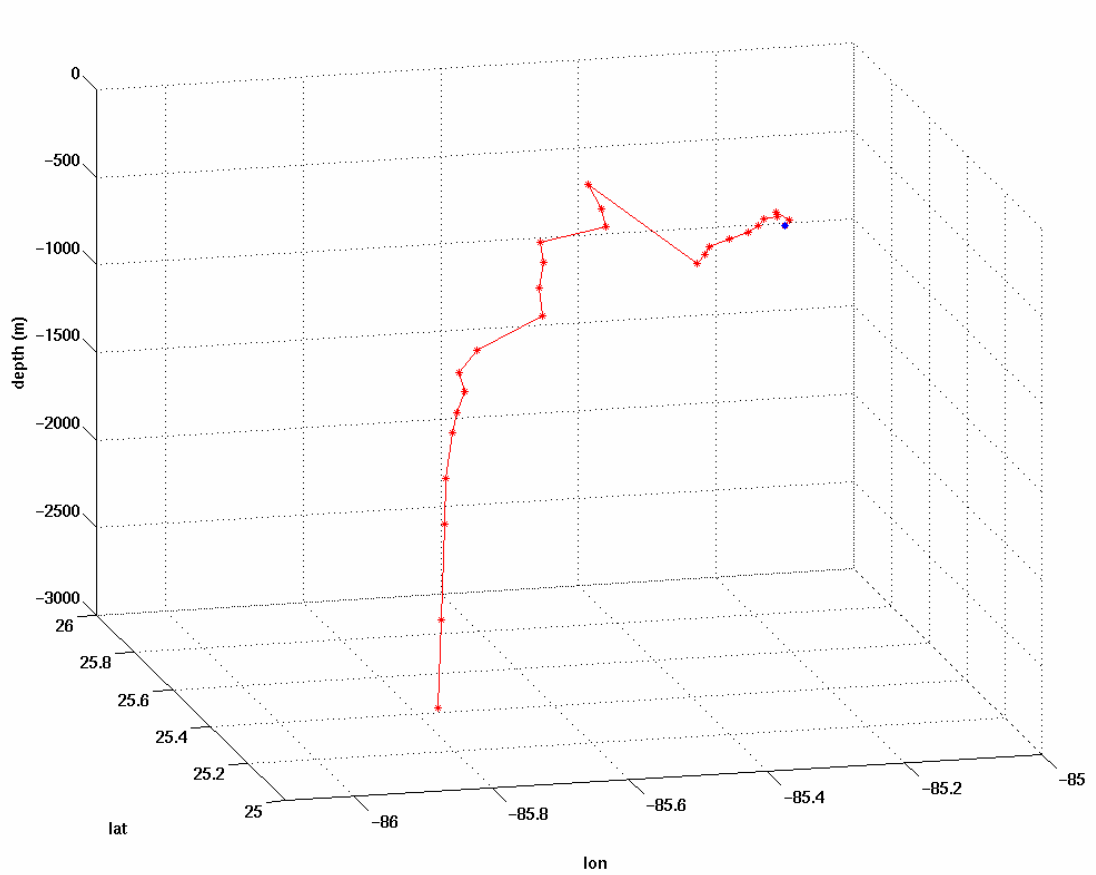


Figure 5-22: Three-dimensional view of the hyperbolic structure A1. This figure shows the position of the hyperbolic trajectory in each of the 27 depths on April 7. The blue dot denotes the position at 10 meters.

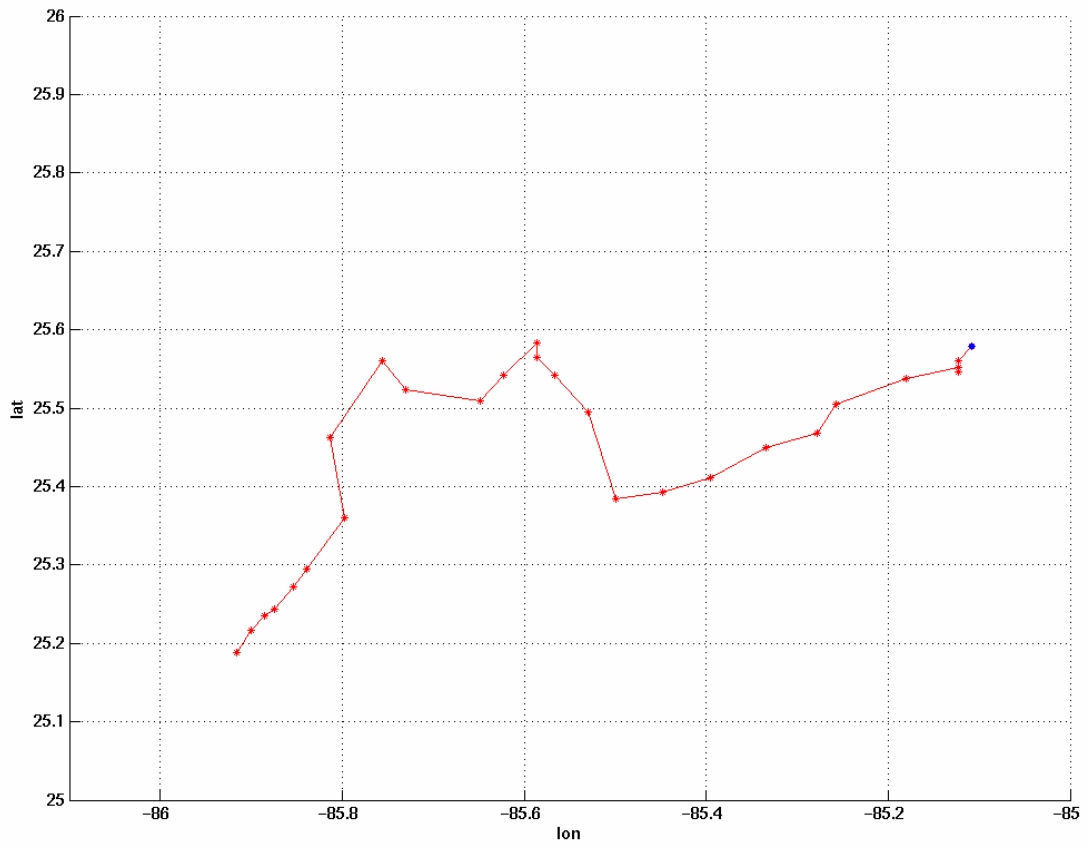


Figure 5-23: Plan view of the hyperbolic structure A1. This figure shows the position of the hyperbolic trajectory in each of the 27 depths on April 11. The blue dot denotes the position at 10 meters.

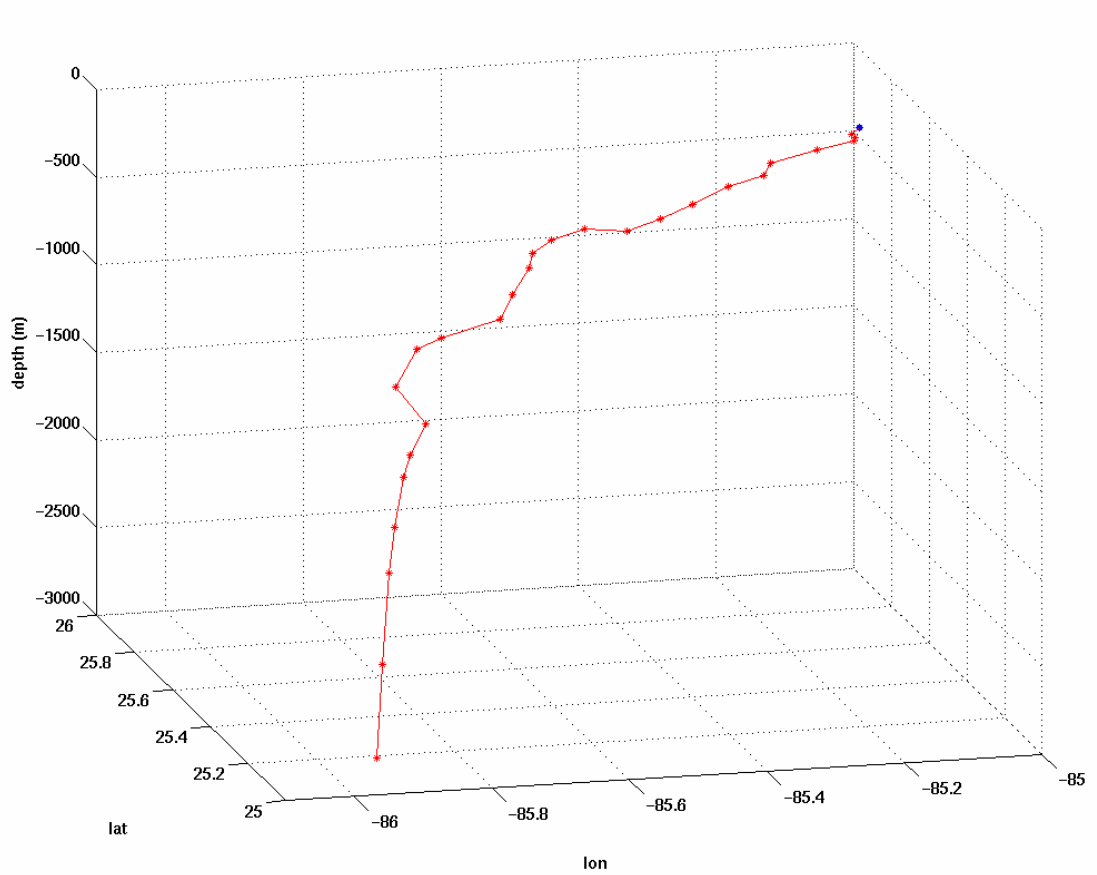


Figure 5-24: Three-dimensional view of the hyperbolic structure A1. This figure shows the position of the hyperbolic trajectory in each of the 27 depths on April 11. The blue dot denotes the position at 10 meters.

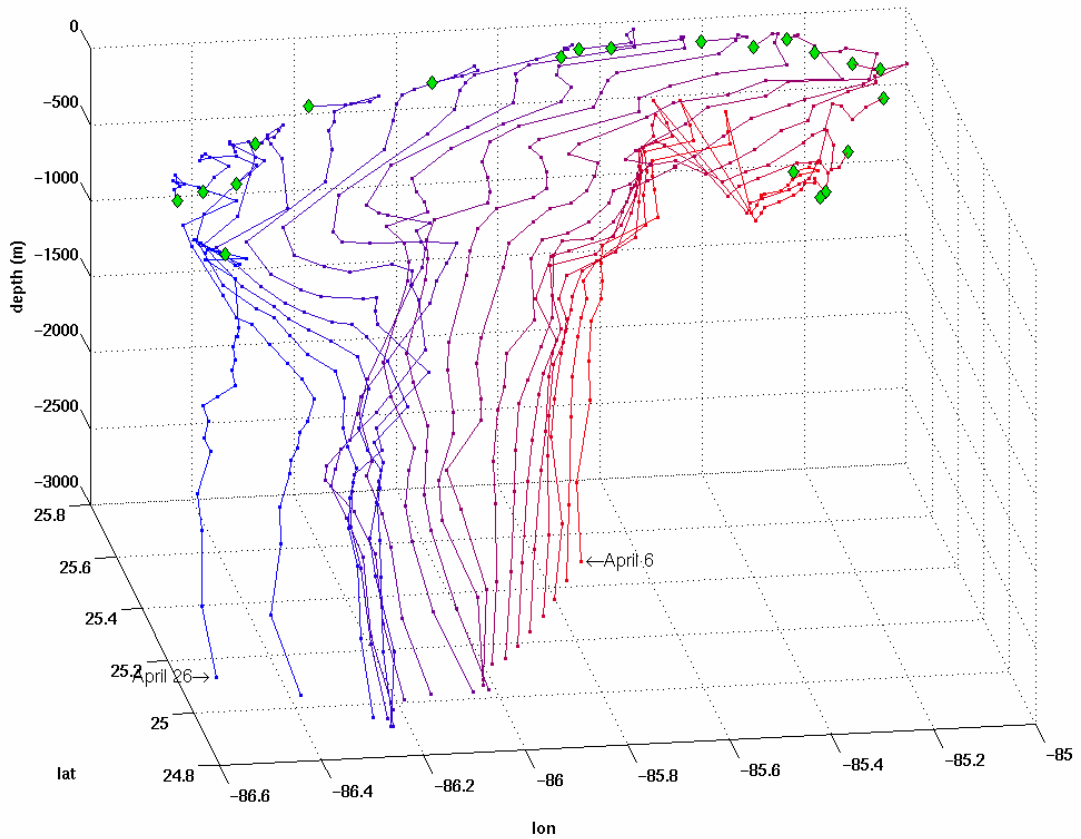


Figure 5-25: Three-dimensional view of the hyperbolic structure A1. This figure shows the position of the hyperbolic trajectory in each of the 27 depths from April 6 (red) to April 26 (blue). The changing colors from red to blue represent passing time. The green diamond denotes the position at 10 m.

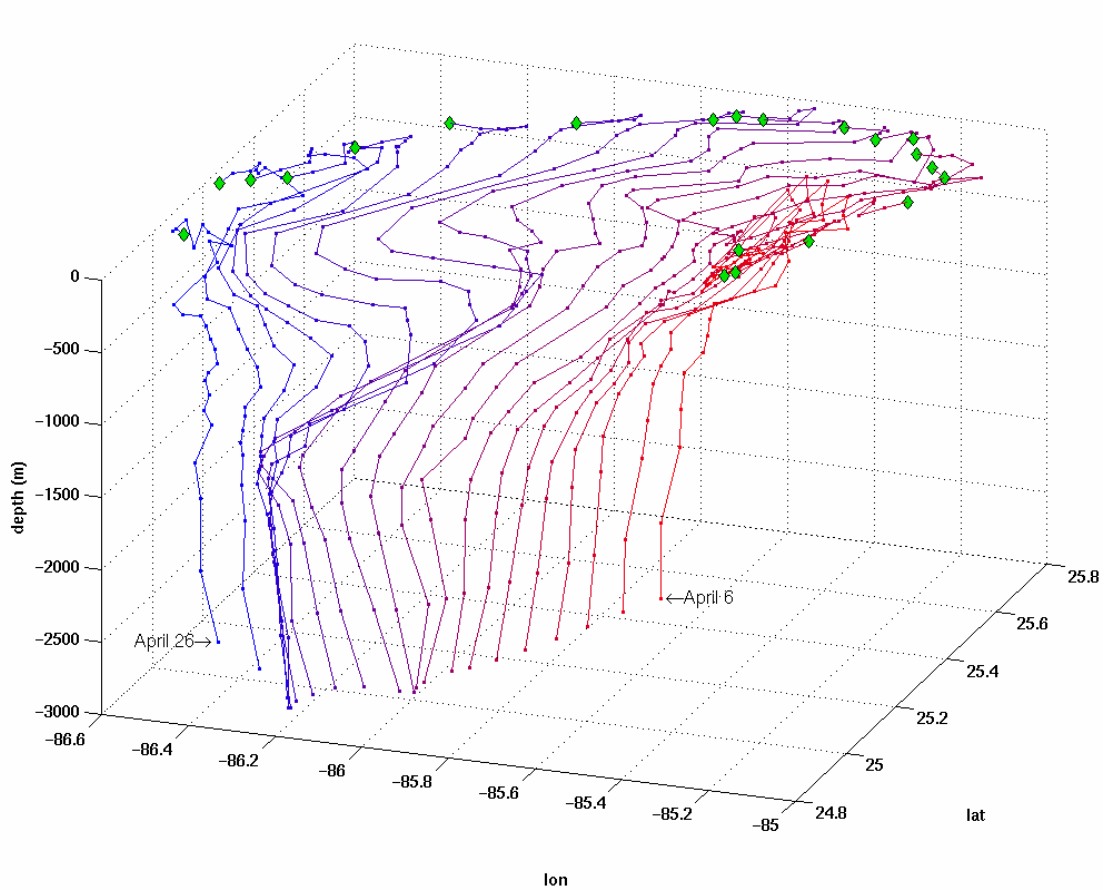


Figure 5-26: Same as Figure 5-25 but shown at a perspective from the right.

In Figures 5-21 through 5-26, lines connecting A1's position with depth are shown based on the assumption that the hyperbolic structure is a single entity throughout the water column. An alternate explanation is that there are really two hyperbolic structures, one shallower and than 400 m and one deeper than 400 m.

Two reasons for rejecting the two-structure hypothesis were given in Section 5.2.3. These are the similarity of movements throughout the water column, as shown by inspection of the average distances traveled of the hyperbolic trajectories,

and similarity of the life span at each level. Examination of velocity fields at different depths provides a third reason to reject the two-structure hypothesis.

Figures 5-27 through 5-30 show the velocity field around A1 at 50, 300, 400, and 1100 m on April 16. The picture is remarkably uniform at all depths. A portion of the cyclone found just to the northwest of the Loop Current noted by Toner et al. (2003) is seen at the southern portion of these figures. Just to the north is an anticyclone. A1 is located just to the east, a typical position for a hyperbolic trajectory. As the figures show, signatures of the cyclone-anticyclone pair exist throughout the water column during this time period. The displacement of the hyperbolic trajectories at the base of the thermo- and haloclines is simply due to the baroclinic structure of these eddies.

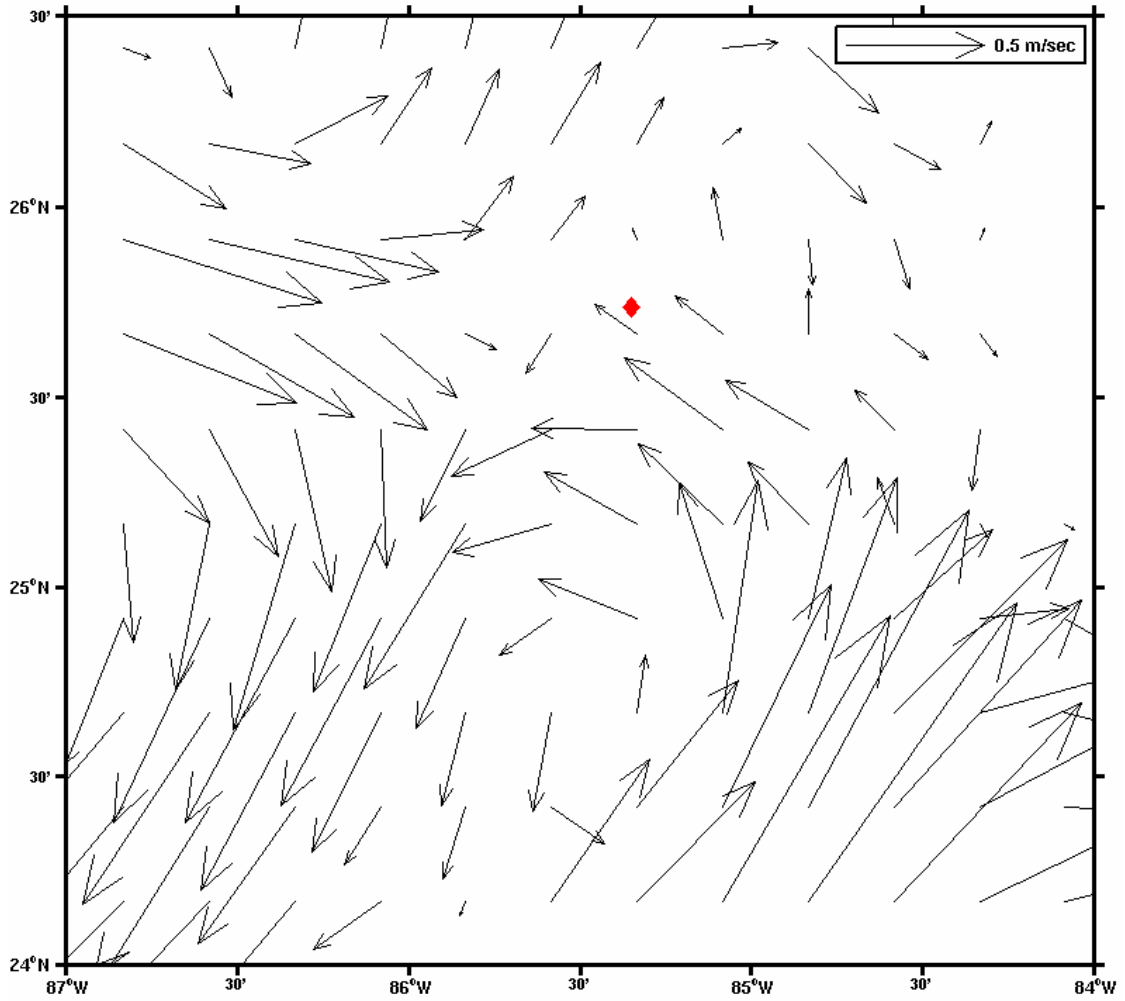


Figure 5-27: Velocities near hyperbolic structure A1 at 50 m on April 16. The red diamond denotes position of the hyperbolic trajectory.

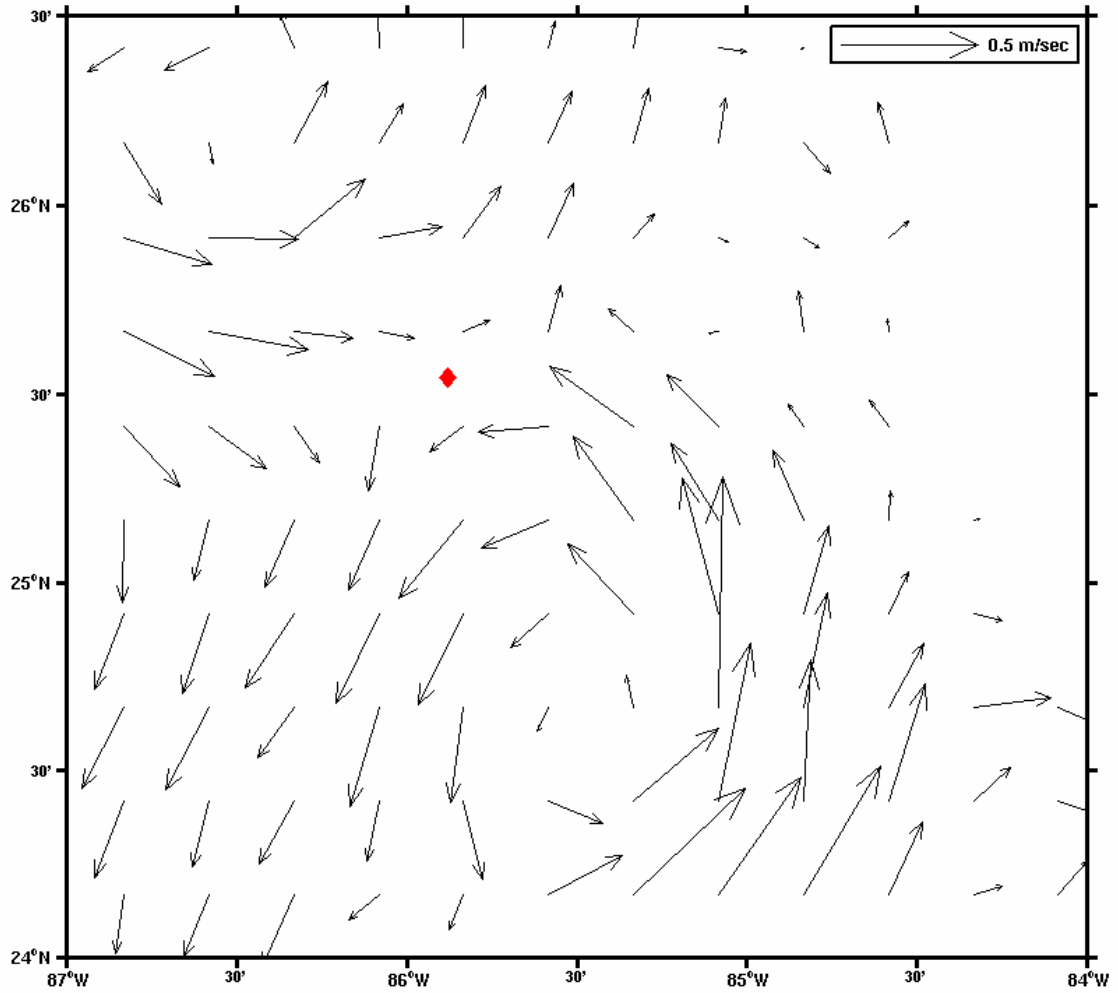


Figure 5-28: Velocities near hyperbolic structure A1 at 300 m on April 16. The red diamond denotes the position of hyperbolic trajectory.

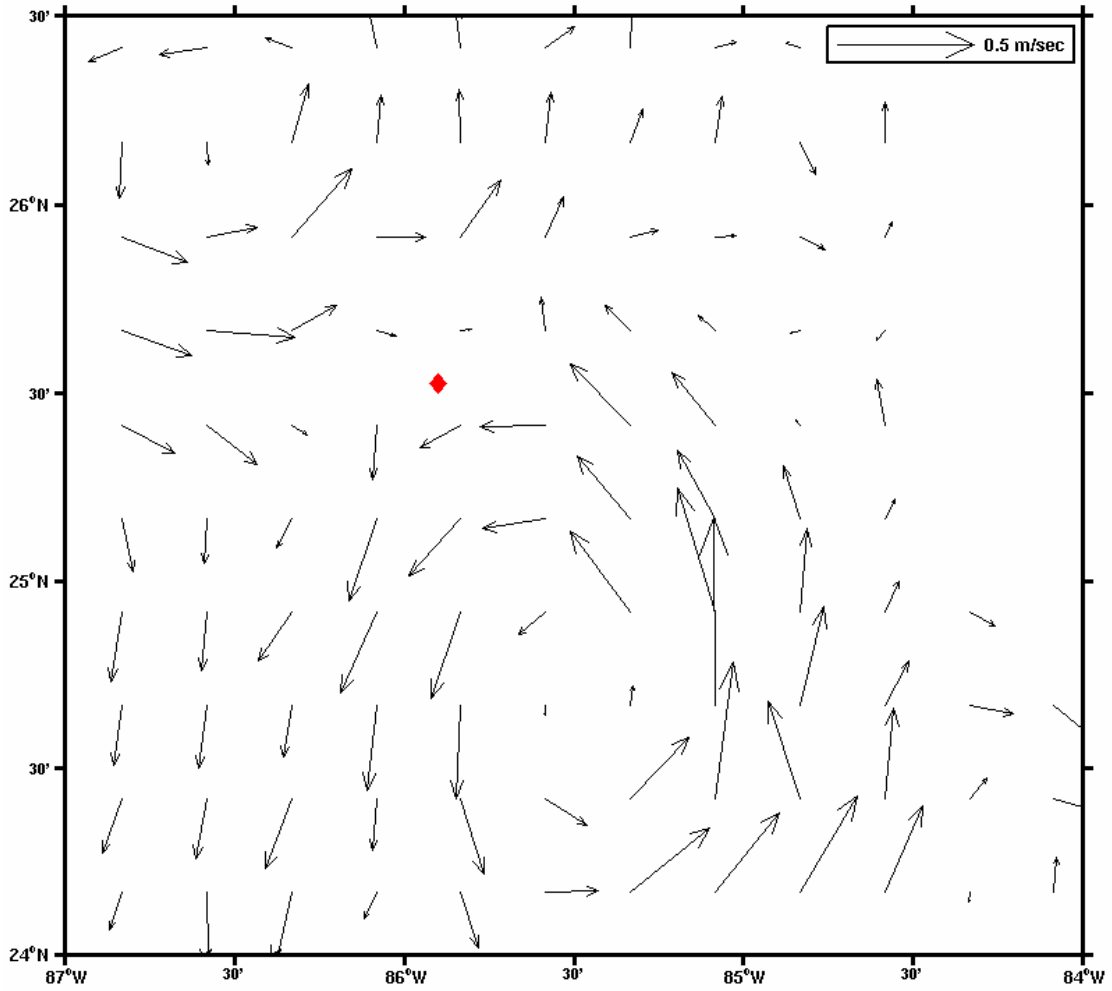


Figure 5-29: Velocities near hyperbolic structure A1 at 400 m on April 16. The red diamond denotes the position of hyperbolic trajectory.

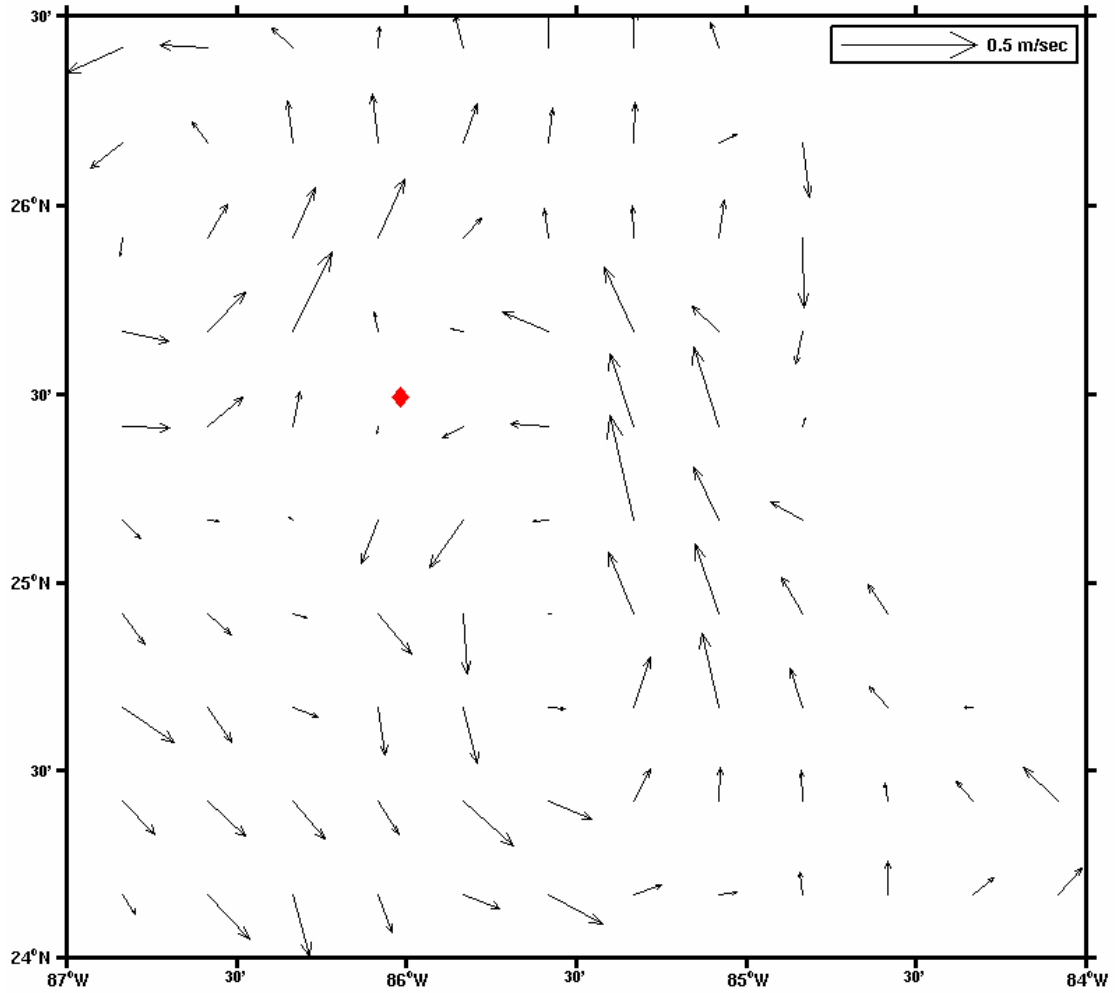


Figure 5-30: Velocities near hyperbolic structure A1 at 1100 m on April 16. The red diamond denotes the position of the hyperbolic trajectory.

5.3 Hyperbolic Structure A2

5.3.1 Hyperbolic Trajectory Paths

Hyperbolic structure A2 was studied from April 10, 1998 to April 20, 1998. Figure 5-31 shows the position of the hyperbolic trajectory from 10 to 125 m. In the upper depths (10-50 m), the paths of the hyperbolic trajectories arc from the northeast to the southwest and then back to the southeast. At the lower depths (75-125 m), the hyperbolic trajectories move in a fairly straight line from the northwest to the southeast. There is a slight change in the shape of the trajectories at 75 meters from the circular motion to the straight-line motion, though from 10-50 m, the circular motion decreased with depth. This change is not nearly as distinct and abrupt as the one we found in A1. This structure clearly maintains its integrity and cannot be interpreted as two separate regions. Also, note that the hyperbolic trajectory moves a much greater total distance in the upper levels than in the lower levels. This is discussed more in Section 5.3.2.

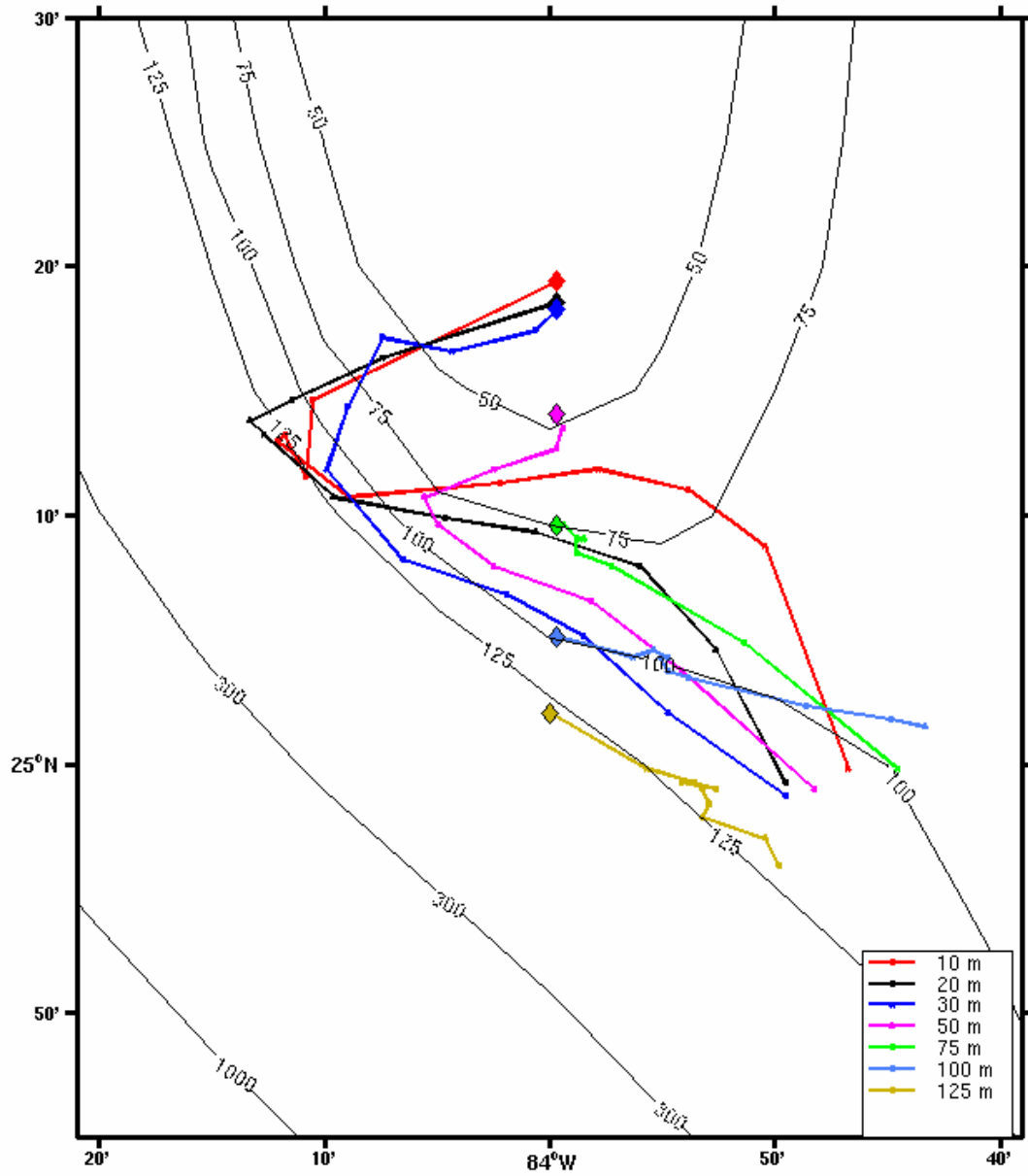


Figure 5-31: Path of the hyperbolic structure A2 from 10 to 125 m. The colors correspond to the depths as noted in the legend. The large diamonds denote the initial position of the hyperbolic trajectory on April 10. The contours are bottom bathymetry (in m).

5.3.2 Distance Moved per Day

The distances moved per day by hyperbolic trajectory A2 at each depth is now examined. Like A1 (see section 5.2.2), there is day-to-day variability as well as variability with depth.

Table 5-10 through 5-12 show the distances moved each day as well as the average distance moved over the period April 10 to April 20. At 10 m (Table 5-10), there is a much wider range of values than what was found for hyperbolic structure A1. The minimum distance in this case is 0.73 km from April 13 to April 14 and the maximum value is 20.15 km from April 10 to April 11. At 50 m (Table 5-11) the minimum value is 0.52 km from April 10 to April 11 and the maximum value is 13.22 km from April 19 to April 20. At 125 m (Table 5-12), the minimum value is 0.73 km from April 15 to April 16 and the maximum is 8.37 km from April 10 to April 11. The smaller range of values is expected since we are going down the water column. Table 5-13 shows that there is also large depth-to-depth variability associated this hyperbolic structure.

Table 5-10: Table of distance traveled in kilometers for hyperbolic trajectory at 10 m for hyperbolic structure A2. The minimum and maximum values are highlighted in yellow.

| Date | Longitude (°W) | Latitude (°N) | East (km) | North (km) | Dist (km) |
|-------------|-----------------------|----------------------|----------------------------------|-------------------|------------------|
| 4/10/98 | -84.00 | 25.32 | | | |
| 4/11/98 | -84.18 | 25.24 | -18.15 | -8.77 | 20.15 |
| 4/12/98 | -84.18 | 25.19 | -0.52 | -5.68 | 5.70 |
| 4/13/98 | -84.20 | 25.22 | -1.56 | 3.10 | 3.47 |
| 4/14/98 | -84.20 | 25.22 | -0.52 | -0.52 | 0.73 |
| 4/15/98 | -84.15 | 25.18 | 5.19 | -4.13 | 6.63 |
| 4/16/98 | -84.04 | 25.19 | 11.42 | 1.03 | 11.47 |
| 4/17/98 | -83.96 | 25.20 | 7.27 | 1.03 | 7.34 |
| 4/18/98 | -83.90 | 25.18 | 6.75 | -1.55 | 6.92 |
| 4/19/98 | -83.84 | 25.15 | 5.71 | -4.13 | 7.05 |
| 4/20/98 | -83.78 | 25.00 | 6.23 | -16.53 | 17.67 |
| | | | | | |
| | | | Average Velocity (km/day) | | 4.36 |

Table 5-11: Table of distance traveled in kilometers for hyperbolic trajectory at 50 m for hyperbolic structure A2. The minimum and maximum values are highlighted in yellow.

| Date | Longitude (°W) | Latitude (°N) | East (km) | North (km) | Dist (km) |
|-------------|-----------------------|----------------------|----------------------------------|-------------------|------------------|
| 4/10/98 | -84.00 | 25.23 | | | |
| 4/11/98 | -84.00 | 25.23 | 0.00 | -0.52 | 0.52 |
| 4/12/98 | -83.99 | 25.23 | 0.52 | -0.52 | 0.73 |
| 4/13/98 | -84.00 | 25.21 | -0.52 | -1.55 | 1.63 |
| 4/14/98 | -84.04 | 25.20 | -4.67 | -1.55 | 4.92 |
| 4/15/98 | -84.09 | 25.18 | -5.19 | -2.06 | 5.59 |
| 4/16/98 | -84.08 | 25.16 | 1.04 | -2.07 | 2.31 |
| 4/17/98 | -84.04 | 25.13 | 4.15 | -3.10 | 5.18 |
| 4/18/98 | -83.97 | 25.11 | 7.27 | -2.58 | 7.71 |
| 4/19/98 | -83.90 | 25.06 | 6.75 | -5.17 | 8.50 |
| 4/20/98 | -83.80 | 24.98 | 9.87 | -8.79 | 13.22 |
| | | | | | |
| | | | Average Velocity (km/day) | | 5.03 |

Table 5-12: Table of distance traveled in kilometers for hyperbolic trajectory at 125 m for hyperbolic structure A2. The minimum and maximum values are highlighted in yellow.

| Date | Longitude (°W) | Latitude (°N) | East (km) | North (km) | Dist (km) |
|---------|----------------|---------------|----------------------------------|------------|-----------|
| 4/10/98 | -84.00 | 25.03 | | | |
| 4/11/98 | -83.93 | 25.00 | 7.28 | -4.14 | 8.37 |
| 4/12/98 | -83.89 | 24.99 | 3.64 | -1.03 | 3.78 |
| 4/13/98 | -83.90 | 24.99 | -1.04 | 0.00 | 1.04 |
| 4/14/98 | -83.88 | 24.98 | 2.60 | -0.52 | 2.65 |
| 4/15/98 | -83.89 | 24.99 | -1.56 | 0.52 | 1.64 |
| 4/16/98 | -83.89 | 24.98 | 0.52 | -0.52 | 0.73 |
| 4/17/98 | -83.88 | 24.97 | 0.52 | -1.03 | 1.16 |
| 4/18/98 | -83.89 | 24.96 | -0.52 | -1.03 | 1.16 |
| 4/19/98 | -83.84 | 24.95 | 4.68 | -1.55 | 4.93 |
| 4/20/98 | -83.83 | 24.93 | 1.04 | -2.07 | 2.32 |
| | | | | | |
| | | | Average Velocity (km/day) | | 2.78 |

Table 5-13: Depth-to-depth variability in km on April 10-11 and April 15-16.

| Depth (m) | 11-Apr | 16-Apr |
|-----------|--------|--------|
| 10 | 20.15 | 11.47 |
| 50 | 0.52 | 2.31 |
| 125 | 8.37 | 0.73 |

The average distance moved at each depth for hyperbolic structure A2 is shown in Table 5-14 below. The average values are all small; much smaller than the average values of A1 at corresponding layers. There is also an increase in the average from 10 m to 20 m, which is different than the trend found for A1. The values are all close, which implies that the structure is fairly uniform though the water column.

Table 5-14: Mean distance traveled for hyperbolic structure A2. The distances are in km/day.

| | Mean Distance |
|------------------|----------------------|
| Depth (m) | km/day |
| 0 | N/A |
| 10 | 4.36 |
| 20 | 7.6 |
| 30 | 6.73 |

| | Mean Distance |
|------------------|----------------------|
| Depth (m) | km/day |
| 50 | 5.03 |
| 75 | 3.3 |
| 100 | 3.01 |
| 125 | 2.78 |

5.3.3 Chaotic Properties of the Hyperbolic Trajectories

The chaotic nature of trajectories near hyperbolic structure A1 (section 5.2.3) can also be seen for A2. Figures 5-32 and 5-33 show trajectories of particles nearby the hyperbolic trajectory for 10 and 50 m depths. At 10 m (Figure 5-32) the particles to the east (blue), west (red) and south (green) initially follow a similar pattern as the hyperbolic trajectory but they move a much greater distance on that path. The particle to the north (magenta) diverges to the north of the hyperbolic trajectory. At 50 m (Figure 5-33), the particle to the south (green) again follows a similar pattern but it moves a much great distance than the hyperbolic trajectory. The particles to the east (blue) and west (red) diverge to the north and follow similar patterns as each other. The particle to the north gets affected by the topography and only moves a small distance, as shown in the zoomed image of Figure 5-33.

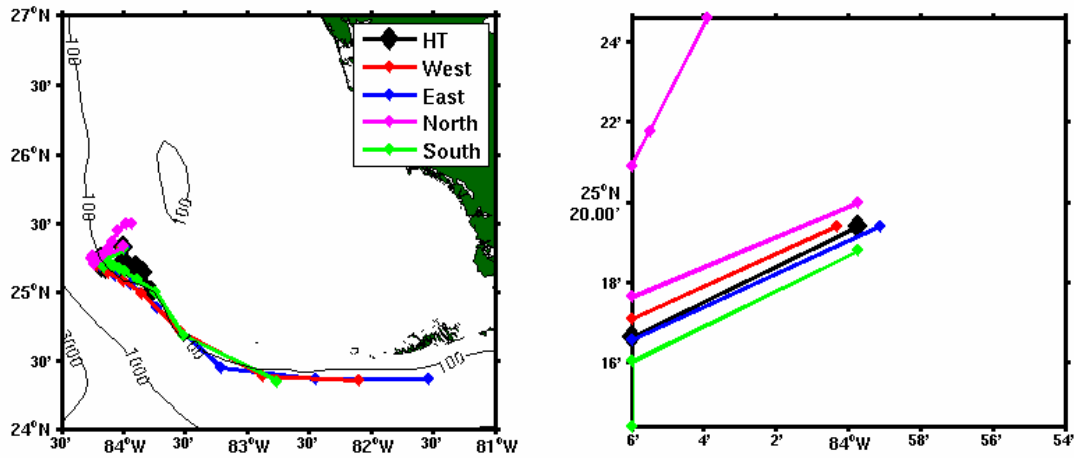


Figure 5-32: Paths of the hyperbolic trajectory and four particles initialized 1 km north, south, east and west of it at 10 m from April 10 to April 20. Colors correspond to positions as noted by the legend. The image to the right is zoomed in on the initial positions. The contours are bottom bathymetry (in m).

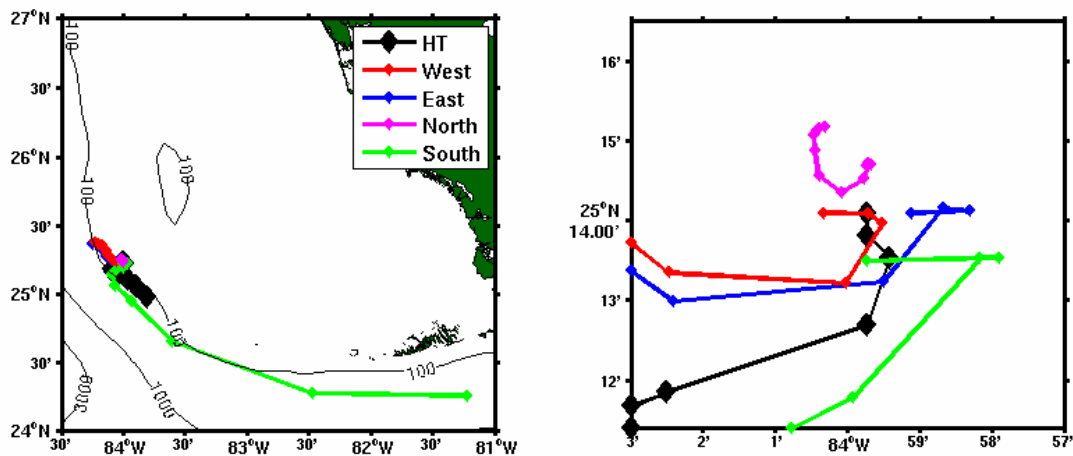


Figure 5-33: Same as Figure 5-32 for 50 m.

Figure 5-34 and Figure 5-35 show the natural log of the separation of the hyperbolic trajectory and the nearby particles over the first 6 days. A line of slope f (Coriolis parameter) is again shown for comparison. At 10 m (Figure 5-34), the separation of the particles is fairly consistent, as evident by the almost straight lines. The rates of separation are one order of magnitude less than Coriolis, $0.05 f$. At 50 m (Figure 5-35), there is a very similar pattern with the same consistent rates of separation and approximate equal separation values. The rates are again $0.05 f$. The decrease in the rates of separation when compared to those for A1 could be due to hyperbolic structure A2's location on the shelf, rather than in the deep Gulf, like A1. Of course, other factors may also be important.

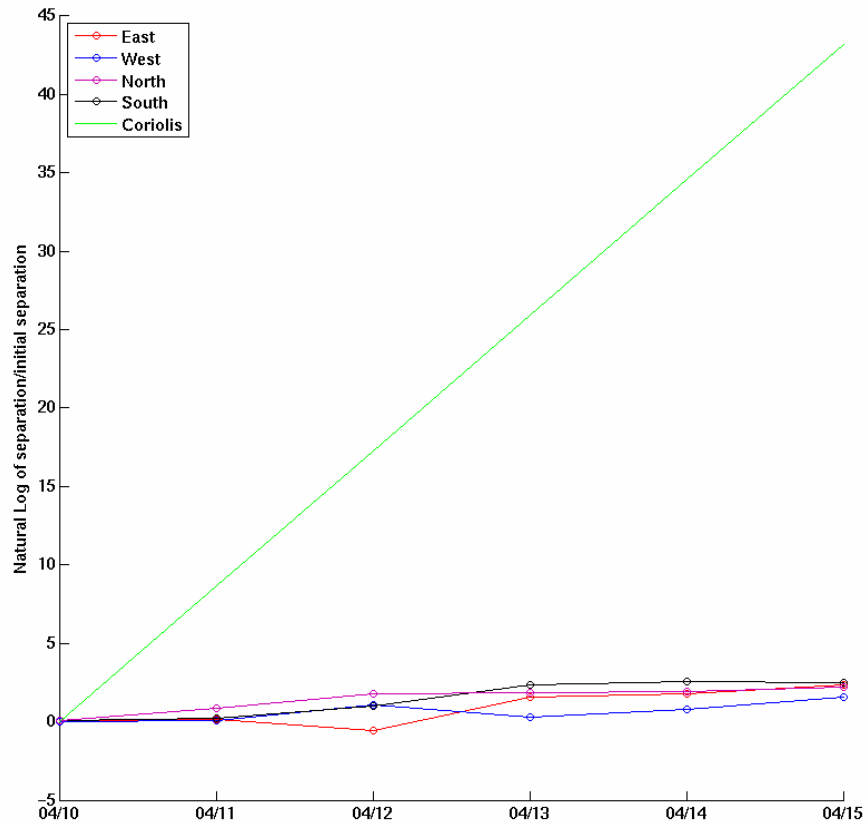


Figure 5-34: Natural log of separation/initial separation versus time for the hyperbolic trajectory and four particles initialized 1km to the north, south, east, and west of hyperbolic trajectory A2 at 10 m. The colors correspond to the positions as noted in the legend. The green line is a line with slope of f (Coriolis parameter).

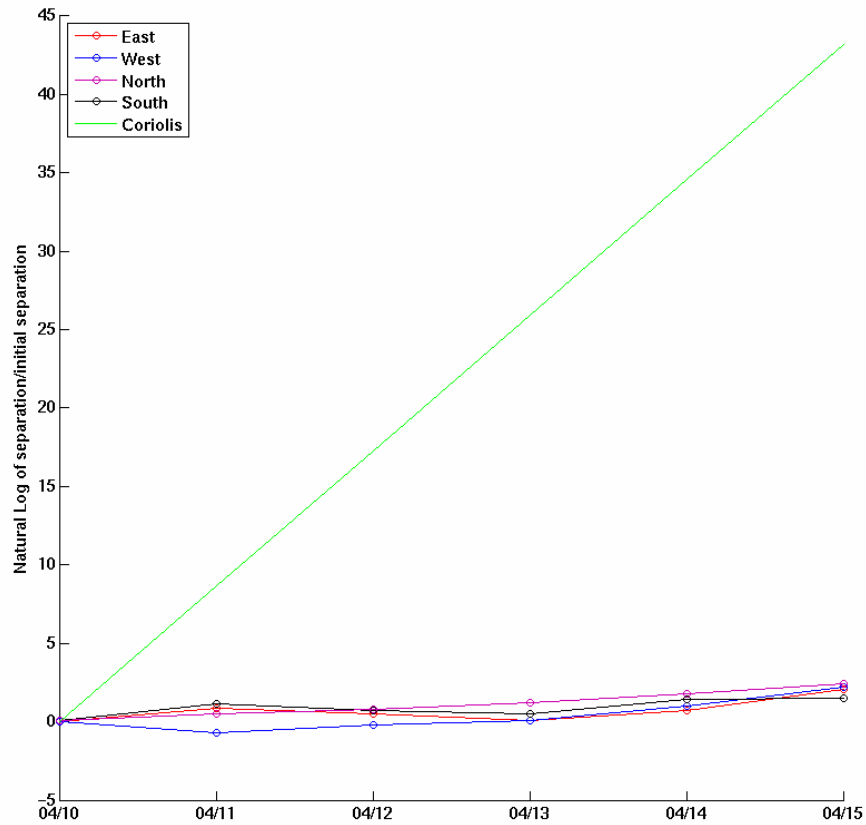


Figure 5-35: Same as Figure 5-34 for 50 m.

We find also that the hyperbolic trajectories for A2 and the particles initialized 1 km to the north, south, east and west of the hyperbolic trajectory follow different contours of geopotential, salinity and temperature. At 10 m (Figure 5-36), the particles clearly diverge from the geopotential after 2 days. All the particles follow similar patterns of temperature as well as salinity, though in both these cases, the divergences are not clear until five and seven days respectively.

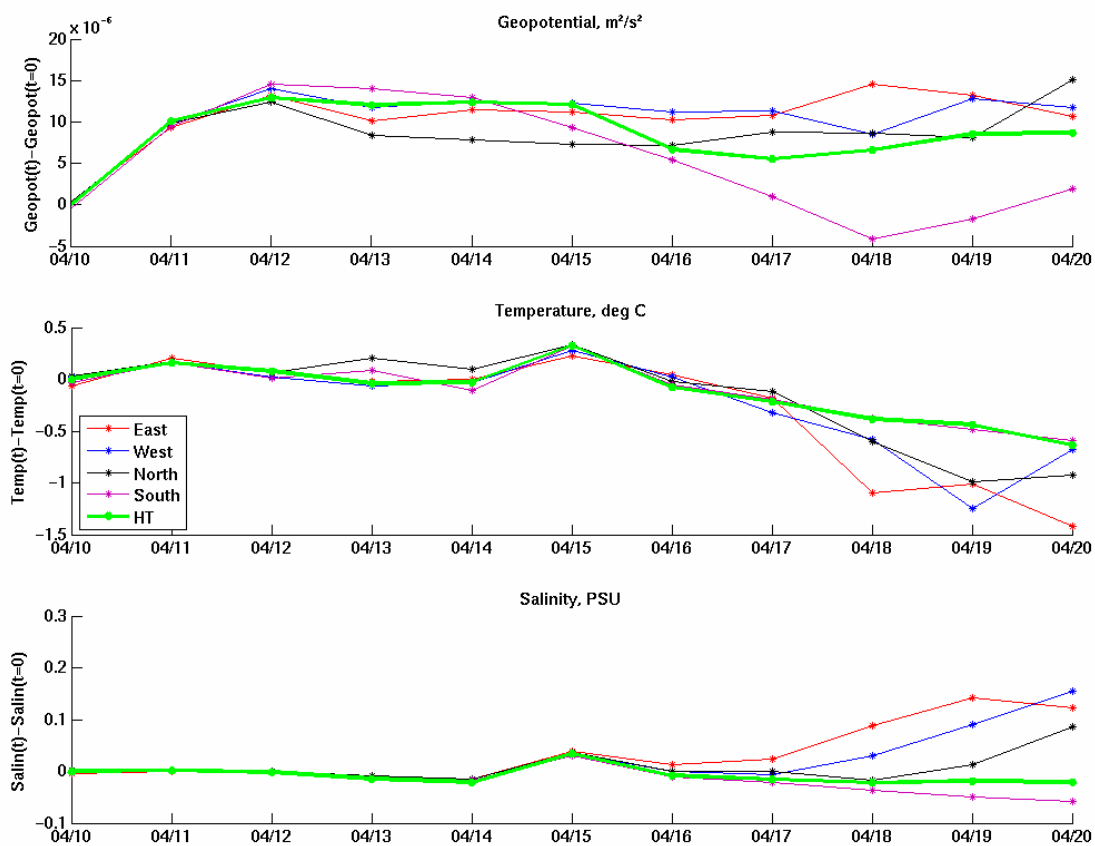


Figure 5-36: Difference in geopotential, temperature and salinity from the hyperbolic trajectory’s initial value for the hyperbolic trajectory and four particles initialized 1 km north, south, east and west of the hyperbolic trajectory at 10 m. The colors correspond to positions as denoted in the legend above. Shown from April 10 to April 20.

5.3.4 Vertical Extent of Hyperbolic Structure A2

Hyperbolic structure A2 closely hugs the shelf break during its entire lifetime and can be tracked at depths down to 125 m, as shown in Figure 5-31. The local bottom topography strongly influences the position of the hyperbolic trajectory

associated with A2 at each depth. Figure 5-37 shows that hyperbolic trajectory likes up against the bottom when it first forms on April 10.

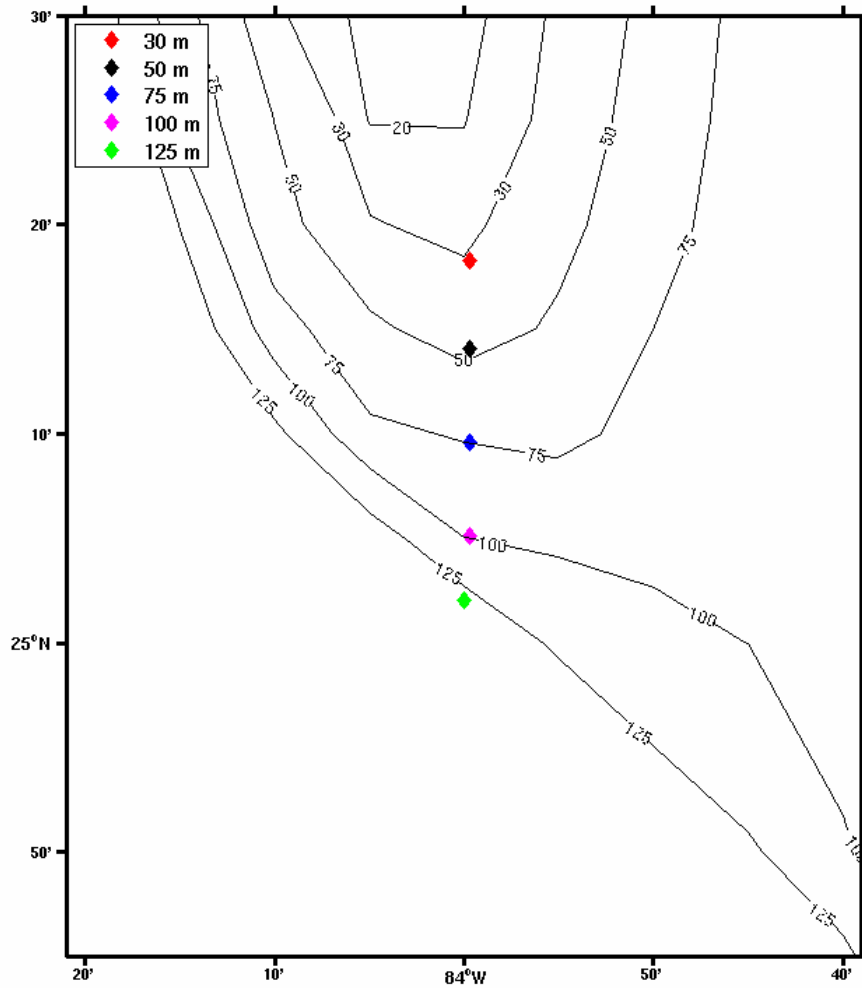


Figure 5-37: Positions of the hyperbolic trajectories associated with A2 for five depths ranging from 30 to 125 m on April 10. The colors correspond to the depths as noted in the legend.

As shown in Figure 5-31, the hyperbolic trajectories for A2 at 10-50 m move away from the bottom toward deeper water with time. The hyperbolic trajectories at 75-125 m remain affected by the bathymetry. The hyperbolic trajectories at both 100 and 125 m follow their respective depth contours. Therefore, it is noted that the lower levels remain affected by the bottom bathymetry throughout the whole lifetime of the hyperbolic structure.

5.3.5 Three-Dimensional Structure

Figures 5-38 through 5-41 show plan and three-dimensional views of A2 in a 50 km x 50 km area around the hyperbolic structure on April 11 and April 15, 1998. The hyperbolic trajectories start in the northwest and move to the southeast. Figures 5-42 and 5-43 show the movement of the hyperbolic structure from April 10 to April 20 from two different perspectives.

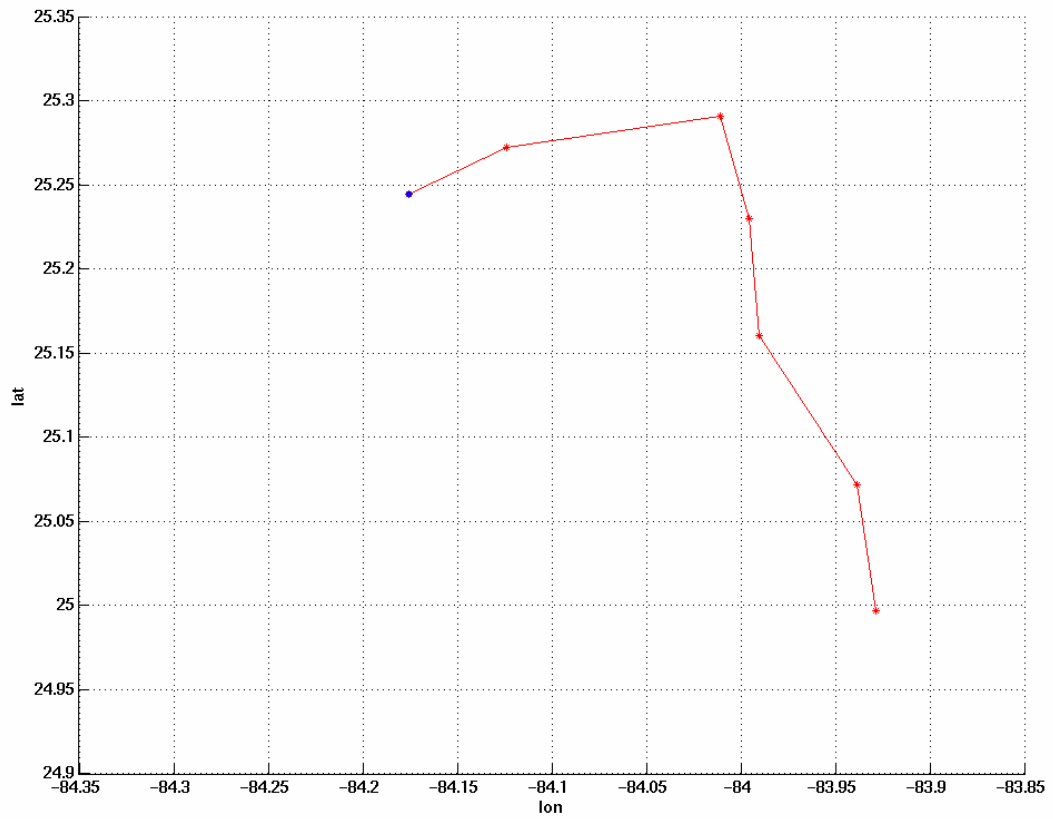


Figure 5-38: Plan view of the hyperbolic structure A2 on April 11. The blue dot denotes the position at 10 m.

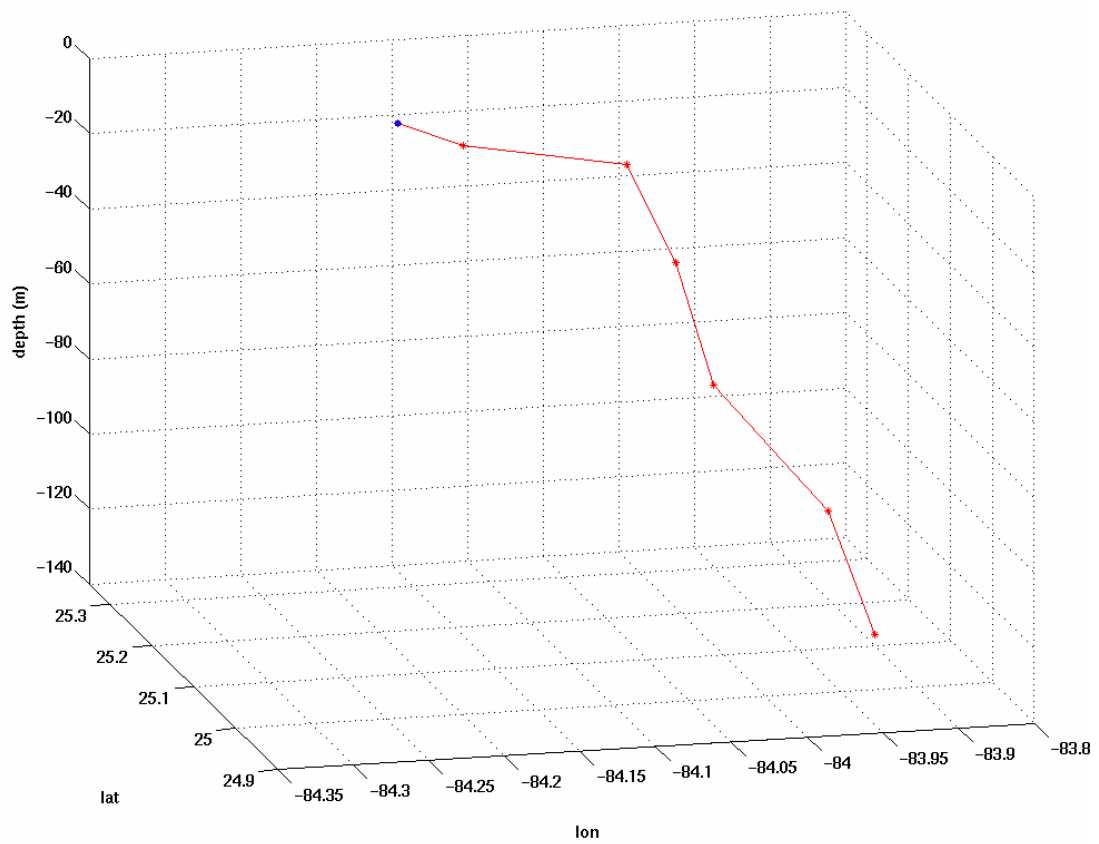


Figure 5-39: Three-dimensional view of the hyperbolic structure A2 on April 11. The blue dot denotes the position at 10 m.

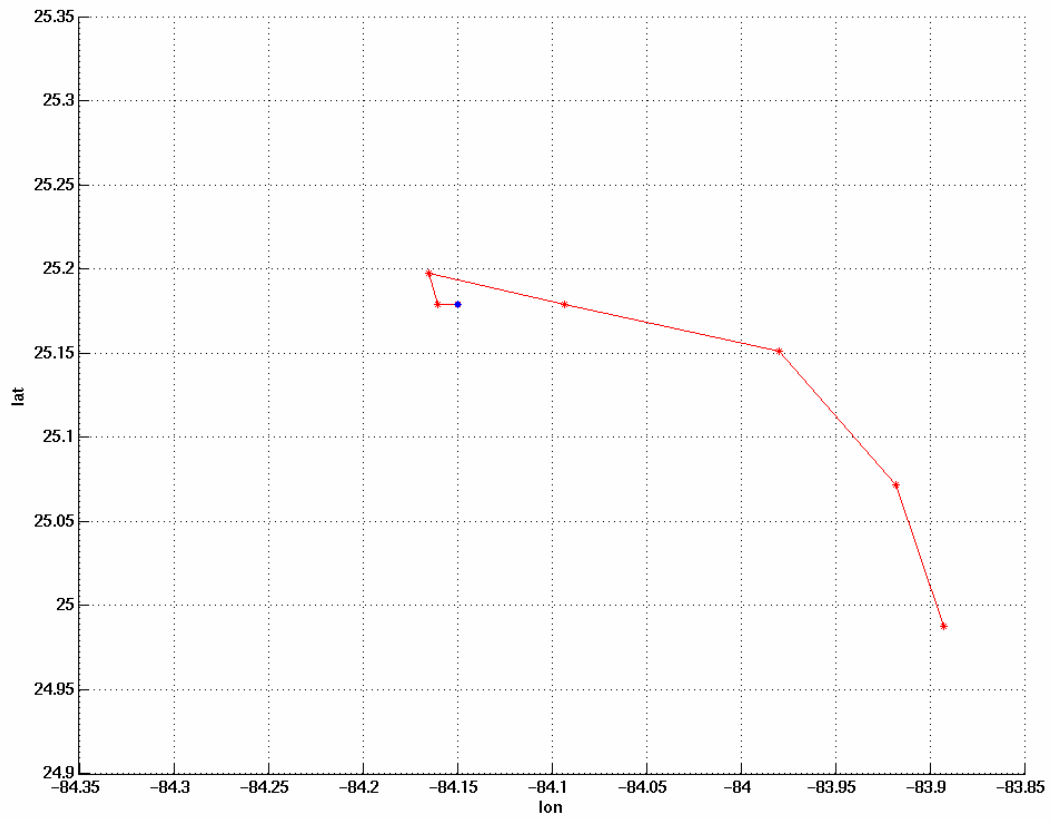


Figure 5-40: Plan view of the hyperbolic structure A2 on April 15. The blue dot denotes the position at 10 m.

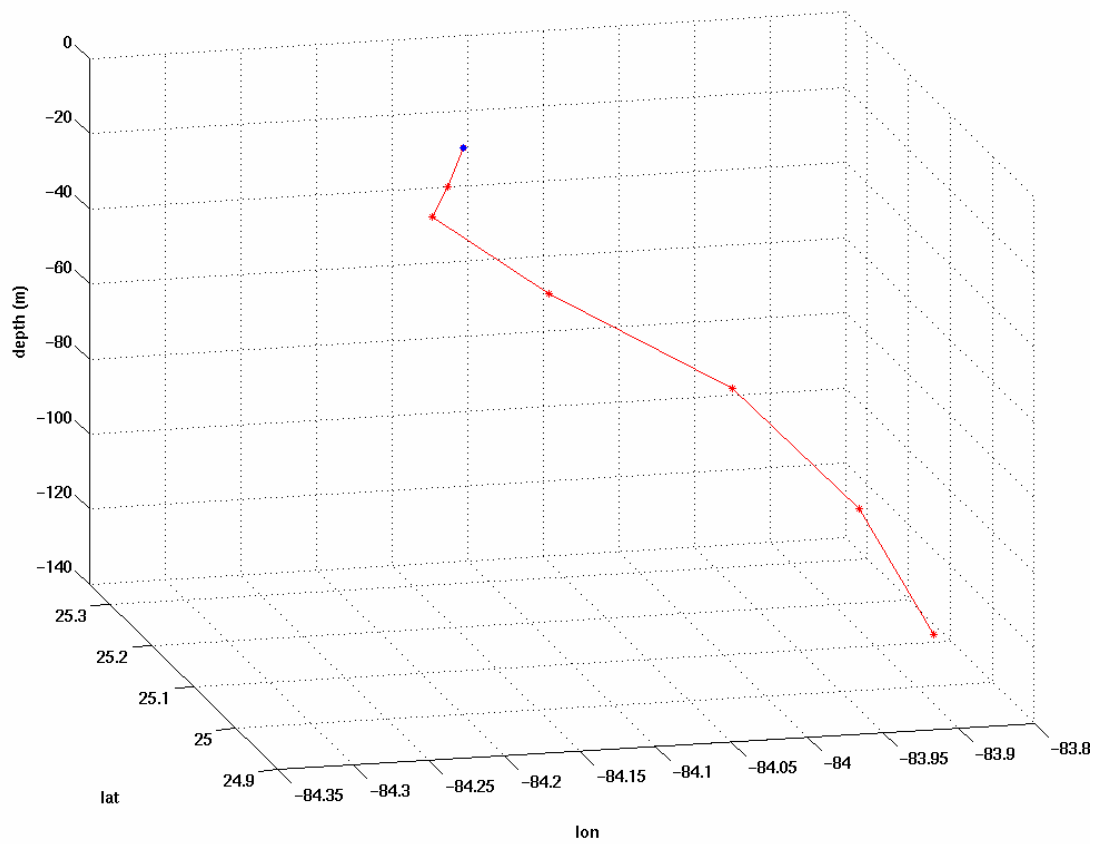


Figure 5-41: Three-dimensional view of the hyperbolic structure A2 on April 15. The blue dot denotes the position at 10 m.

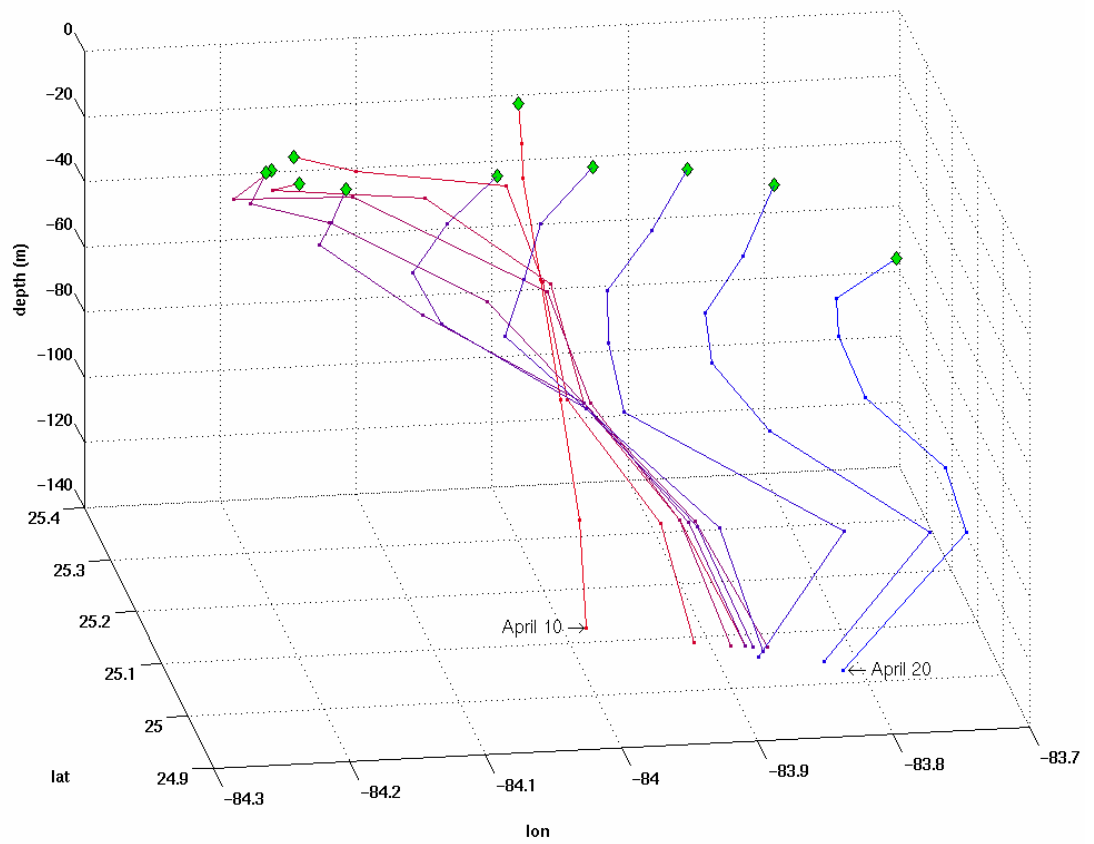


Figure 5-42: Three-dimensional view of the evolution of hyperbolic structure A2 from April 10 (red) to April 20 (blue). The green diamond denotes the position at 10 m.

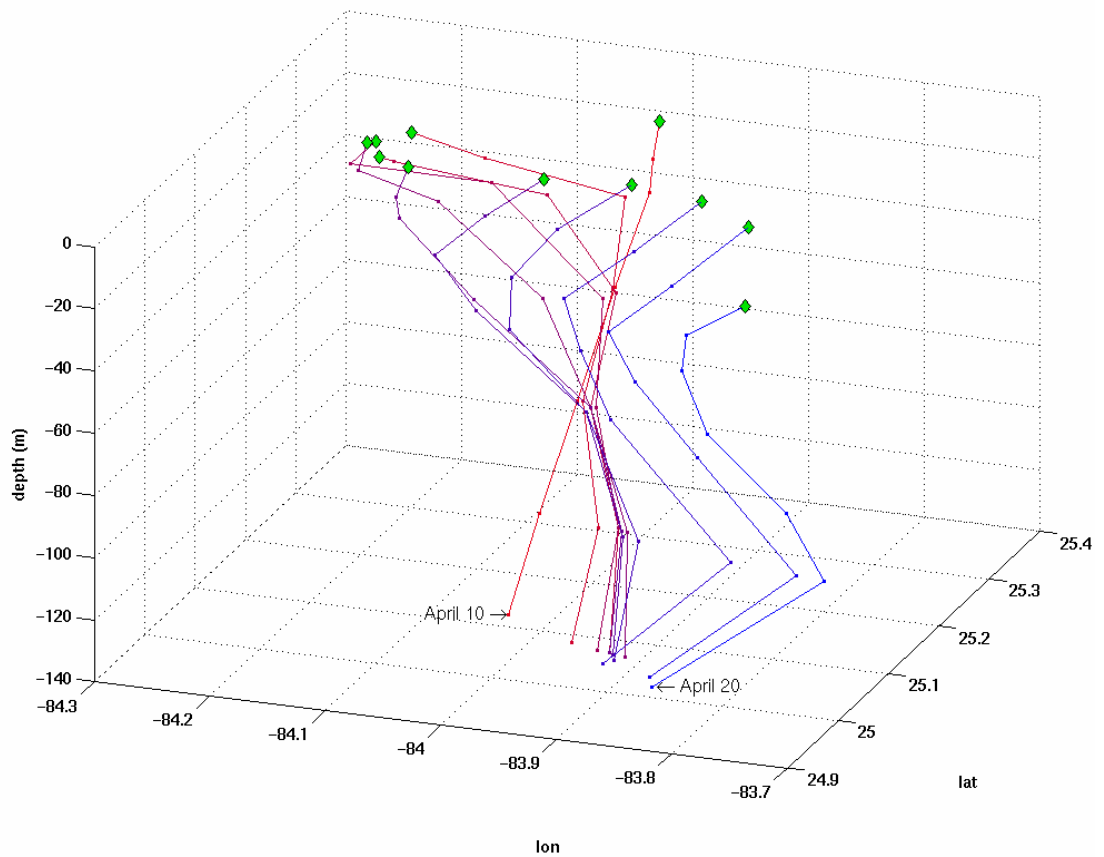


Figure 5-43: Same as Figure 5-42 but at a perspective from the right.

5.4 Advective Channel

The outflowing manifold of A1 and the inflowing manifold of A2 form an advective channel. Toner et al. (2003) showed that these manifolds at 50 meters align closely with a chlorophyll plume. This advective channel, though, is not only at 50-meters; it extends from the surface to 75 m.

5.4.1 Depth of the Channel

The advective channel is only present up to 75 m. Figure 5-44 and Figure 5-45, shown on April 16, show that below 75 m, no advective channel is present. The surface is ignored, consistent with the previous results and upon closer inspection the channel at 10 m is not clearly defined, due to the effect of surface processes. At 20 m, the channel between the two curves is clearly defined. At 30 m, 50 m and 75 m, the channel between the two curves is wide and clearly shown. At 100 m the channel is no longer defined since the outflowing manifold does not form the channel. At 125 m, the channel is clearly not defined since the outflowing manifold of hyperbolic structure A1 does not have time to form the advective channel with the inflowing manifold of hyperbolic structure A2. At 150 m A2 is no longer present. Therefore, the channel begins at 20 m and ends somewhere between 75 m and 100 m.

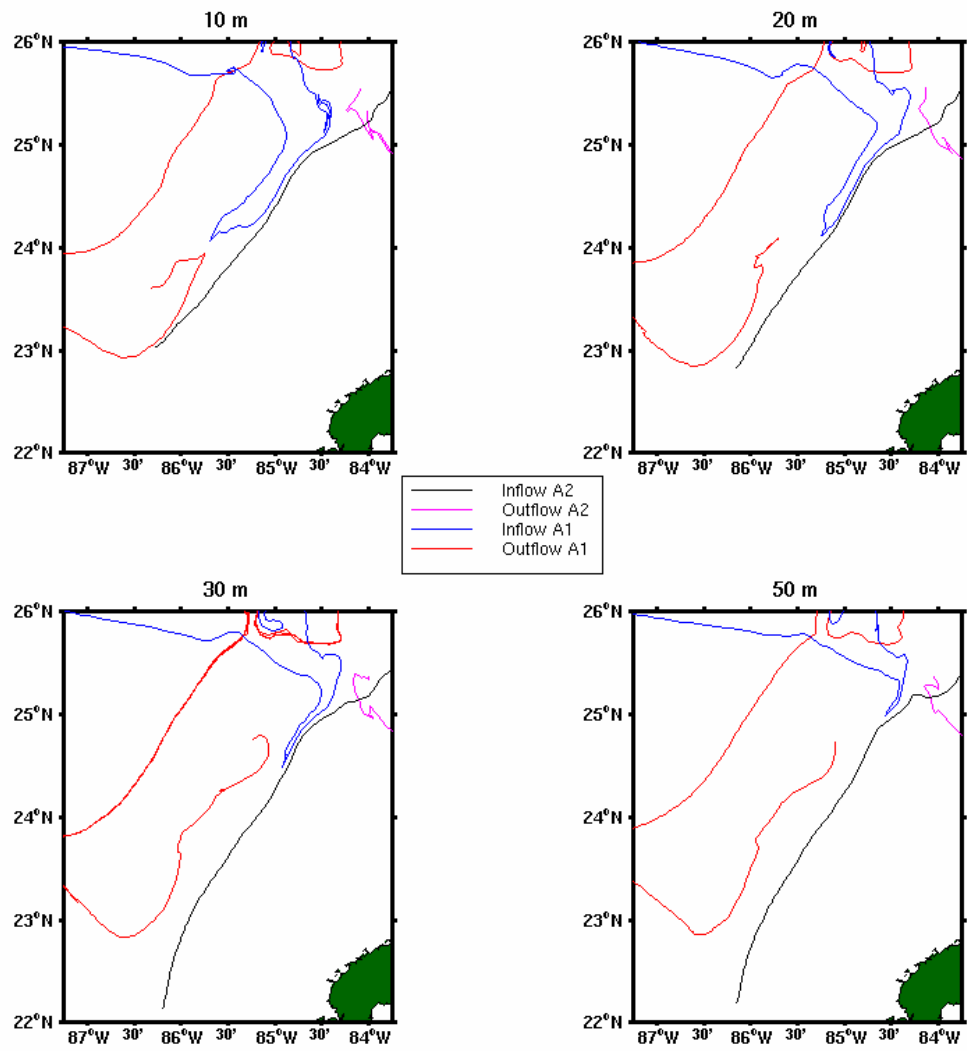


Figure 5-44: Inflowing and outflowing manifolds for depths 10-50 m for both A1 and A2 on April 16, 1998.

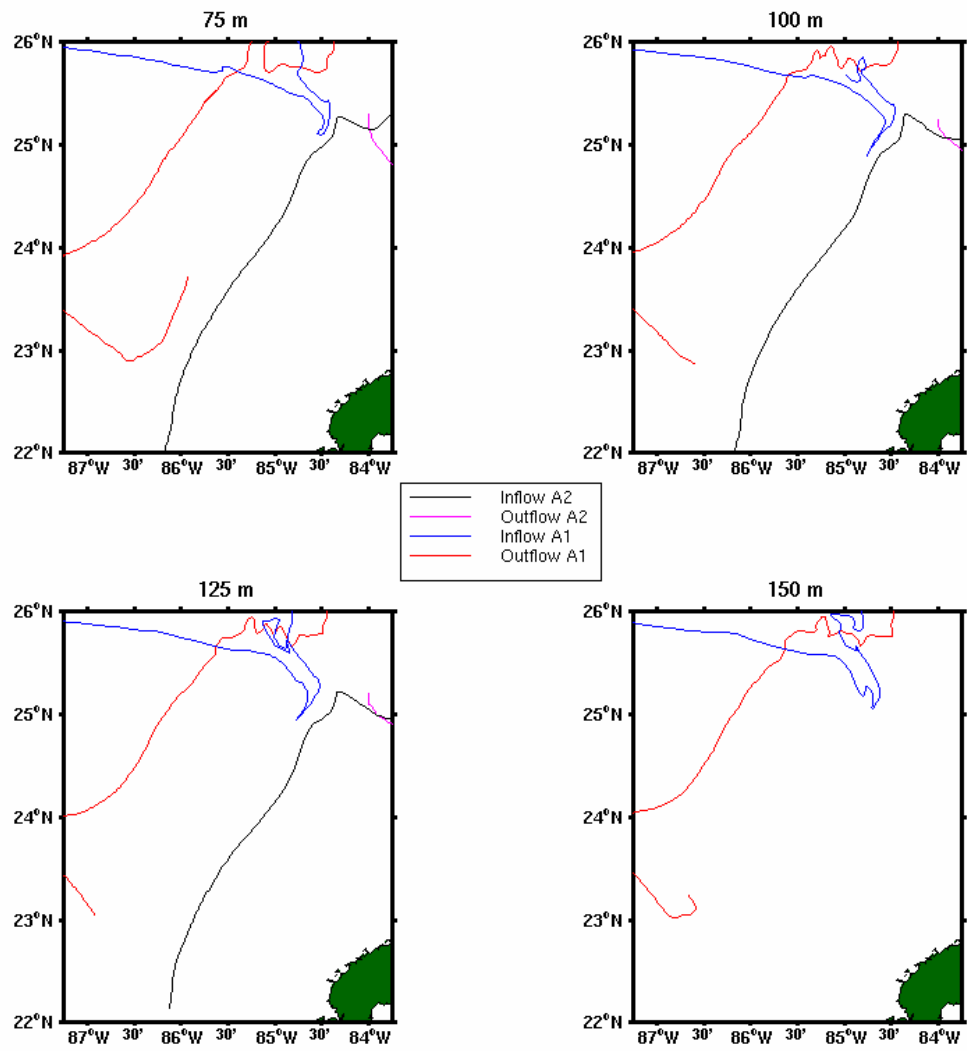


Figure 5-45: Inflowing and outflowing manifolds at depths 75-125 m for both A1 and A2 and 150 m for A1 on April 16, 1998.

5.4.2 Three-Dimensional Channel

From April 14 to April 18, 1998, a three-dimensional advective channel exists at depths 10-75 m, formed by the outflowing manifolds of A1 and the inflowing manifolds of A2. Figures 5-46 through 5-50 show daily pictures of the advective channel during this period.

On April 14 (Figure 5-46), the advective channel is well defined between 20 and 75 m. The outflowing manifolds of A1 have just begun to curl to far enough to the northeast to create the advective channel. On April 15 (Figure 5-47), the channel is more clearly defined down to 75 m. On April 16 and 17 (Figures 5-48 and 5-49), there is no channel at 10 m or 100 m. On April 18 (Figure 5-50) the advective channel is present only at 75 and 100 m, though it is not nearly as clearly defined as in Figure 5-48.

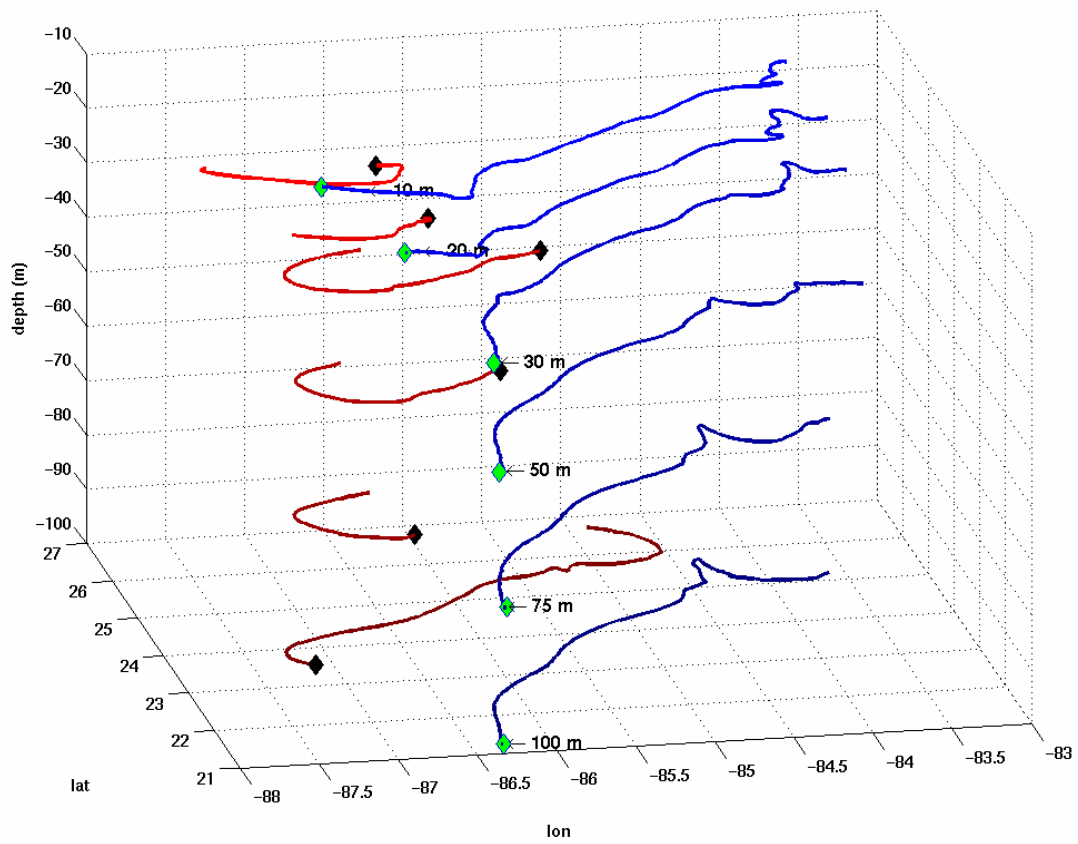


Figure 5-46: Advective channel formed by the inflowing A2 manifolds (blue) and the outflowing manifolds (red) on April 14, 1998 for depths 10-100 m. The shade of the manifold gets darker with depth.

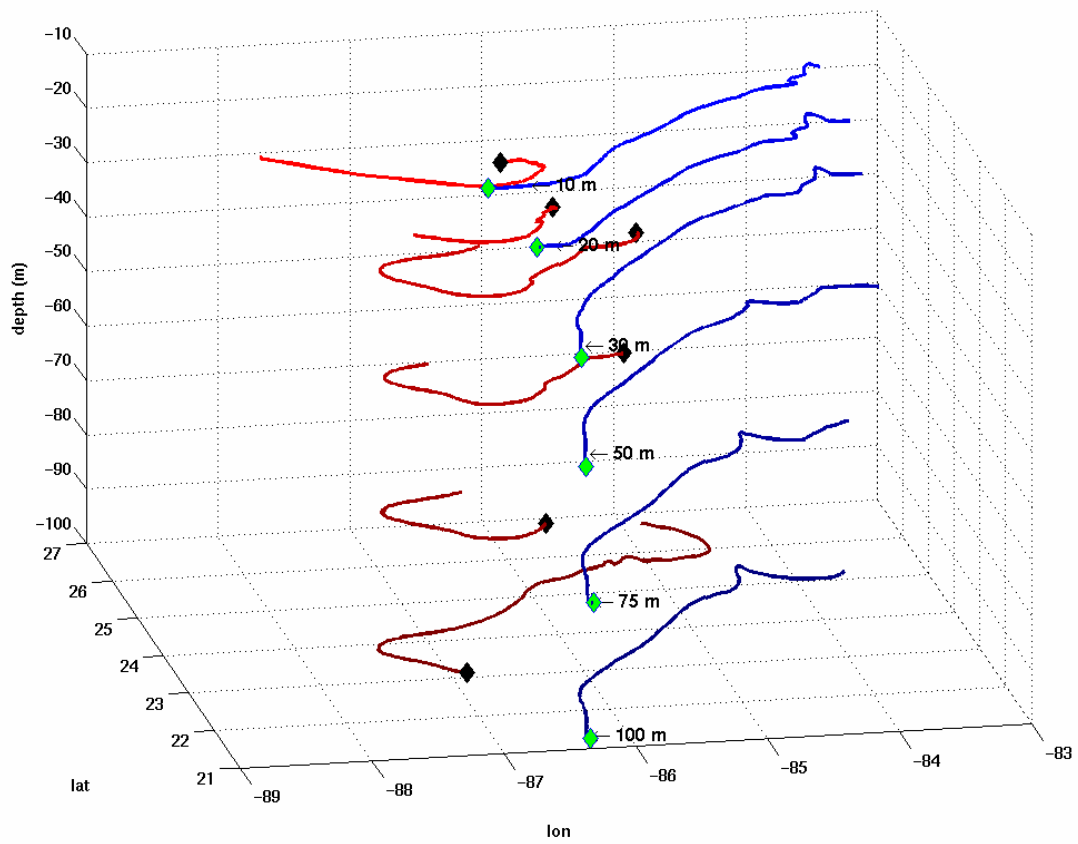


Figure 5-47: Same as Figure 5-46 for April 15, 1998.

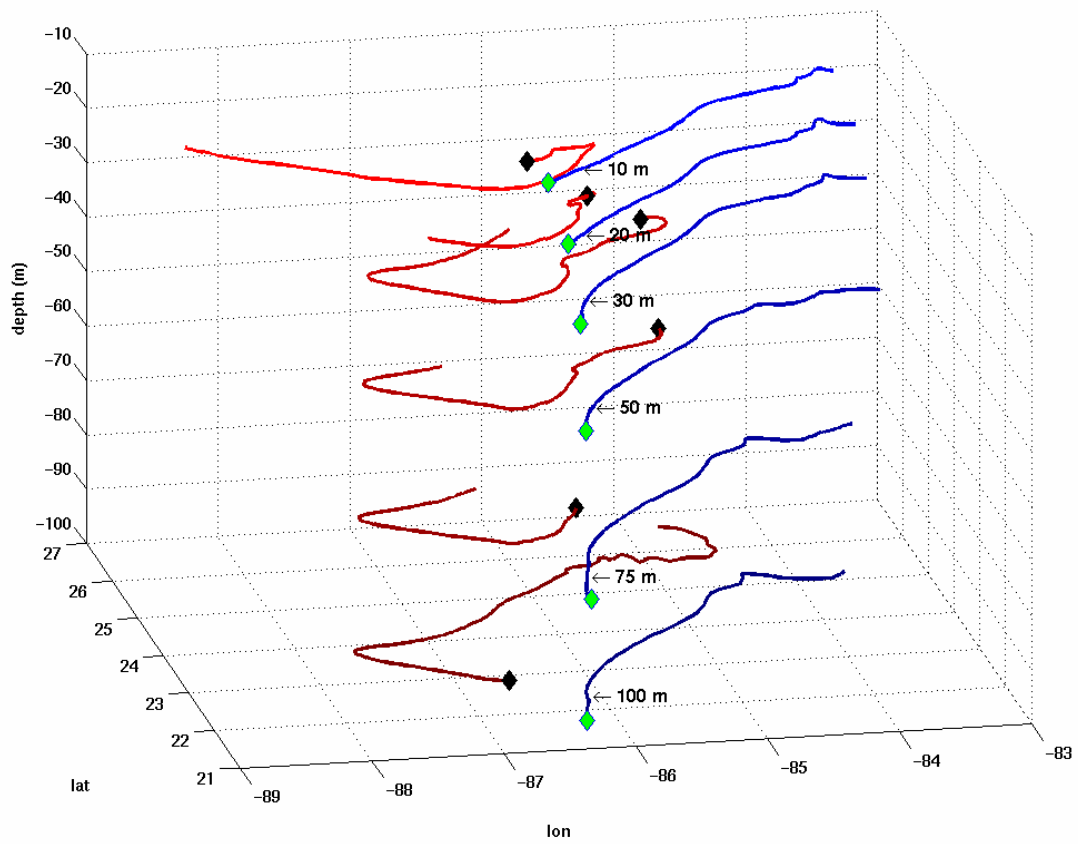


Figure 5-48: Same as Figure 5-46 for April 16, 1998.

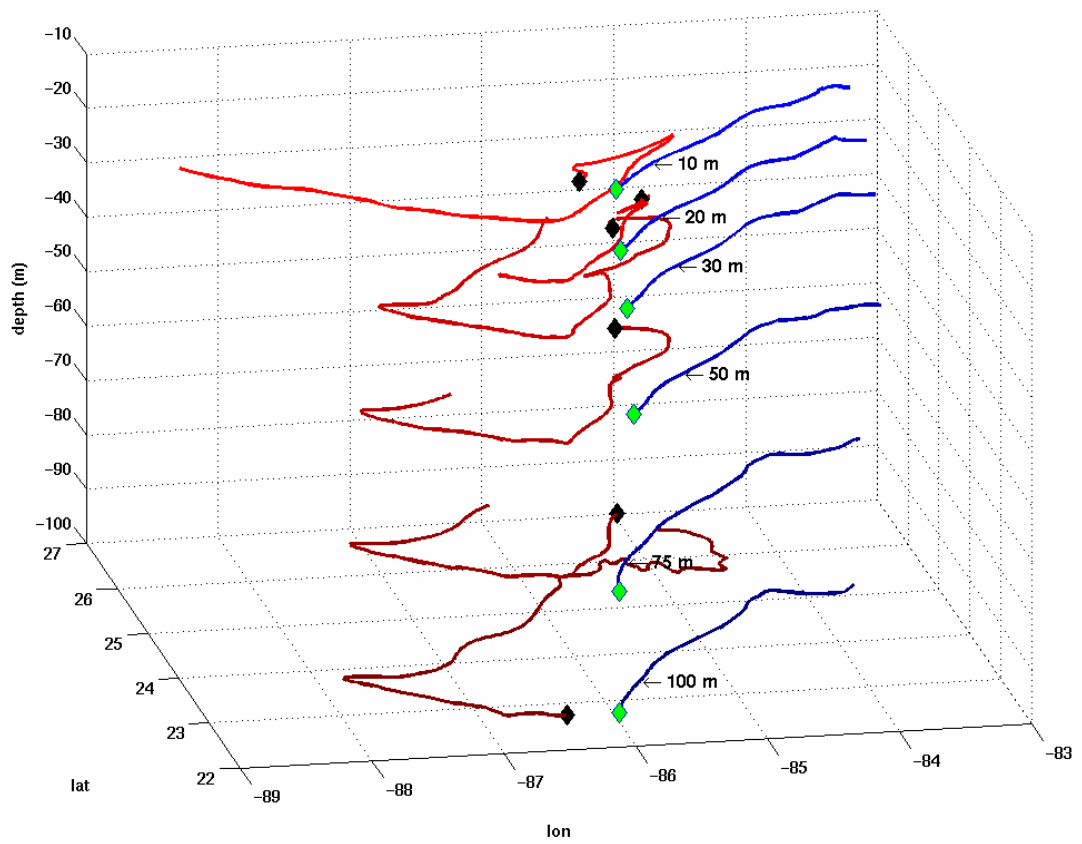


Figure 5-49: Same as Figure 5-46 for April 17, 1998.

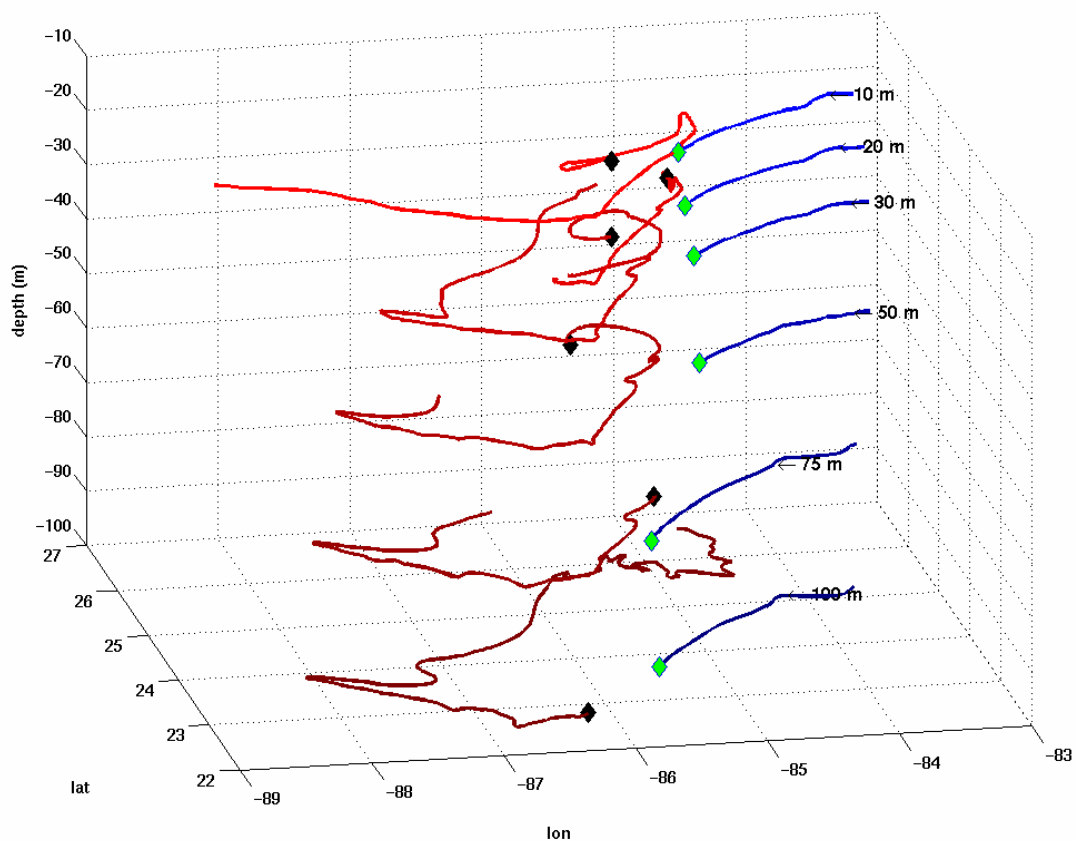


Figure 5-50: Same as Figure 5-46 for April 18, 1998.

5.4.3 Volume Transport

Toner et al. (2003) showed that the advective channel was capable of advecting chlorophyll off the Campeche Shelf and moving it 200 km across the deep Gulf to the West Florida Shelf. With a three-dimensional picture of the channel, estimates of the volume flux through the channel can be made.

Two transects across the advective channel were constructed to estimate volume flux on April 16, 1998. An example showing the transect positions at 50 m on April 16 is shown in Figure 5-51. The procedure for estimating volume flux is

1. At each depth, pick points on the outflowing manifold of A1 and inflowing manifold of A2 to define the transect.
2. The interpolated CUPOM velocities (u,v) at five points along the transect are averaged and the mean velocity component normal to the transect line is determined.
3. Transport at each depth is determined by multiplying the mean normal flow along the transect by the width of the transect.
4. Finally, volume flux is determined by multiplying each layer transport by the layer thickness and summing over all layers.

Using the above procedure, the estimated volume flux across transect A (B) was 1.4 Sv (2.6 Sv) on April 16. Details of the calculations are shown in Table 5-15.

Table 5-15: Details of the volume flux estimate calculation along two transects spanning the advect channel on April 16, 1998.

| A | South-Western Transect | | | | | |
|--|-----------------------------------|--------------------|--------------------|--------------------|---|--------------------------------------|
| <u>Depth (m)</u> | <u>Lon1</u> | <u>Lat1</u> | <u>Lon2</u> | <u>Lat2</u> | <u>Mass flux (m²/s)</u> | <u>Channel width (km)</u> |
| 20 | -85.85 | 23.38 | -85.772 | 23.34 | 7306 | 9.30 |
| 30 | -86.1 | 23.26 | -85.88 | 23.10 | 18589 | 28.65 |
| 50 | -86.13 | 23.16 | -85.86 | 23.00 | 24960 | 32.84 |
| 75 | -86.21 | 23.03 | -85.99 | 22.87 | 15558 | 28.68 |
| | | | | | | |
| Volume Flux (m³/s) | 1403740 | | | | | |
| | | | | | | |
| B | North-Eastern Transect | | | | | |
| <u>Depth (m)</u> | <u>Lon1</u> | <u>Lat1</u> | <u>Lon2</u> | <u>Lat2</u> | <u>Mass flux (m²/s)</u> | <u>Channel width (km)</u> |
| 20 | -85.49 | 24.16 | -85.30 | 24.06 | 18408 | 22.26 |
| 30 | -85.62 | 24.20 | -85.24 | 23.97 | 38868 | 45.94 |
| 50 | -85.63 | 24.17 | -85.25 | 23.93 | 39538 | 46.91 |
| 75 | -85.94 | 23.66 | -85.58 | 23.49 | 29955 | 41.50 |
| | | | | | | |
| Volume Flux (m³/s) | 2579313 | | | | | |

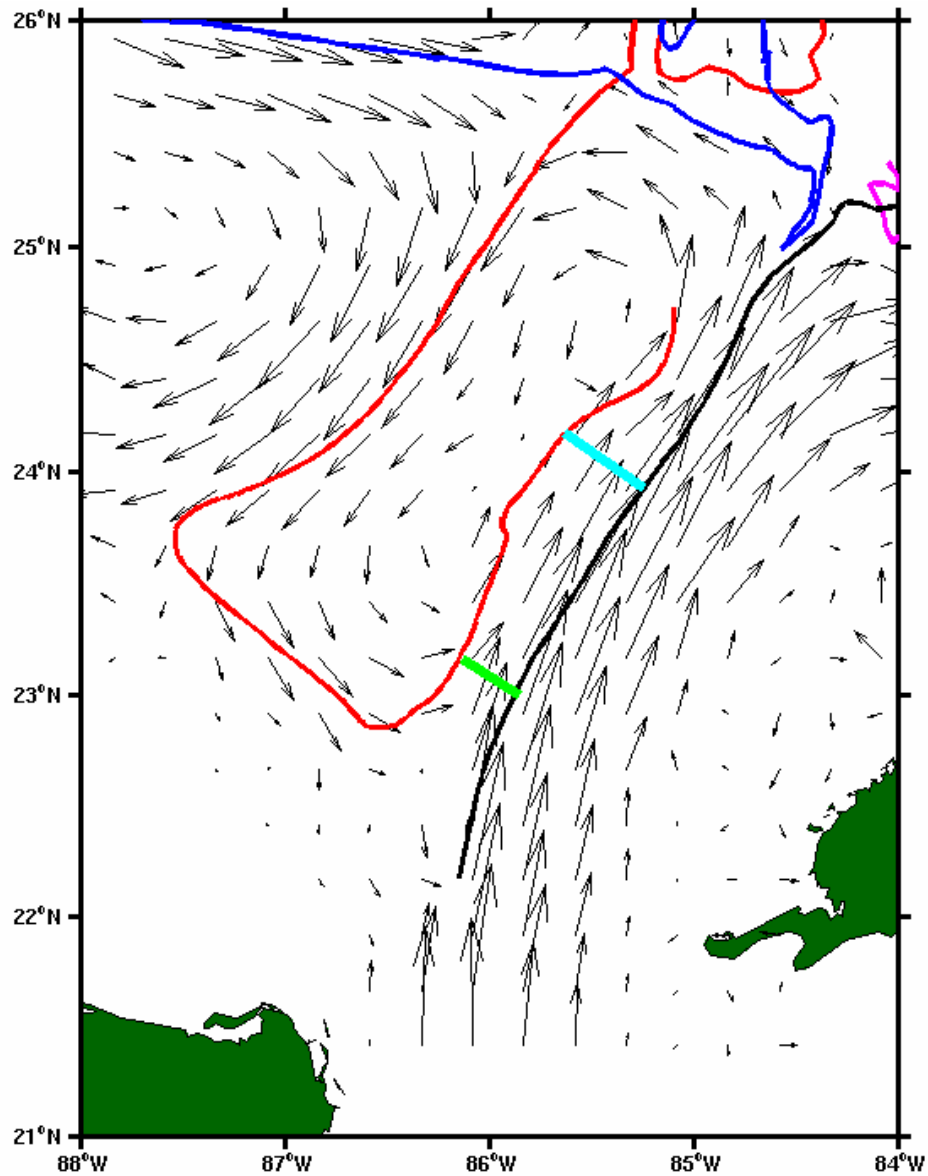


Figure 5-51: Position of transects A (green) and B (light blue) used for the volume flux estimates on April 16, 1998 at 50 m. The inflowing (outflowing) manifolds of A1 are shown in blue (red) and the inflowing (outflowing) manifolds of A2 are shown in black (magenta). The vectors are the model velocity vectors at grid points.

Is a volume flux that varies by a factor of two significant? In most volume flux calculations, variability on the order of several Sverdrups is expected. The volume of water that enters the Gulf of Mexico through the Yucatan Channel varies on the order of 5 Sverdrups. The same can be said for eddy transport. Here, the variability of transport is on the same order as the transport itself. The differences could be due, though not limited, to the following factors.

- Upwelling or down welling occurring between the two transects, changing the volume fluxes between the transects.
- Perpendicularity of the transect to both manifolds is not guaranteed since the two manifolds are not necessarily parallel.
- The average velocity of the channel was found using five interpolated points. A more precise numerical integration scheme might reduce the variability.

More accurate transport calculations will require substantially more development.

Chapter 6

CONCLUSIONS

This study extended the pioneering work of Toner et al. (2003) to include 28 levels of the Colorado University Princeton Ocean Model (CUPOM). The analysis of two hyperbolic structures with depth provides answers to the questions posed in Chapter 1.

- Hyperbolic structures A1 and A2 extend from the surface to the bottom, which for A1 is 3000 m and for A2 is 125 m. This established that hyperbolic structures are not necessarily near surface features.
- The baroclinic structure of A1 is affected by the vertical structure of the water column. The initial position of the hyperbolic trajectories between 300 m and 400 m is offset by 50 km. This occurs at the bottom of the thermocline and halocline. Yet, the analysis in Chapter 7 suggests that the hyperbolic trajectory is a single feature.
- The distances traveled by the hyperbolic trajectories varied with time and with depth. A1 had minimum and maximum distances traveled ranging from 0.73 to 19.73 m/day. Hyperbolic structure A2 displayed similar ranges between the minimum and maximum distances.
- There is a chaotic nature associated with hyperbolic structures. Particles initialized 1 km to the north, south, east and west of the hyperbolic trajectory separate from path of the hyperbolic trajectory exponentially fast. The rate of separation for hyperbolic structure A1 is $0.125 f$ in the upper levels

decreasing to $0.075 f$ in the lower levels where f is the Coriolis parameter. The rate of separation for hyperbolic structure A2 is $0.05 f$.

New results about the advective channel reported by Toner et al. (2003) were found. These include:

- The advective channel is only present at depths from 20 m to 75 m.
- The advective channel is present only from April 14 to April 18.
- Volume flux of the channel at two transects, southwest and northeast, varied between 1.4 and 2.6 Sverdrups on April 16, 1998.

The findings above could have far reaching implications outside of the Gulf of Mexico. Toner et al. (2003) first showed that material curves of the hyperbolic trajectories created an advective pathway. Since these hyperbolic trajectories were found between counter-rotating eddies, this research could be applied to other eddy rich areas, such as the Agulhas Current in Africa, the East Australian Current, and the Gulf Stream on the East Coast of the United States. Do they have similar baroclinic nature, movement, time and depth variability, lifespan, and chaotic properties as those reported here?

Chapter 7

FUTURE STUDIES

As with all research, discovery leads to more questions. The previous research can be improved and extended in many ways. Here are perhaps the most important issues.

- The volume transport calculations described in 5.4.3, however they are only rough estimates. How can they be made more accurate? These estimates could be improved by using the actual interpolated velocities along the entire transect of the channel rather than the average between the 5 points along the channel. The channel transect is also an area for improvement. How should the points be chosen? Should the transect be taken at the front, middle, or end of the channel? How can the transect be made exactly perpendicular to the channel? At present, the two endpoints of the channel were picked by hand so that the perpendicularity of the transect was not ensured. The perpendicularity would provide us with the true velocity normal to the channel. Also, the velocities at the five points along the transect were interpolated, which could be one area of concern. Another area of concern is the vertical resolution. Are more levels required? How should the channel at in-between depths be treated? In Figure 5-32, the channel is present at 75 m and not at 100 m; at what depth does the channel end?

- At present, the interpolation scheme cannot be applied when the template includes boundary points. Hence, the present study restricted analysis at A2 to 125 m since the interpolation scheme had to incorporate boundary points below this depth. The present interpolation scheme for velocity, salinity and temperature must be improved to properly account for boundary conditions on the slope. This might extend the hyperbolic structure to deeper levels.
- Sigma coordinates are more appropriate in the study of geophysical fluid dynamics. Their use might uncover new details about the vertical motion of trajectories.

There are also other studies dealing with hyperbolic structures that can be completed in the Gulf of Mexico.

- How do other hyperbolic structures in the Gulf of Mexico compare to the two studied here? Is there a normal life span for a hyperbolic structure or do they vary greatly? How often do they form? Where are they located? Hyperbolic structure A1 was clearly stronger than A2; is it generally true that hyperbolic structures in the deep Gulf tend to be stronger than those on the continental shelf?
- Hyperbolic structures create advective pathways that advect water in the Gulf of Mexico great distances over a short period of time. Ortner et al. (1995) found that Mississippi River flood waters reached the Gulf Stream via the Loop Current. But how did these waters reach the Loop Current? Toner et al. (2003) showed the evolution of a chlorophyll plume extending 500 km from the Louisiana Shelf toward the northern Yucatan. He found

two hyperbolic trajectories with associated manifolds in the vicinity of mouth of the Mississippi River. Are hyperbolic structures responsible for advecting the Mississippi River flood waters into the Loop Current and hence out of the Gulf of Mexico? Finally, what role do hyperbolic structures play in advective exchange between eddies and ambient waters in the Gulf of Mexico?

- Haddad and Carder (1979) and Tester and Steindinger (1997) suggest that upwelled intrusions of nutrient-rich Gulf of Mexico slope water onto the West Florida Shelf leads to the formation of red tides. Here I showed that the advective channel transported water from the Yucatan to the West Florida Shelf. The presence of hyperbolic structures and an associated advective channel could provide an alternate explanation for this movement of water. If so, the dynamical systems theory might be useful in predicting red tides.
- I have shown that hyperbolic structures can exist down to the ocean bottom. What roles might these structures play deep ocean dynamics?
- What makes a region of the ocean hyperbolic? Why do particles suddenly gain and lose this distinguishing character? What is the significance of the extensive vertical structure of hyperbolic regions?

Appendix A

MATERIAL CURVES

A material object consists of the same particles at all times. There are material curves, surfaces and volumes. Following the example outlined by Jaunzemis (1967), a material curve consists of those particles whose material coordinates satisfy the equations

$$X_i = F_i(u) \quad (1)$$

where u is a scalar parameter which ranges in some interval $u_0 \leq u \leq u_1$. A continuous material line is traced out, starting at $X_i(u_0)$ and ending at the particle $X_i(u_1)$ where X_i identifies individual particles.

The particles that satisfy (1) are mapped by a motion

$$x_i(t) = \chi_i(X_i, t) \quad (2)$$

into a family of space curves

$$x_i = \chi_i(F(u), t) \equiv f_i(u), \quad (3)$$

where t represents time.

A material surface is defined

$$X_i = X_i(u, v), \quad (4)$$

where u, v are surface coordinates. The particles that satisfy (4) are mapped into a family of surfaces in space

$$x_i = \chi_i(X_i(u, v), t) = v_i(u, v, t), \quad (5)$$

where x_i identifies geographic coordinates. An example of a material surface is the surface of the ocean.

Although not directly related to my research, there are also material volumes, defined by

$$\mathbf{X}_i = \mathbf{X}_i(u, v, w) \quad (6)$$

where u, v, w are curvilinear coordinates in space and its particles are mapped into regions of space defined by

$$x_i = \chi_i(\mathbf{X}(u, v, w), t) = \zeta_i(u, v, w, t). \quad (7)$$

By the axiom of impenetrability (no two particles can occupy the same point at the same time), and continuity of particles along any material object, material curves and surfaces form impermeable boundaries for advection. In contrast, particles freely cross curves, surfaces, and volumes defined by geographic coordinates.

Appendix B

HYPERBOLIC TRAJECTORY TABLES

Tables of distances traveled in other layers not listed in the results section.

Table B-1: Table of Distances traveled at 0 m for hyperbolic structure A1.

| Date | Longitude (°W) | Latitude (°N) | East (km) | North (km) | Dist (km) |
|-------------|---------------------------|--------------------------|--------------------------------------|-----------------------|------------------|
| 4/6/98 | -85.35 | 25.22 | | | |
| 4/7/98 | -85.35 | 25.14 | 0.00 | -8.78 | 8.78 |
| 4/8/98 | -85.35 | 25.20 | 0.00 | 6.71 | 6.71 |
| 4/9/98 | -85.29 | 25.23 | 6.23 | 3.10 | 6.95 |
| 4/10/98 | -85.13 | 25.39 | 16.08 | 18.05 | 24.18 |
| 4/11/98 | -85.13 | 25.50 | -0.52 | 11.33 | 11.34 |
| 4/12/98 | -85.32 | 25.48 | -18.64 | -1.54 | 18.70 |
| 4/13/98 | -85.61 | 25.49 | -29.51 | 0.51 | 29.52 |
| 4/14/98 | -85.75 | 25.51 | -13.46 | 2.57 | 13.71 |
| 4/15/98 | -85.83 | 25.52 | -8.28 | 1.03 | 8.35 |
| 4/16/98 | -85.78 | 25.63 | 5.18 | 11.84 | 12.92 |
| 4/17/98 | -85.77 | 25.65 | 1.03 | 2.57 | 2.77 |
| 4/18/98 | -85.83 | 25.68 | -6.20 | 3.09 | 6.93 |
| 4/19/98 | -85.76 | 25.72 | 6.72 | 5.14 | 8.46 |
| 4/20/98 | -85.89 | 25.72 | -12.92 | -0.51 | 12.93 |
| 4/21/98 | -86.13 | 25.65 | -23.77 | -7.20 | 24.84 |
| 4/22/98 | -86.35 | 25.48 | -22.23 | -19.04 | 29.27 |
| 4/23/98 | -86.38 | 25.33 | -3.62 | -16.49 | 16.88 |
| 4/24/98 | -86.49 | 25.26 | -10.37 | -8.25 | 13.25 |
| 4/25/98 | -86.58 | 25.19 | -8.82 | -7.74 | 11.73 |
| 4/26/98 | -86.56 | 25.02 | 1.04 | -19.11 | 19.14 |
| | | | | | |
| | | | Average Velocity (km/day) | | 14.37 |

Table B-2: Table of Distances traveled at 10 m for hyperbolic structure A1.

| Date | Longitude (°W) | Latitude (°N) | East (km) | North (km) | Dist (km) |
|-------------|-----------------------|----------------------|----------------------------------|-------------------|------------------|
| 4/6/98 | -85.37 | 25.21 | | | |
| 4/7/98 | -85.34 | 25.11 | 2.59 | -11.36 | 11.65 |
| 4/8/98 | -85.33 | 25.13 | 1.56 | 2.07 | 2.59 |
| 4/9/98 | -85.25 | 25.28 | 8.31 | 16.52 | 18.49 |
| 4/10/98 | -85.13 | 25.47 | 11.93 | 21.13 | 24.27 |
| 4/11/98 | -85.11 | 25.58 | 2.07 | 12.35 | 12.53 |
| 4/12/98 | -85.15 | 25.61 | -4.66 | 3.09 | 5.59 |
| 4/13/98 | -85.22 | 25.65 | -6.21 | 5.14 | 8.06 |
| 4/14/98 | -85.26 | 25.71 | -4.14 | 6.17 | 7.43 |
| 4/15/98 | -85.33 | 25.69 | -7.24 | -2.57 | 7.68 |
| 4/16/98 | -85.42 | 25.72 | -9.30 | 3.60 | 9.98 |
| 4/17/98 | -85.60 | 25.71 | -18.09 | -1.03 | 18.12 |
| 4/18/98 | -85.66 | 25.71 | -6.20 | 0.00 | 6.20 |
| 4/19/98 | -85.70 | 25.69 | -4.13 | -2.57 | 4.87 |
| 4/20/98 | -85.98 | 25.61 | -27.40 | -8.23 | 28.60 |
| 4/21/98 | -86.24 | 25.55 | -25.86 | -6.69 | 26.71 |
| 4/22/98 | -86.37 | 25.42 | -13.97 | -14.93 | 20.45 |
| 4/23/98 | -86.45 | 25.27 | -7.25 | -15.98 | 17.55 |
| 4/24/98 | -86.52 | 25.25 | -7.26 | -2.58 | 7.71 |
| 4/25/98 | -86.58 | 25.22 | -5.71 | -3.10 | 6.49 |
| 4/26/98 | -86.53 | 25.01 | 4.15 | -23.24 | 23.61 |
| | | | | | |
| | | | Average Velocity (km/day) | | 13.43 |

Table B-3: Table of Distances traveled at 20 m for hyperbolic structure A1.

| Date | Longitude (°W) | Latitude (°N) | East (km) | North (km) | Dist (km) |
|-------------|-----------------------|----------------------|----------------------------------|-------------------|------------------|
| 4/6/98 | -85.33 | 25.23 | | | |
| 4/7/98 | -85.33 | 25.14 | 0.52 | -9.81 | 9.82 |
| 4/8/98 | -85.32 | 25.14 | 0.52 | -0.52 | 0.73 |
| 4/9/98 | -85.28 | 25.23 | 4.67 | 9.81 | 10.86 |
| 4/10/98 | -85.17 | 25.44 | 10.90 | 24.23 | 26.57 |
| 4/11/98 | -85.12 | 25.56 | 4.66 | 12.87 | 13.69 |
| 4/12/98 | -85.12 | 25.58 | 0.52 | 2.57 | 2.62 |
| 4/13/98 | -85.16 | 25.66 | -4.66 | 8.23 | 9.46 |
| 4/14/98 | -85.23 | 25.73 | -6.72 | 7.71 | 10.23 |
| 4/15/98 | -85.28 | 25.74 | -4.65 | 1.03 | 4.76 |
| 4/16/98 | -85.33 | 25.73 | -5.17 | -0.51 | 5.19 |
| 4/17/98 | -85.46 | 25.74 | -12.92 | 0.51 | 12.93 |
| 4/18/98 | -85.56 | 25.73 | -9.82 | -0.51 | 9.83 |
| 4/19/98 | -85.69 | 25.72 | -13.43 | -1.03 | 13.47 |
| 4/20/98 | -85.91 | 25.64 | -22.22 | -9.25 | 24.07 |
| 4/21/98 | -86.16 | 25.55 | -25.34 | -9.78 | 27.16 |
| 4/22/98 | -86.36 | 25.43 | -19.66 | -13.90 | 24.08 |
| 4/23/98 | -86.41 | 25.31 | -5.18 | -12.89 | 13.89 |
| 4/24/98 | -86.48 | 25.30 | -7.26 | -0.52 | 7.28 |
| 4/25/98 | -86.57 | 25.27 | -8.82 | -4.13 | 9.73 |
| 4/26/98 | -86.56 | 25.03 | 0.52 | -25.82 | 25.82 |
| | | | | | |
| | | | Average Velocity (km/day) | | 13.11 |

Table B-4: Table of Distances traveled at 30 m for hyperbolic structure A1.

| Date | Longitude (°W) | Latitude (°N) | East (km) | North (km) | Dist (km) |
|-------------|-----------------------|----------------------|----------------------------------|-------------------|------------------|
| 4/6/98 | -85.32 | 25.22 | | | |
| 4/7/98 | -85.33 | 25.19 | -1.56 | -3.10 | 3.47 |
| 4/8/98 | -85.30 | 25.21 | 3.11 | 2.06 | 3.74 |
| 4/9/98 | -85.29 | 25.23 | 1.04 | 1.55 | 1.86 |
| 4/10/98 | -85.21 | 25.41 | 8.82 | 20.11 | 21.96 |
| 4/11/98 | -85.12 | 25.55 | 8.29 | 15.45 | 17.53 |
| 4/12/98 | -85.10 | 25.58 | 2.07 | 4.12 | 4.61 |
| 4/13/98 | -85.15 | 25.68 | -4.66 | 10.29 | 11.29 |
| 4/14/98 | -85.24 | 25.73 | -8.79 | 6.17 | 10.74 |
| 4/15/98 | -85.27 | 25.74 | -3.10 | 1.03 | 3.27 |
| 4/16/98 | -85.34 | 25.75 | -7.75 | 0.51 | 7.77 |
| 4/17/98 | -85.45 | 25.75 | -10.85 | 0.51 | 10.86 |
| 4/18/98 | -85.56 | 25.77 | -10.33 | 2.06 | 10.53 |
| 4/19/98 | -85.67 | 25.74 | -11.36 | -3.08 | 11.77 |
| 4/20/98 | -85.87 | 25.66 | -20.67 | -8.74 | 22.44 |
| 4/21/98 | -86.11 | 25.57 | -23.78 | -10.80 | 26.12 |
| 4/22/98 | -86.34 | 25.46 | -22.77 | -11.84 | 25.66 |
| 4/23/98 | -86.37 | 25.37 | -3.11 | -10.31 | 10.76 |
| 4/24/98 | -86.44 | 25.35 | -7.26 | -1.55 | 7.42 |
| 4/25/98 | -86.54 | 25.29 | -10.37 | -6.70 | 12.35 |
| 4/26/98 | -86.57 | 25.03 | -2.59 | -28.91 | 29.03 |
| | | | | | |
| | | | Average Velocity (km/day) | | 12.66 |

Table B-5: Table of Distances traveled at 75 m for hyperbolic structure A1.

| Date | Longitude (°W) | Latitude (°N) | East (km) | North (km) | Dist (km) |
|-------------|-----------------------|----------------------|----------------------------------|-------------------|------------------|
| 4/6/98 | -85.37 | 25.22 | | | |
| 4/7/98 | -85.35 | 25.20 | 2.08 | -2.06 | 2.93 |
| 4/8/98 | -85.31 | 25.28 | 4.15 | 8.26 | 9.24 |
| 4/9/98 | -85.26 | 25.40 | 5.19 | 13.40 | 14.37 |
| 4/10/98 | -85.22 | 25.50 | 3.63 | 10.82 | 11.41 |
| 4/11/98 | -85.18 | 25.54 | 4.14 | 4.63 | 6.21 |
| 4/12/98 | -85.14 | 25.57 | 3.62 | 3.09 | 4.76 |
| 4/13/98 | -85.13 | 25.58 | 1.55 | 1.54 | 2.19 |
| 4/14/98 | -85.18 | 25.58 | -5.17 | 0.51 | 5.20 |
| 4/15/98 | -85.27 | 25.65 | -9.31 | 7.20 | 11.77 |
| 4/16/98 | -85.39 | 25.70 | -11.89 | 6.17 | 13.40 |
| 4/17/98 | -85.45 | 25.73 | -6.20 | 3.08 | 6.93 |
| 4/18/98 | -85.55 | 25.75 | -9.30 | 1.54 | 9.43 |
| 4/19/98 | -85.75 | 25.72 | -20.15 | -3.08 | 20.38 |
| 4/20/98 | -85.92 | 25.67 | -17.05 | -5.14 | 17.81 |
| 4/21/98 | -86.14 | 25.59 | -22.75 | -9.26 | 24.56 |
| 4/22/98 | -86.31 | 25.50 | -16.55 | -9.78 | 19.23 |
| 4/23/98 | -86.41 | 25.47 | -10.35 | -3.60 | 10.96 |
| 4/24/98 | -86.48 | 25.42 | -6.73 | -5.67 | 8.80 |
| 4/25/98 | -86.55 | 25.32 | -7.25 | -10.31 | 12.60 |
| 4/26/98 | -86.51 | 25.01 | 4.15 | -35.11 | 35.35 |
| | | | | | |
| | | | Average Velocity (km/day) | | 12.38 |

Table B-6: Table of Distances traveled at 100 m for hyperbolic structure A1.

| Date | Longitude (°W) | Latitude (°N) | East (km) | North (km) | Dist (km) |
|-------------|-----------------------|----------------------|----------------------------------|-------------------|------------------|
| 4/6/98 | -85.38 | 25.21 | | | |
| 4/7/98 | -85.36 | 25.19 | 2.08 | -2.06 | 2.93 |
| 4/8/98 | -85.33 | 25.23 | 2.59 | 4.64 | 5.32 |
| 4/9/98 | -85.30 | 25.30 | 3.63 | 7.22 | 8.08 |
| 4/10/98 | -85.26 | 25.42 | 4.15 | 12.89 | 13.54 |
| 4/11/98 | -85.26 | 25.50 | 0.00 | 9.79 | 9.79 |
| 4/12/98 | -85.27 | 25.53 | -1.04 | 3.09 | 3.26 |
| 4/13/98 | -85.28 | 25.60 | -1.55 | 7.72 | 7.87 |
| 4/14/98 | -85.32 | 25.61 | -4.14 | 1.03 | 4.26 |
| 4/15/98 | -85.41 | 25.64 | -8.79 | 3.60 | 9.50 |
| 4/16/98 | -85.60 | 25.67 | -19.13 | 2.57 | 19.30 |
| 4/17/98 | -85.70 | 25.70 | -10.34 | 4.11 | 11.13 |
| 4/18/98 | -85.76 | 25.71 | -5.69 | 1.03 | 5.78 |
| 4/19/98 | -85.87 | 25.69 | -11.37 | -3.08 | 11.78 |
| 4/20/98 | -86.00 | 25.64 | -12.92 | -4.63 | 13.73 |
| 4/21/98 | -86.18 | 25.57 | -17.58 | -7.72 | 19.20 |
| 4/22/98 | -86.32 | 25.49 | -13.97 | -9.27 | 16.76 |
| 4/23/98 | -86.41 | 25.44 | -8.80 | -5.15 | 10.20 |
| 4/24/98 | -86.48 | 25.42 | -7.77 | -3.09 | 8.36 |
| 4/25/98 | -86.54 | 25.32 | -6.22 | -10.31 | 12.04 |
| 4/26/98 | -86.51 | 25.02 | 3.11 | -34.07 | 34.22 |
| | | | | | |
| | | | Average Velocity (km/day) | | 11.35 |

Table B-7: Table of Distances traveled at 125 m for hyperbolic structure A1.

| Date | Longitude (°W) | Latitude (°N) | East (km) | North (km) | Dist (km) |
|-------------|-----------------------|----------------------|----------------------------------|-------------------|------------------|
| 4/6/98 | -85.40 | 25.21 | | | |
| 4/7/98 | -85.38 | 25.19 | 2.08 | -2.06 | 2.93 |
| 4/8/98 | -85.35 | 25.23 | 2.08 | 4.64 | 5.09 |
| 4/9/98 | -85.31 | 25.30 | 4.15 | 8.25 | 9.24 |
| 4/10/98 | -85.28 | 25.41 | 3.11 | 11.86 | 12.26 |
| 4/11/98 | -85.28 | 25.47 | 0.52 | 6.18 | 6.20 |
| 4/12/98 | -85.30 | 25.53 | -2.07 | 6.69 | 7.01 |
| 4/13/98 | -85.33 | 25.57 | -3.62 | 4.12 | 5.48 |
| 4/14/98 | -85.41 | 25.58 | -7.24 | 1.54 | 7.41 |
| 4/15/98 | -85.51 | 25.62 | -10.35 | 4.63 | 11.34 |
| 4/16/98 | -85.62 | 25.65 | -11.38 | 3.60 | 11.93 |
| 4/17/98 | -85.72 | 25.69 | -9.31 | 3.60 | 9.98 |
| 4/18/98 | -85.79 | 25.70 | -7.75 | 1.03 | 7.82 |
| 4/19/98 | -85.90 | 25.67 | -10.34 | -2.57 | 10.65 |
| 4/20/98 | -86.03 | 25.64 | -13.44 | -3.60 | 13.91 |
| 4/21/98 | -86.18 | 25.55 | -15.51 | -9.78 | 18.34 |
| 4/22/98 | -86.33 | 25.50 | -14.49 | -5.66 | 15.56 |
| 4/23/98 | -86.40 | 25.48 | -7.25 | -2.06 | 7.53 |
| 4/24/98 | -86.46 | 25.44 | -5.70 | -4.64 | 7.34 |
| 4/25/98 | -86.55 | 25.36 | -9.32 | -8.76 | 12.79 |
| 4/26/98 | -86.55 | 25.12 | -0.52 | -26.31 | 26.32 |
| | | | | | |
| | | | Average Velocity (km/day) | | 10.46 |

Table B-8: Table of Distances traveled at 150 m for hyperbolic structure A1.

| Date | Longitude (°W) | Latitude (°N) | East (km) | North (km) | Dist (km) |
|-------------|-----------------------|----------------------|----------------------------------|-------------------|------------------|
| 4/6/98 | -85.43 | 25.21 | | | |
| 4/7/98 | -85.41 | 25.18 | 2.08 | -3.61 | 4.17 |
| 4/8/98 | -85.38 | 25.23 | 3.11 | 5.16 | 6.03 |
| 4/9/98 | -85.33 | 25.32 | 4.15 | 10.83 | 11.60 |
| 4/10/98 | -85.30 | 25.40 | 3.11 | 8.25 | 8.81 |
| 4/11/98 | -85.33 | 25.45 | -3.11 | 5.67 | 6.46 |
| 4/12/98 | -85.38 | 25.50 | -4.66 | 5.66 | 7.34 |
| 4/13/98 | -85.45 | 25.55 | -7.25 | 5.66 | 9.20 |
| 4/14/98 | -85.51 | 25.57 | -6.21 | 2.57 | 6.72 |
| 4/15/98 | -85.58 | 25.60 | -6.21 | 2.57 | 6.72 |
| 4/16/98 | -85.64 | 25.63 | -6.72 | 3.09 | 7.40 |
| 4/17/98 | -85.69 | 25.65 | -5.17 | 2.57 | 5.78 |
| 4/18/98 | -85.79 | 25.69 | -9.82 | 4.11 | 10.65 |
| 4/19/98 | -85.91 | 25.66 | -11.89 | -3.08 | 12.28 |
| 4/20/98 | -86.04 | 25.62 | -13.44 | -4.11 | 14.06 |
| 4/21/98 | -86.20 | 25.53 | -15.52 | -9.78 | 18.34 |
| 4/22/98 | -86.32 | 25.50 | -12.42 | -4.12 | 13.09 |
| 4/23/98 | -86.36 | 25.50 | -4.14 | 1.03 | 4.27 |
| 4/24/98 | -86.40 | 25.45 | -3.62 | -5.66 | 6.72 |
| 4/25/98 | -86.50 | 25.35 | -10.36 | -11.85 | 15.74 |
| 4/26/98 | -86.53 | 25.11 | -3.11 | -26.32 | 26.50 |
| | | | | | |
| | | | Average Velocity (km/day) | | 10.09 |

Table B-9: Table of Distances traveled at 250 m for hyperbolic structure A1.

| Date | Longitude (°W) | Latitude (°N) | East (km) | North (km) | Dist (km) |
|-------------|-----------------------|----------------------|----------------------------------|-------------------|------------------|
| 4/6/98 | -85.44 | 25.23 | | | |
| 4/7/98 | -85.44 | 25.20 | 0.00 | -3.61 | 3.61 |
| 4/8/98 | -85.45 | 25.24 | -1.04 | 4.64 | 4.76 |
| 4/9/98 | -85.45 | 25.30 | -0.52 | 7.22 | 7.24 |
| 4/10/98 | -85.43 | 25.36 | 2.59 | 5.67 | 6.24 |
| 4/11/98 | -85.45 | 25.39 | -2.07 | 4.12 | 4.62 |
| 4/12/98 | -85.51 | 25.43 | -6.22 | 3.61 | 7.19 |
| 4/13/98 | -85.62 | 25.46 | -10.88 | 3.61 | 11.46 |
| 4/14/98 | -85.72 | 25.49 | -10.36 | 3.60 | 10.97 |
| 4/15/98 | -85.79 | 25.52 | -7.25 | 3.09 | 7.88 |
| 4/16/98 | -85.82 | 25.57 | -2.59 | 5.66 | 6.23 |
| 4/17/98 | -85.84 | 25.58 | -2.59 | 1.54 | 3.01 |
| 4/18/98 | -85.92 | 25.57 | -7.24 | -1.03 | 7.32 |
| 4/19/98 | -86.00 | 25.56 | -8.28 | -1.54 | 8.42 |
| 4/20/98 | -86.10 | 25.51 | -9.83 | -5.66 | 11.35 |
| 4/21/98 | -86.24 | 25.40 | -14.49 | -12.36 | 19.05 |
| 4/22/98 | -86.34 | 25.30 | -9.84 | -10.31 | 14.26 |
| 4/23/98 | -86.44 | 25.29 | -10.37 | -2.06 | 10.57 |
| 4/24/98 | -86.50 | 25.30 | -6.22 | 1.55 | 6.41 |
| 4/25/98 | -86.55 | 25.26 | -5.19 | -4.13 | 6.63 |
| 4/26/98 | -86.54 | 25.13 | 1.04 | -14.97 | 15.00 |
| | | | | | |
| | | | Average Velocity (km/day) | | 8.61 |

Table B-10: Table of Distances traveled at 500 m for hyperbolic structure A1.

| Date | Longitude (°W) | Latitude (°N) | East (km) | North (km) | Dist (km) |
|-------------|-----------------------|----------------------|----------------------------------|-------------------|------------------|
| 4/6/98 | -85.39 | 25.65 | | | |
| 4/7/98 | -85.45 | 25.69 | -6.72 | 3.60 | 7.62 |
| 4/8/98 | -85.49 | 25.70 | -4.14 | 1.54 | 4.41 |
| 4/9/98 | -85.52 | 25.69 | -3.10 | -1.03 | 3.27 |
| 4/10/98 | -85.54 | 25.63 | -1.03 | -6.68 | 6.76 |
| 4/11/98 | -85.57 | 25.54 | -3.10 | -9.78 | 10.26 |
| 4/12/98 | -85.59 | 25.49 | -2.07 | -6.18 | 6.52 |
| 4/13/98 | -85.62 | 25.48 | -3.62 | -1.03 | 3.77 |
| 4/14/98 | -85.68 | 25.51 | -6.21 | 3.60 | 7.18 |
| 4/15/98 | -85.77 | 25.54 | -8.80 | 3.09 | 9.33 |
| 4/16/98 | -85.89 | 25.53 | -11.90 | -1.03 | 11.95 |
| 4/17/98 | -86.04 | 25.49 | -15.01 | -4.63 | 15.71 |
| 4/18/98 | -86.13 | 25.42 | -9.32 | -7.73 | 12.11 |
| 4/19/98 | -86.23 | 25.31 | -9.84 | -11.34 | 15.02 |
| 4/20/98 | -86.29 | 25.23 | -5.70 | -9.80 | 11.34 |
| 4/21/98 | -86.35 | 25.14 | -6.75 | -9.29 | 11.48 |
| 4/22/98 | -86.39 | 25.10 | -4.15 | -5.16 | 6.63 |
| 4/23/98 | -86.42 | 25.08 | -2.60 | -1.55 | 3.02 |
| 4/24/98 | -86.46 | 25.08 | -3.64 | -0.52 | 3.67 |
| 4/25/98 | -86.50 | 25.05 | -4.68 | -3.10 | 5.61 |
| 4/26/98 | -86.52 | 24.98 | -1.56 | -7.75 | 7.91 |
| | | | | | |
| | | | Average Velocity (km/day) | | 8.18 |

Table B-11: Table of Distances traveled at 700 m for hyperbolic structure A1.

| Date | Longitude (°W) | Latitude (°N) | East (km) | North (km) | Dist (km) |
|-------------|-----------------------|----------------------|----------------------------------|-------------------|------------------|
| 4/6/98 | -85.53 | 25.67 | | | |
| 4/7/98 | -85.54 | 25.71 | -0.52 | 4.11 | 4.14 |
| 4/8/98 | -85.54 | 25.72 | 0.00 | 1.54 | 1.54 |
| 4/9/98 | -85.55 | 25.71 | -1.03 | -1.03 | 1.46 |
| 4/10/98 | -85.56 | 25.65 | -1.55 | -6.68 | 6.86 |
| 4/11/98 | -85.59 | 25.58 | -2.59 | -7.72 | 8.14 |
| 4/12/98 | -85.62 | 25.52 | -3.10 | -6.69 | 7.38 |
| 4/13/98 | -85.65 | 25.52 | -3.62 | 0.00 | 3.62 |
| 4/14/98 | -85.73 | 25.53 | -7.25 | 0.51 | 7.26 |
| 4/15/98 | -85.79 | 25.56 | -6.73 | 3.09 | 7.40 |
| 4/16/98 | -85.89 | 25.55 | -9.31 | -1.03 | 9.37 |
| 4/17/98 | -86.01 | 25.52 | -12.42 | -2.57 | 12.68 |
| 4/18/98 | -86.01 | 25.48 | -0.52 | -4.63 | 4.66 |
| 4/19/98 | -86.05 | 25.41 | -3.62 | -7.73 | 8.53 |
| 4/20/98 | -86.13 | 25.33 | -7.77 | -8.76 | 11.71 |
| 4/21/98 | -86.21 | 25.21 | -8.81 | -13.41 | 16.05 |
| 4/22/98 | -86.30 | 25.13 | -8.30 | -9.29 | 12.46 |
| 4/23/98 | -86.35 | 25.10 | -5.19 | -2.58 | 5.80 |
| 4/24/98 | -86.39 | 25.09 | -4.16 | -2.07 | 4.64 |
| 4/25/98 | -86.44 | 25.06 | -4.68 | -3.10 | 5.61 |
| 4/26/98 | -86.51 | 25.05 | -7.27 | -0.52 | 7.29 |
| | | | | | |
| | | | Average Velocity (km/day) | | 7.33 |

Table B-12: Table of Distances traveled at 800 m for hyperbolic structure A1.

| Date | Longitude (°W) | Latitude (°N) | East (km) | North (km) | Dist (km) |
|-------------|-----------------------|----------------------|----------------------------------|-------------------|------------------|
| 4/6/98 | -85.53 | 25.67 | | | |
| 4/7/98 | -85.54 | 25.70 | -0.52 | 2.57 | 2.62 |
| 4/8/98 | -85.55 | 25.70 | -1.03 | 0.00 | 1.03 |
| 4/9/98 | -85.56 | 25.67 | -1.03 | -3.08 | 3.25 |
| 4/10/98 | -85.58 | 25.60 | -2.58 | -7.20 | 7.65 |
| 4/11/98 | -85.62 | 25.54 | -4.14 | -6.69 | 7.87 |
| 4/12/98 | -85.65 | 25.51 | -2.59 | -3.60 | 4.44 |
| 4/13/98 | -85.69 | 25.51 | -4.66 | 0.51 | 4.69 |
| 4/14/98 | -85.76 | 25.57 | -6.21 | 6.18 | 8.76 |
| 4/15/98 | -85.86 | 25.58 | -10.35 | 1.03 | 10.40 |
| 4/16/98 | -85.99 | 25.55 | -12.93 | -3.09 | 13.30 |
| 4/17/98 | -86.09 | 25.53 | -9.83 | -2.06 | 10.05 |
| 4/18/98 | -86.03 | 25.51 | 5.18 | -2.57 | 5.78 |
| 4/19/98 | -85.97 | 25.46 | 6.73 | -5.66 | 8.80 |
| 4/20/98 | -86.08 | 25.36 | -11.39 | -10.82 | 15.71 |
| 4/21/98 | -86.17 | 25.27 | -9.33 | -10.31 | 13.91 |
| 4/22/98 | -86.25 | 25.17 | -7.26 | -10.32 | 12.62 |
| 4/23/98 | -86.30 | 25.11 | -5.71 | -6.71 | 8.81 |
| 4/24/98 | -86.36 | 25.07 | -5.71 | -5.17 | 7.70 |
| 4/25/98 | -86.41 | 25.04 | -4.68 | -3.10 | 5.61 |
| 4/26/98 | -86.50 | 25.06 | -9.87 | 2.58 | 10.21 |
| | | | | | |
| | | | Average Velocity (km/day) | | 8.16 |

Table B-13: Table of Distances traveled at 900 m for hyperbolic structure A1.

| Date | Longitude (°W) | Latitude (°N) | East (km) | North (km) | Dist (km) |
|-------------|-----------------------|----------------------|----------------------------------|-------------------|------------------|
| 4/6/98 | -85.52 | 25.68 | | | |
| 4/7/98 | -85.55 | 25.66 | -2.58 | -2.06 | 3.30 |
| 4/8/98 | -85.57 | 25.63 | -1.55 | -2.57 | 3.00 |
| 4/9/98 | -85.59 | 25.59 | -2.59 | -4.63 | 5.30 |
| 4/10/98 | -85.62 | 25.55 | -3.10 | -4.63 | 5.58 |
| 4/11/98 | -85.65 | 25.51 | -2.59 | -4.63 | 5.31 |
| 4/12/98 | -85.69 | 25.50 | -4.14 | -0.51 | 4.17 |
| 4/13/98 | -85.73 | 25.53 | -4.14 | 3.09 | 5.17 |
| 4/14/98 | -85.79 | 25.58 | -5.69 | 5.15 | 7.67 |
| 4/15/98 | -85.90 | 25.57 | -11.38 | -1.54 | 11.49 |
| 4/16/98 | -86.01 | 25.53 | -10.87 | -3.60 | 11.45 |
| 4/17/98 | -86.06 | 25.52 | -4.66 | -1.03 | 4.77 |
| 4/18/98 | -86.02 | 25.50 | 3.62 | -2.57 | 4.44 |
| 4/19/98 | -85.99 | 25.44 | 2.59 | -6.70 | 7.18 |
| 4/20/98 | -86.08 | 25.37 | -8.81 | -8.24 | 12.06 |
| 4/21/98 | -86.17 | 25.28 | -9.33 | -9.80 | 13.53 |
| 4/22/98 | -86.21 | 25.18 | -4.15 | -10.84 | 11.60 |
| 4/23/98 | -86.25 | 25.11 | -3.63 | -7.75 | 8.56 |
| 4/24/98 | -86.31 | 25.06 | -5.71 | -5.68 | 8.06 |
| 4/25/98 | -86.38 | 25.03 | -7.27 | -2.58 | 7.72 |
| 4/26/98 | -86.50 | 25.08 | -12.47 | 5.17 | 13.50 |
| | | | | | |
| | | | Average Velocity (km/day) | | 7.69 |

Table B-14: Table of Distances traveled at 1000 m for hyperbolic structure A1.

| Date | Longitude (°W) | Latitude (°N) | East (km) | North (km) | Dist (km) |
|-------------|-----------------------|----------------------|----------------------------------|-------------------|------------------|
| 4/6/98 | -85.53 | 25.63 | | | |
| 4/7/98 | -85.56 | 25.60 | -3.10 | -3.09 | 4.38 |
| 4/8/98 | -85.59 | 25.56 | -3.10 | -4.63 | 5.57 |
| 4/9/98 | -85.64 | 25.51 | -5.17 | -5.66 | 7.67 |
| 4/10/98 | -85.68 | 25.50 | -4.14 | -0.51 | 4.17 |
| 4/11/98 | -85.73 | 25.52 | -4.66 | 2.06 | 5.09 |
| 4/12/98 | -85.74 | 25.56 | -0.52 | 4.12 | 4.15 |
| 4/13/98 | -85.77 | 25.57 | -3.62 | 1.03 | 3.77 |
| 4/14/98 | -85.84 | 25.56 | -6.73 | -1.03 | 6.80 |
| 4/15/98 | -85.92 | 25.54 | -8.28 | -2.06 | 8.53 |
| 4/16/98 | -86.01 | 25.52 | -8.80 | -2.57 | 9.17 |
| 4/17/98 | -86.05 | 25.51 | -4.14 | -1.03 | 4.27 |
| 4/18/98 | -86.03 | 25.49 | 2.07 | -2.57 | 3.30 |
| 4/19/98 | -86.01 | 25.43 | 1.55 | -5.67 | 5.87 |
| 4/20/98 | -86.07 | 25.37 | -5.18 | -7.73 | 9.30 |
| 4/21/98 | -86.17 | 25.28 | -10.37 | -9.28 | 13.91 |
| 4/22/98 | -86.18 | 25.14 | -1.56 | -15.48 | 15.56 |
| 4/23/98 | -86.25 | 25.04 | -6.23 | -11.37 | 12.96 |
| 4/24/98 | -86.30 | 25.01 | -5.72 | -3.10 | 6.50 |
| 4/25/98 | -86.36 | 25.02 | -5.72 | 0.52 | 5.74 |
| 4/26/98 | -86.50 | 25.08 | -14.03 | 7.23 | 15.79 |
| | | | | | |
| | | | Average Velocity (km/day) | | 7.63 |

Table B-15: Table of Distances traveled at 1200 m for hyperbolic structure A1.

| Date | Longitude (°W) | Latitude (°N) | East (km) | North (km) | Dist (km) |
|-------------|-----------------------|----------------------|----------------------------------|-------------------|------------------|
| 4/6/98 | -85.65 | 25.58 | | | |
| 4/7/98 | -85.70 | 25.52 | -5.17 | -7.21 | 8.87 |
| 4/8/98 | -85.74 | 25.46 | -3.62 | -6.18 | 7.16 |
| 4/9/98 | -85.77 | 25.46 | -2.59 | -0.52 | 2.64 |
| 4/10/98 | -85.78 | 25.47 | -1.04 | 1.55 | 1.86 |
| 4/11/98 | -85.81 | 25.46 | -3.62 | -1.03 | 3.77 |
| 4/12/98 | -85.80 | 25.39 | 1.55 | -8.24 | 8.39 |
| 4/13/98 | -85.83 | 25.38 | -3.63 | -0.52 | 3.66 |
| 4/14/98 | -85.95 | 25.33 | -11.92 | -6.19 | 13.43 |
| 4/15/98 | -86.02 | 25.31 | -6.74 | -1.55 | 6.91 |
| 4/16/98 | -86.11 | 25.28 | -9.33 | -3.61 | 10.01 |
| 4/17/98 | -86.16 | 25.25 | -5.19 | -3.10 | 6.04 |
| 4/18/98 | -86.21 | 25.19 | -4.67 | -6.71 | 8.17 |
| 4/19/98 | -86.24 | 25.13 | -3.11 | -7.23 | 7.87 |
| 4/20/98 | -86.23 | 25.07 | 1.56 | -6.72 | 6.89 |
| 4/21/98 | -86.24 | 25.01 | -1.56 | -6.72 | 6.90 |
| 4/22/98 | -86.26 | 24.96 | -1.56 | -5.69 | 5.90 |
| 4/23/98 | -86.28 | 24.93 | -2.08 | -3.10 | 3.74 |
| 4/24/98 | -86.31 | 24.94 | -3.64 | 1.55 | 3.96 |
| 4/25/98 | -86.39 | 25.01 | -7.80 | 7.24 | 10.64 |
| 4/26/98 | -86.55 | 25.12 | -16.11 | 12.92 | 20.65 |
| | | | | | |
| | | | Average Velocity (km/day) | | 7.37 |

Table B-16: Table of Distances traveled at 1300 m for hyperbolic structure A1.

| Date | Longitude (°W) | Latitude (°N) | East (km) | North (km) | Dist (km) |
|-------------|-----------------------|----------------------|----------------------------------|-------------------|------------------|
| 4/6/98 | -85.65 | 25.57 | | | |
| 4/7/98 | -85.70 | 25.51 | -4.66 | -7.21 | 8.58 |
| 4/8/98 | -85.74 | 25.47 | -4.14 | -4.12 | 5.84 |
| 4/9/98 | -85.76 | 25.44 | -1.55 | -3.61 | 3.93 |
| 4/10/98 | -85.78 | 25.40 | -2.07 | -4.12 | 4.61 |
| 4/11/98 | -85.80 | 25.36 | -2.07 | -4.64 | 5.08 |
| 4/12/98 | -85.83 | 25.34 | -3.63 | -2.58 | 4.45 |
| 4/13/98 | -85.91 | 25.32 | -7.26 | -2.06 | 7.54 |
| 4/14/98 | -85.97 | 25.29 | -6.74 | -3.61 | 7.65 |
| 4/15/98 | -86.03 | 25.27 | -6.22 | -2.06 | 6.56 |
| 4/16/98 | -86.11 | 25.23 | -7.78 | -4.13 | 8.81 |
| 4/17/98 | -86.17 | 25.18 | -5.71 | -5.68 | 8.05 |
| 4/18/98 | -86.25 | 25.12 | -7.79 | -6.20 | 9.95 |
| 4/19/98 | -86.29 | 25.03 | -4.15 | -10.85 | 11.62 |
| 4/20/98 | -86.31 | 24.99 | -2.60 | -3.62 | 4.45 |
| 4/21/98 | -86.24 | 24.98 | 7.80 | -1.55 | 7.95 |
| 4/22/98 | -86.25 | 24.93 | -1.04 | -5.17 | 5.28 |
| 4/23/98 | -86.26 | 24.90 | -1.04 | -3.10 | 3.27 |
| 4/24/98 | -86.30 | 24.92 | -4.68 | 1.55 | 4.93 |
| 4/25/98 | -86.39 | 25.01 | -9.36 | 9.83 | 13.57 |
| 4/26/98 | -86.54 | 25.12 | -14.55 | 12.92 | 19.46 |
| | | | | | |
| | | | Average Velocity (km/day) | | 7.58 |

Table B-17: Table of Distances traveled at 1400 m for hyperbolic structure A1.

| Date | Longitude (°W) | Latitude (°N) | East (km) | North (km) | Dist (km) |
|-------------|-----------------------|----------------------|----------------------------------|-------------------|------------------|
| 4/6/98 | -85.66 | 25.57 | | | |
| 4/7/98 | -85.72 | 25.50 | -5.69 | -7.72 | 9.59 |
| 4/8/98 | -85.76 | 25.45 | -4.14 | -5.15 | 6.61 |
| 4/9/98 | -85.77 | 25.41 | -1.55 | -4.64 | 4.89 |
| 4/10/98 | -85.80 | 25.37 | -3.11 | -4.12 | 5.16 |
| 4/11/98 | -85.84 | 25.30 | -3.63 | -8.25 | 9.01 |
| 4/12/98 | -85.87 | 25.27 | -3.63 | -2.58 | 4.45 |
| 4/13/98 | -85.93 | 25.25 | -5.19 | -2.06 | 5.58 |
| 4/14/98 | -85.98 | 25.21 | -5.71 | -4.64 | 7.36 |
| 4/15/98 | -86.05 | 25.16 | -6.75 | -5.16 | 8.49 |
| 4/16/98 | -86.11 | 25.12 | -6.23 | -5.16 | 8.09 |
| 4/17/98 | -86.16 | 25.04 | -4.67 | -8.78 | 9.95 |
| 4/18/98 | -86.25 | 25.00 | -9.35 | -4.65 | 10.45 |
| 4/19/98 | -86.34 | 24.99 | -9.36 | -1.03 | 9.41 |
| 4/20/98 | -86.33 | 24.97 | 1.56 | -1.55 | 2.20 |
| 4/21/98 | -86.30 | 24.95 | 3.12 | -2.59 | 4.05 |
| 4/22/98 | -86.26 | 24.92 | 4.16 | -3.10 | 5.19 |
| 4/23/98 | -86.26 | 24.89 | -0.52 | -3.10 | 3.15 |
| 4/24/98 | -86.31 | 24.92 | -4.68 | 3.10 | 5.62 |
| 4/25/98 | -86.41 | 25.02 | -9.88 | 10.34 | 14.30 |
| 4/26/98 | -86.55 | 25.12 | -14.55 | 11.37 | 18.47 |
| | | | | | |
| | | | Average Velocity (km/day) | | 7.60 |

Table B-18: Table of Distances traveled at 1500 m for hyperbolic structure A1.

| Date | Longitude (°W) | Latitude (°N) | East (km) | North (km) | Dist (km) |
|-------------|-----------------------|----------------------|----------------------------------|-------------------|------------------|
| 4/6/98 | -85.68 | 25.54 | | | |
| 4/7/98 | -85.73 | 25.48 | -4.14 | -6.18 | 7.44 |
| 4/8/98 | -85.77 | 25.43 | -4.66 | -6.18 | 7.74 |
| 4/9/98 | -85.80 | 25.38 | -2.59 | -4.64 | 5.31 |
| 4/10/98 | -85.82 | 25.34 | -2.07 | -5.15 | 5.56 |
| 4/11/98 | -85.85 | 25.27 | -3.63 | -7.22 | 8.08 |
| 4/12/98 | -85.90 | 25.24 | -4.67 | -3.10 | 5.60 |
| 4/13/98 | -85.95 | 25.22 | -4.67 | -2.58 | 5.33 |
| 4/14/98 | -85.99 | 25.19 | -4.15 | -3.61 | 5.50 |
| 4/15/98 | -86.06 | 25.14 | -6.75 | -5.16 | 8.50 |
| 4/16/98 | -86.12 | 25.08 | -6.75 | -6.71 | 9.52 |
| 4/17/98 | -86.17 | 25.02 | -5.19 | -7.23 | 8.91 |
| 4/18/98 | -86.26 | 25.00 | -8.84 | -1.55 | 8.97 |
| 4/19/98 | -86.34 | 24.99 | -8.32 | -1.03 | 8.38 |
| 4/20/98 | -86.34 | 24.97 | 0.52 | -2.59 | 2.64 |
| 4/21/98 | -86.30 | 24.95 | 3.64 | -2.59 | 4.46 |
| 4/22/98 | -86.27 | 24.90 | 3.64 | -5.17 | 6.33 |
| 4/23/98 | -86.27 | 24.89 | 0.00 | -1.03 | 1.03 |
| 4/24/98 | -86.31 | 24.92 | -4.68 | 3.62 | 5.92 |
| 4/25/98 | -86.41 | 25.03 | -9.36 | 11.38 | 14.73 |
| 4/26/98 | -86.53 | 25.12 | -12.99 | 10.85 | 16.93 |
| | | | | | |
| | | | Average Velocity (km/day) | | 7.34 |

Table B-19: Table of Distances traveled at 1750 m for hyperbolic structure A1.

| Date | Longitude (°W) | Latitude (°N) | East (km) | North (km) | Dist (km) |
|-------------|-----------------------|----------------------|----------------------------------|-------------------|------------------|
| 4/6/98 | -85.69 | 25.53 | | | |
| 4/7/98 | -85.74 | 25.48 | -4.66 | -6.18 | 7.74 |
| 4/8/98 | -85.79 | 25.40 | -5.70 | -8.76 | 10.45 |
| 4/9/98 | -85.82 | 25.33 | -2.59 | -7.22 | 7.67 |
| 4/10/98 | -85.84 | 25.28 | -2.07 | -6.19 | 6.53 |
| 4/11/98 | -85.87 | 25.24 | -3.63 | -3.61 | 5.12 |
| 4/12/98 | -85.92 | 25.21 | -4.15 | -3.61 | 5.50 |
| 4/13/98 | -85.97 | 25.17 | -5.19 | -4.13 | 6.63 |
| 4/14/98 | -86.07 | 25.15 | -9.86 | -2.58 | 10.19 |
| 4/15/98 | -86.09 | 25.11 | -2.60 | -4.13 | 4.88 |
| 4/16/98 | -86.13 | 25.06 | -4.15 | -5.68 | 7.04 |
| 4/17/98 | -86.18 | 25.03 | -4.68 | -4.13 | 6.24 |
| 4/18/98 | -86.23 | 25.00 | -5.20 | -3.10 | 6.05 |
| 4/19/98 | -86.28 | 25.01 | -5.20 | 1.55 | 5.42 |
| 4/20/98 | -86.30 | 24.99 | -2.08 | -2.58 | 3.32 |
| 4/21/98 | -86.30 | 24.96 | 0.00 | -3.62 | 3.62 |
| 4/22/98 | -86.28 | 24.91 | 2.60 | -5.17 | 5.79 |
| 4/23/98 | -86.26 | 24.90 | 1.56 | -1.03 | 1.87 |
| 4/24/98 | -86.31 | 24.95 | -4.68 | 5.69 | 7.37 |
| 4/25/98 | -86.42 | 25.04 | -11.44 | 10.34 | 15.42 |
| 4/26/98 | -86.56 | 25.11 | -14.55 | 7.23 | 16.25 |
| | | | | | |
| | | | Average Velocity (km/day) | | 7.16 |

Table B-20: Table of Distances traveled at 2000 m for hyperbolic structure A1.

| Date | Longitude (°W) | Latitude (°N) | East (km) | North (km) | Dist (km) |
|-------------|-----------------------|----------------------|----------------------------------|-------------------|------------------|
| 4/6/98 | -85.69 | 25.53 | | | |
| 4/7/98 | -85.74 | 25.47 | -5.18 | -6.69 | 8.46 |
| 4/8/98 | -85.80 | 25.40 | -5.70 | -7.73 | 9.60 |
| 4/9/98 | -85.82 | 25.33 | -2.59 | -7.73 | 8.15 |
| 4/10/98 | -85.85 | 25.27 | -2.59 | -6.19 | 6.71 |
| 4/11/98 | -85.89 | 25.23 | -3.63 | -4.13 | 5.50 |
| 4/12/98 | -85.92 | 25.20 | -3.63 | -4.13 | 5.50 |
| 4/13/98 | -85.97 | 25.16 | -4.67 | -4.65 | 6.59 |
| 4/14/98 | -86.04 | 25.14 | -7.27 | -1.55 | 7.43 |
| 4/15/98 | -86.09 | 25.10 | -4.67 | -4.13 | 6.24 |
| 4/16/98 | -86.12 | 25.07 | -3.12 | -4.13 | 5.18 |
| 4/17/98 | -86.16 | 25.03 | -4.68 | -4.13 | 6.24 |
| 4/18/98 | -86.21 | 25.02 | -4.68 | -1.55 | 4.93 |
| 4/19/98 | -86.25 | 24.99 | -3.64 | -2.58 | 4.46 |
| 4/20/98 | -86.27 | 24.98 | -2.60 | -1.03 | 2.80 |
| 4/21/98 | -86.29 | 24.94 | -1.56 | -4.65 | 4.91 |
| 4/22/98 | -86.27 | 24.91 | 2.08 | -3.62 | 4.18 |
| 4/23/98 | -86.26 | 24.90 | 1.04 | -0.52 | 1.16 |
| 4/24/98 | -86.29 | 24.95 | -3.64 | 5.17 | 6.33 |
| 4/25/98 | -86.42 | 25.05 | -12.48 | 10.86 | 16.54 |
| 4/26/98 | -86.55 | 25.11 | -14.03 | 7.23 | 15.78 |
| | | | | | |
| | | | Average Velocity (km/day) | | 6.83 |

Table B-21: Table of Distances traveled at 2500 m for hyperbolic structure A1.

| Date | Longitude (°W) | Latitude (°N) | East (km) | North (km) | Dist (km) |
|-------------|-----------------------|----------------------|----------------------------------|-------------------|------------------|
| 4/6/98 | -85.72 | 25.50 | | | |
| 4/7/98 | -85.76 | 25.43 | -3.62 | -8.76 | 9.48 |
| 4/8/98 | -85.79 | 25.36 | -3.11 | -7.73 | 8.33 |
| 4/9/98 | -85.82 | 25.31 | -3.63 | -4.64 | 5.89 |
| 4/10/98 | -85.86 | 25.26 | -4.15 | -5.67 | 7.03 |
| 4/11/98 | -85.90 | 25.22 | -3.63 | -5.16 | 6.31 |
| 4/12/98 | -85.93 | 25.18 | -3.11 | -3.61 | 4.77 |
| 4/13/98 | -85.97 | 25.15 | -3.63 | -3.61 | 5.12 |
| 4/14/98 | -85.99 | 25.12 | -2.60 | -3.10 | 4.04 |
| 4/15/98 | -86.02 | 25.10 | -2.60 | -3.10 | 4.04 |
| 4/16/98 | -86.07 | 25.06 | -5.19 | -4.13 | 6.64 |
| 4/17/98 | -86.12 | 25.05 | -4.68 | -1.03 | 4.79 |
| 4/18/98 | -86.18 | 25.03 | -6.76 | -2.07 | 7.06 |
| 4/19/98 | -86.23 | 25.01 | -4.16 | -2.07 | 4.64 |
| 4/20/98 | -86.26 | 24.97 | -3.64 | -4.65 | 5.91 |
| 4/21/98 | -86.27 | 24.94 | -0.52 | -3.10 | 3.15 |
| 4/22/98 | -86.23 | 24.90 | 3.64 | -4.14 | 5.51 |
| 4/23/98 | -86.25 | 24.91 | -2.08 | 0.52 | 2.14 |
| 4/24/98 | -86.28 | 24.96 | -3.12 | 6.21 | 6.95 |
| 4/25/98 | -86.43 | 25.07 | -15.08 | 11.37 | 18.89 |
| 4/26/98 | -86.55 | 25.11 | -12.47 | 5.17 | 13.50 |
| | | | | | |
| | | | Average Velocity (km/day) | | 6.71 |

Table B-22: Table of Distances traveled at 3000 m for hyperbolic structure A1.

| Date | Longitude (°W) | Latitude (°N) | East (km) | North (km) | Dist (km) |
|-------------|-----------------------|----------------------|----------------------------------|-------------------|------------------|
| 4/6/98 | -85.72 | 25.50 | | | |
| 4/7/98 | -85.76 | 25.43 | -4.66 | -7.73 | 9.02 |
| 4/8/98 | -85.80 | 25.36 | -4.14 | -7.73 | 8.77 |
| 4/9/98 | -85.84 | 25.30 | -3.63 | -6.70 | 7.62 |
| 4/10/98 | -85.88 | 25.24 | -4.15 | -6.19 | 7.45 |
| 4/11/98 | -85.92 | 25.19 | -3.63 | -5.68 | 6.74 |
| 4/12/98 | -85.95 | 25.15 | -3.63 | -4.65 | 5.90 |
| 4/13/98 | -85.98 | 25.13 | -3.12 | -2.07 | 3.74 |
| 4/14/98 | -86.01 | 25.07 | -3.12 | -6.20 | 6.94 |
| 4/15/98 | -86.02 | 25.05 | -0.52 | -2.58 | 2.64 |
| 4/16/98 | -86.01 | 25.03 | 0.52 | -2.07 | 2.13 |
| 4/17/98 | -86.04 | 25.03 | -3.12 | -0.52 | 3.16 |
| 4/18/98 | -86.13 | 25.03 | -8.32 | 0.00 | 8.32 |
| 4/19/98 | -86.18 | 25.01 | -5.72 | -1.55 | 5.92 |
| 4/20/98 | -86.21 | 24.97 | -3.12 | -4.14 | 5.18 |
| 4/21/98 | -86.24 | 24.94 | -2.08 | -3.62 | 4.17 |
| 4/22/98 | -86.24 | 24.91 | 0.00 | -3.10 | 3.10 |
| 4/23/98 | -86.23 | 24.91 | 0.52 | 0.00 | 0.52 |
| 4/24/98 | -86.26 | 24.95 | -3.12 | 4.14 | 5.18 |
| 4/25/98 | -86.38 | 25.04 | -11.96 | 10.34 | 15.81 |
| 4/26/98 | -86.52 | 25.13 | -14.55 | 9.30 | 17.27 |
| | | | | | |
| | | | Average Velocity (km/day) | | 6.48 |

Table B-23: Table of Distances traveled at 0 m for hyperbolic structure A2.

| Date | Longitude (°W) | Latitude (°N) | East (km) | North (km) | Dist (km) |
|---------|----------------|---------------|----------------------------------|------------|-----------|
| 4/10/98 | -84.00 | 25.40 | | | |
| 4/11/98 | -84.10 | 25.05 | -9.84 | -38.19 | 39.44 |
| 4/12/98 | -84.03 | 24.88 | 7.27 | -19.13 | 20.47 |
| 4/13/98 | -84.05 | 24.98 | -2.60 | 10.86 | 11.17 |
| 4/14/98 | -84.05 | 25.06 | 0.52 | 8.79 | 8.80 |
| 4/15/98 | -83.93 | 25.06 | 11.43 | 0.52 | 11.44 |
| 4/16/98 | -83.88 | 25.10 | 5.20 | 3.62 | 6.33 |
| 4/17/98 | -83.84 | 25.08 | 4.16 | -1.55 | 4.43 |
| 4/18/98 | -83.78 | 25.13 | 5.71 | 5.17 | 7.70 |
| 4/19/98 | -83.79 | 25.16 | -0.52 | 4.13 | 4.16 |
| 4/20/98 | -83.68 | 25.02 | 11.42 | -16.53 | 20.09 |
| | | | | | |
| | | | Average Velocity (km/day) | | 13.40 |

Table B-24: Table of Distances traveled at 20 m for hyperbolic structure A2.

| Date | Longitude (°W) | Latitude (°N) | East (km) | North (km) | Dist (km) |
|---------|----------------|---------------|----------------------------------|------------|-----------|
| 4/10/98 | -84.00 | 25.31 | | | |
| 4/11/98 | -84.12 | 25.27 | -12.96 | -4.13 | 13.60 |
| 4/12/98 | -84.19 | 25.24 | -6.74 | -3.10 | 7.42 |
| 4/13/98 | -84.22 | 25.23 | -3.11 | -1.55 | 3.48 |
| 4/14/98 | -84.21 | 25.22 | 1.04 | -1.03 | 1.46 |
| 4/15/98 | -84.16 | 25.18 | 5.19 | -4.65 | 6.96 |
| 4/16/98 | -84.08 | 25.16 | 8.31 | -1.55 | 8.45 |
| 4/17/98 | -84.01 | 25.16 | 6.75 | -1.03 | 6.83 |
| 4/18/98 | -83.93 | 25.13 | 7.79 | -2.58 | 8.20 |
| 4/19/98 | -83.88 | 25.08 | 5.71 | -6.20 | 8.43 |
| 4/20/98 | -83.83 | 24.99 | 5.20 | -9.82 | 11.11 |
| | | | | | |
| | | | Average Velocity (km/day) | | 7.59 |

Table B-25: Table of Distances traveled at 30 m for hyperbolic structure A2.

| Date | Longitude (°W) | Latitude (°N) | East (km) | North (km) | Dist (km) |
|---------|----------------|---------------|----------------------------------|------------|-----------|
| 4/10/98 | -84.00 | 25.30 | | | |
| 4/11/98 | -84.01 | 25.29 | -1.56 | -1.55 | 2.19 |
| 4/12/98 | -84.07 | 25.28 | -6.22 | -1.55 | 6.41 |
| 4/13/98 | -84.12 | 25.29 | -5.19 | 1.03 | 5.29 |
| 4/14/98 | -84.15 | 25.24 | -2.59 | -5.16 | 5.77 |
| 4/15/98 | -84.17 | 25.20 | -1.56 | -4.64 | 4.90 |
| 4/16/98 | -84.11 | 25.14 | 5.71 | -6.71 | 8.81 |
| 4/17/98 | -84.03 | 25.11 | 7.79 | -2.58 | 8.21 |
| 4/18/98 | -83.97 | 25.09 | 5.71 | -3.10 | 6.50 |
| 4/19/98 | -83.91 | 25.03 | 6.23 | -5.68 | 8.44 |
| 4/20/98 | -83.83 | 24.98 | 8.83 | -6.20 | 10.79 |
| | | | | | |
| | | | Average Velocity (km/day) | | 6.73 |

Table B-26: Table of Distances traveled at 75 m for hyperbolic structure A2.

| Date | Longitude (°W) | Latitude (°N) | East (km) | North (km) | Dist (km) |
|---------|----------------|---------------|----------------------------------|------------|-----------|
| 4/10/98 | -84.00 | 25.16 | | | |
| 4/11/98 | -83.99 | 25.16 | 0.52 | 0.00 | 0.52 |
| 4/12/98 | -83.98 | 25.15 | 1.04 | -1.03 | 1.46 |
| 4/13/98 | -83.97 | 25.15 | 0.52 | 0.00 | 0.52 |
| 4/14/98 | -83.98 | 25.15 | -0.52 | 0.00 | 0.52 |
| 4/15/98 | -83.98 | 25.15 | 0.00 | 0.00 | 0.00 |
| 4/16/98 | -83.98 | 25.14 | 0.00 | -1.03 | 1.03 |
| 4/17/98 | -83.98 | 25.14 | 0.00 | 0.00 | 0.00 |
| 4/18/98 | -83.95 | 25.13 | 2.60 | -1.03 | 2.79 |
| 4/19/98 | -83.86 | 25.08 | 9.87 | -5.68 | 11.39 |
| 4/20/98 | -83.74 | 25.00 | 11.43 | -9.30 | 14.74 |
| | | | | | |
| | | | Average Velocity (km/day) | | 3.30 |

Table B-27: Table of Distances traveled at 100 m for hyperbolic structure A2.

| Date | Longitude (°W) | Latitude (°N) | East (km) | North (km) | Dist (km) |
|-------------|-----------------------|----------------------|----------------------------------|-------------------|------------------|
| 4/10/98 | -84.00 | 25.09 | | | |
| 4/11/98 | -83.94 | 25.07 | 5.71 | -1.55 | 5.92 |
| 4/12/98 | -83.92 | 25.08 | 1.56 | 0.52 | 1.64 |
| 4/13/98 | -83.92 | 25.08 | 0.00 | 0.00 | 0.00 |
| 4/14/98 | -83.91 | 25.07 | 1.04 | -0.52 | 1.16 |
| 4/15/98 | -83.92 | 25.07 | -0.52 | 0.00 | 0.52 |
| 4/16/98 | -83.91 | 25.06 | 0.52 | -1.03 | 1.16 |
| 4/17/98 | -83.90 | 25.06 | 1.56 | -0.52 | 1.64 |
| 4/18/98 | -83.81 | 25.04 | 8.83 | -2.07 | 9.07 |
| 4/19/98 | -83.75 | 25.03 | 6.24 | -1.03 | 6.32 |
| 4/20/98 | -83.72 | 25.03 | 2.60 | -0.52 | 2.65 |
| | | | | | |
| | | | Average Velocity (km/day) | | 3.01 |

Bibliography

- Biggs, D.C., and F.E. Muller-Karger. 1994. Ship and satellite observations of chlorophyll stocks in warm- and cold-core rings in the western Gulf of Mexico. *J. Geophys. Res.*, Vol. 99, 7371-7384.
- Biggs, D.C. G.S. Fargion, P. Hamilton and R.R. Leben. 1996. Cleavage of a Gulf of Mexico Loop Current eddy by a deep water cyclone. *J. Geophys. Res.* Vol. 101, 20629-20641.
- Candella, Julio, Sorayda Tanahara, Michel Crepon, Bernard Barnier, and Julio Sheinbaum. 2003. Yucatan Channel flow: Observations versus CLIPPER ATL6 and MERCATOR PAM models. *J. Geophys. Research.* Vol. 108. No. C12. 15-1- 15-24.
- Cochrane, J.D. 1969. Separation of an anticyclone and subsequent developments in the Loop Current. *Contributions on the Physical Oceanography of the Gulf of Mexico.* Edited by L.R.A. Capurio and J.L. Reid. 91-106. Gulf Publishing, Houston, TX.
- Coulliette, C. and S. Wiggins. 2000. Intergyre transport in a wind-driven, quasigeostrophic double gyre: An application of lobe dynamics. *Nonlinear Processes in Geophysics.* 7, 59-85.
- Denman, K.L., and M.R. Abbott. 1994. Time scales of pattern evolution from cross-spectrum analysis of advanced very high resolution radiometer and coastal zone color scanner imagery. *J. Geophys. Res.*, 99, 7433-7442.
- Dietrich, D.E. and C.A. Lin. 1994. Numerical studies of eddy shedding in the Gulf of Mexico. *J. Geophys. Res.*, 99, 7599-7615.
- Dietrich, D.E., C.A. Lin, A. Mestas-Nunez. 1997. A high resolution numerical study of Gulf of Mexico fronts and eddies. *Meteorol. Atmos. Phys.* 64, 187-201.
- Elliot, B.A. 1979. Anticyclonic rings and the energetics of the circulation of the Gulf of Mexico. Ph.D. dissertation, Texas A & M University, College Station, TX.
- , 1982. Anticyclonic rings in the Gulf of Mexico. *J. Phys. Oceanogr.*, 12, 1292-1309.

- Gilbes, F.C. Thomas, J.J. Walsh and F.E. Muller-Karger. 1996. An episodic chlorophyll plume on the west Florida shelf. *Cont. Shelf Res.*, 16, 1201-1224.
- Gower, J.F.R.K., K.L. Denman and R.J. Holyer. 1980. Phytoplankton patchiness indicates the fluctuation spectrum of mesoscale oceanic structures. *Nature*, 288, 157-159.
- Haddad, K.D. and K.L. Carder. 1979. Ocean Intrusion: One possible initiation mechanism of red tide blooms on the west coast of Florida, in *Toxic Dinoflagellate Blooms*, edited by D.L. Taylor and H.H. Seliger, pp. 269-274, Elsevier Sci., New York.
- Haller, G. and A.C. Poje. 1998. Finite time transport in aperiodic flows. *Physica D*. Vol. 119, 352-380.
- Haller, G. 2000. Finding finite-time invariant manifolds in two-dimensional velocity fields. *Chaos*. Vol. 10, 99-108.
- Hamilton, P., T.J. Berger and W. Johnson. 2002. On the structure and motions of cyclones in the northern Gulf of Mexico. *J. Geophys. Res.*, Vol. 107 (C12), 3028, doi:10.1029/1999JC000270.
- Hua, B.L., P. Klein. 1998. An exact criterion for the stirring properties of nearly two-dimensional turbulence. *Physica D*. Vol. 113, 98-110.
- Hurlburt, H.E., and J.D. Thompson. 1980. A numerical study of Loop Current intrusions and eddy shedding. *J. Phys. Oceanog.* 10, 1611-1651.
- Ichiye, T. 1962. Circulation and water mass distribution in the Gulf of Mexico. *Geofis. Int.*, 2, 47-76.
- Indest, A.W., A.D. Kirwan, Jr., J.K. Lewis, P. Reinersman. 1989. A synopsis of mesoscale eddies in the Gulf of Mexico. *Mesoscale/Synoptic Coherent Structures in Geophysical Turbulence*. Elsevier Science Publishers. Amsterdam, 485-500.
- Jaunzemis, Walter. 1967. *Continuum Mechanics*. MacMillan Company. New York. 145-148.
- Kantha, L.H. and C.A. Clayson. 1994. An improved mixed layer model for geophysical applications. *J. Geophys. Res.*, 99, 235-266.

- Kantha, L.H., J.K. Choi, R. Leben, C. Cooper, M. Vogel, and J. Feeny. 1999. Hindcasts and real-time nowcast/forecast of currents in the Gulf of Mexico, paper presented at Offshore Technol. Conference, Offshore Technol., Houston, Tex., 3-6 May.
- Kantha, Lakshmi, 2004. PRIVATE COMMUNICATION.
- Kantha, L. H., 2005. Development, testing and implementation of a real-time nowcast/forecast capability for the Gulf of Mexico. *Kaiyo*, 37, 239-256.
- Kirwan, A.D. Jr., 2005. Dynamics of "critical" trajectories. Accepted for publication in *Progress in Oceanography*.
- Kirwan, A.D. Jr., W.J. Merrel, Jr., J.K. Lewis, R.E. Whitaker. 1984a. Lagrangian observations of an anticyclonic ring in the western Gulf of Mexico. *J. Geophys. Res.*, 89, 11, 727-740.
- Kirwan, A.D. Jr., W.J. Merrel, Jr., J.K. Lewis, R.E. Whitaker, and R. Legeckis. 1984b. A model for the analysis of drifter data with an application to a warm core ring in the Gulf of Mexico. *J. Geophys. Res.*, 89(C3), 3425-3438.
- Kuznetsov, L. M. Toner, A.D. Kirwan Jr. C.K.R.T. Jones, L.H. Kantha, and J. Choi. 2002. The Loop Current and adjacent rings delineated by Lagrangian analysis of the near-surface flow. *J. Marine Research*, 60, 405-429.
- Lewis, J.K. and A.D. Kirwan Jr., 1985. Some observations of ring-topography and ring-ring interactions in the Gulf of Mexico. *J. Geophys. Res.*, 94, 8163-8178.
- 1987. Genesis of a Gulf of Mexico ring as determined from kinematic analysis. *J. Geophys. Res.*, 92, 8163-8178.
- Lewis, J.K., 1990. Analysis of drifting buoy trajectories from Gulf of Mexico physical Oceanography program year 5, Proc. Annu. Info. Transfer Meet., 10 Dec. 1989. 169-174.
- Lopez, J.W., and L.H. Kantha. 2000. A data-assimilative numerical model of the North Indian Ocean. *J. Atmos. Ocean Tech.* 17, 1525-1540.
- Mellor, G.L. and T. Yamada. 1982. Development of a turbulence closure model for geophysical fluid problems. *Rev. Geophys.*, 20, 851-875.
- Merrell, W.J. and J.M. Morrison. 1981. On the circulation of the Western Gulf of Mexico with observations from 1978. *J. Geophys. Res.* 86(C5), 4181-4185.

- Merrell, W.J. and A.M. Vazquez. 1983. Observations of changing mesoscale circulation patterns in the western Gulf of Mexico. *J. Geophys. Res.* 88 (C12), 7721-7723.
- Mezic, I and S. Wiggins. 1994. On the integrability and perturbation of three-dimensional fluid flow with symmetry. *J. Nonlinear Sci.* Vol. 4, 157-194.
- Miller, P.D., C.K.R.T. Jones, A.M. Rogerson, L.J. Pratt. 1997. Quantifying transport in numerically generated velocity fields. *Physica D.* 110. 105-122.
- Muller-Karger, F.E., J.J. Walsh, R.H. Evans, and M.B. Meyers. 1991. On the seasonal phytoplankton concentration and sea surface temperature cycles of the Gulf of Mexico as determined by satellites. *J. Geophys. Res.*, 88, 7721-7723.
- Neumann, G. and W.J. Pierson Jr., 1966. *Principles of Physical Oceanography.* Prentice-Hall, Inc., Englewood Cliffs, NJ. 131.
- Oey, L., H.C. Lee and W.J. Schmitz, Jr., 2003. Effects of winds and Caribbean eddies on the frequency of Loop Current Eddy shedding: A numerical model study. *J. Geophys. Res.*, 108, 3324, doi: 10.1029/2002JC001698.
- Oey, L. 2004. Vorticity flux through the Yucatan Channel and Loop Current variability in the Gulf of Mexico. *J. Geophys. Res.*, 109, C10004, doi:10.1029/2004JC002400.
- Okubo, A. 1970. Horizontal dispersion of floatable particles in the vicinity of velocity singularities such as convergences. *Deep-Sea Res.* Vol. 17, 445-454.
- Ortner, P.B, T.N. Lee, P.J. Milne, R.G. Zika, M.E. Clarke, G.P. Podesta, P.K. Swart, P.A. Tester, L.P. Atkinson and W.R. Johnson. 1995. Mississippi River flood waters that reached the Gulf Stream. *J. Geophys. Res.* 100, (C7), 13595-13601.
- Perez, R., F.E. Muller-Karger, I. Victoria, N. Melo, and S. Cerdeira, 1999. Cuban, Mexican, and U.S. researchers probing mysteries of Yucatan Current. *EOS Trans. AGU*, 80, 14, 153.
- Pond, Stephen and George L. Pickard. *Introductory Dynamical Oceanography.* Pergamon Press. Oxford. 1983.
- Romanou, A., E.P Chassignet., W. Sturges. 2004. Gulf of Mexico circulation within a high-resolution numerical simulation of the North Atlantic Ocean. *J. Geophys. Res.* 109, C01003. doi:10.1029/2003JC001770.

- Sturges, W., J.C. Evans, S. Welsh, and W. Holland. 1993. Separation of warm-core rings in the Gulf of Mexico. *J. Phys. Oceanogr.*, 23, 250-268.
- Sturges, W. and R. Leben. 2000. Frequency of ring separations from the Loop Current in the Gulf of Mexico: A revised estimate. *J. Phys. Oceanogr.*, 30, 1814-1819.
- Tester, P.A. and K.A. Steidinger. 1997. *Gymnodinium breve* red tide blooms: Initiation, transport, and consequence of surface circulation. *Limnol. Oceanogr.*, 42, 1039-1051, 1997.
- Toner, M., A.D. Kirwan Jr., L. Kantha and J. Choi. 2001. Can general circulation models be assessed and their output enhanced with drifter data? *J. Geo. Phys. Res.*, 106, 19,563-19,579.
- Toner, M. A.D. Kirwan, Jr., A.C. Poje, L.H. Kantha, F.E. Muller-Karger and C.K.R.T. Jones. 2003. Chlorophyll dispersal by eddy-eddy interactions in the Gulf of Mexico. *J. Geophys. Res.* Vol. 108(C4), 3105. doi:10.1029/2002JC001499.
- Vukovich, F.M. 1995. An updated evaluation of the Loop Current's eddy shedding frequency. *J. Geophys. Res.*, 100, 8655-8659.
- Vukovich, F.M. and B.W. Crissman. 1986. Aspects of warm rings in the Gulf of Mexico. *J. Geophys. Res.*, 91(C2), 2645-2660.
- Weiss, J. 1991. The dynamics of enstrophy transfer in two-dimensional hydrodynamics. *Physica D.* Vol. 48, 273-294.